

AD-A180 354

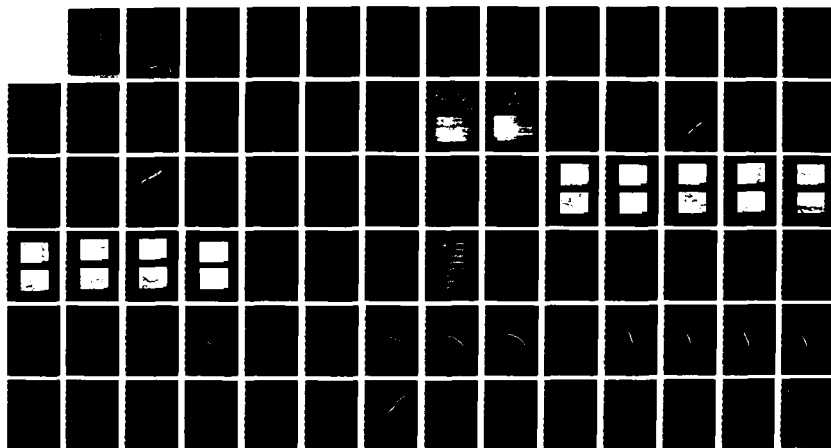
FATIGUE CRACK-GROWTH RESISTANCE OF ALUMINUM ALLOYS  
UNDER SPECTRUM LOADING (U) NORTHROP CORP HAWTHORNE CA  
AIRCRAFT GROUP G V SCARICH ET AL DEC 85

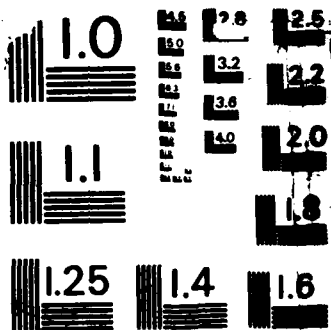
1/1

UNCLASSIFIED

NOR-85-141-VOL-1 N00014-82-C-0425

F/G 11/6 1 NL





MICROCOPY RESOLUTION TEST CHART  
NATIONAL BUREAU OF STANDARDS 1963

DMC FILE COPY

AD-A180 354

**FATIGUE CRACK-GROWTH RESISTANCE  
OF ALUMINUM ALLOYS  
UNDER SPECTRUM LOADING**  
**Volume I — Commercial 2XXX and 7XXX Alloys**

**G. V. SCARICH  
P. E. BRETZ**

**DECEMBER 1985  
NOR 85-141**

**TECHNICAL REPORT  
FINAL REPORT FOR PERIOD 30 SEPTEMBER 1982 THROUGH 31 MARCH 1985  
CONTRACT NO. N00019-82-C-0425**

**APPROVED FOR PUBLIC RELEASE; DISTRIBUTION IS UNLIMITED**

**DEPARTMENT OF THE NAVY  
NAVAL AIR SYSTEMS COMMAND  
WASHINGTON, D.C. 20361**

**LIBRARY COPY**

**JAN 24 1986**

**LANGLEY RESEARCH CENTER  
LIBRARY, NASA  
HAMPTON, VIRGINIA**

**NORTHROP**

**Aircraft Division  
Aircraft Group  
Northrop Corporation  
One Northrop Avenue  
Hawthorne, California 90250**

**MAY 11 1987**

**S D  
SELECTED  
A**

**87-5-11-023**

6a. NAME OF PERFORMING ORGANIZATION Northrop Corporation Aircraft Division	6b. OFFICE SYMBOL <i>(If applicable)</i>	7a. NAME OF MONITORING ORGANIZATION Naval Air Systems Command	
6c. ADDRESS (City, State and ZIP Code) One Northrop Avenue Hawthorne, California 90250	7b. ADDRESS (City, State and ZIP Code) Department of the Navy Washington, DC 20301		
8a. NAME OF FUNDING/SPONSORING ORGANIZATION Naval Air Systems Command	8b. OFFICE SYMBOL <i>(If applicable)</i>	9. PROCUREMENT INSTRUMENT IDENTIFICATION NUMBER N00019-82-C-0425	
8c. ADDRESS (City, State and ZIP Code) Department of the Navy Washington, D.C. 20361	10. SOURCE OF FUNDING NOS		
11. TITLE (Include Security Classification) See Cover	PROGRAM ELEMENT NO.	PROJECT NO.	TASK NO.
12. PERSONAL AUTHOR(S) G.V. Scarich (Northrop) P.E. Bretz (Alcoa)	13. PAGE COUNT 77		
13a. TYPE OF REPORT Technical Report	13b. TIME COVERED FROM 30 Sept 82 TO 31 Mar 85	14. DATE OF REPORT (Yr., Mo., Day) December 1985	
16. SUPPLEMENTARY NOTATION Volume II of this report, "Aluminum Lithium Alloys" contains the results of the balance of the effort of this contract.			
17. COSATI CODES	18. SUBJECT TERMS (Continue on reverse if necessary and identify by block number) 2020 7075 Aluminum Alloys Microstructure 2024 7475 Fatigue Fracture Toughness 2124 7050 Spectrum Loading Constant-Amplitude Loading 2324 7150 Retardation Variable-Amplitude Loading		
19. ABSTRACT (Continue on reverse if necessary and identify by block number)  The purpose of this program is to obtain metallurgical guidelines and test methodologies for selection and development of spectrum fatigue-resistant, high-strength aluminum alloys for application to aircraft structures. This volume (II) of this report describes the results of baseline characterizations of two high-strength aluminum alloys, and compares these results to those obtained in the two previous phases of the program.			
20. DISTRIBUTION/AVAILABILITY OF ABSTRACT UNCLASSIFIED/UNLIMITED <input checked="" type="checkbox"/> SAME AS RPT <input type="checkbox"/> DTIC USERS <input type="checkbox"/>		21. ABSTRACT SECURITY CLASSIFICATION UNCLASSIFIED	
22a. NAME OF RESPONSIBLE INDIVIDUAL W. L. Koegel		22b. TELEPHONE NUMBER <i>(Include Area Code)</i> (212) 692-6025	22c. OFFICE SYMBOL NAVAIR-5304B6

## 19. Abstract (continued)

For fatigue crack-growth testing under constant amplitude loading, the significant observations were that (1) the differences in fatigue crack-growth rates were greatest in the near-threshold regime, where 2024-T351, 2124-T351, and 7475-T651 showed the highest resistance to FCP and (2) FCP resistance varied with the stress intensity factor range ( $\Delta K$ ). For example, in contrast to its excellent near threshold crack-growth resistance, 7475-T651 had the lowest resistance to FCP for  $\Delta K$  greater than 6 MPa  $\sqrt{\text{m}}$ .

For spectrum testing at the maximum peak stress of 145 MPa (21 ksi):

1. The ranking of the alloys by spectrum life is the same for both spectrums, except for 2020-T651. The alloys ranked as follows with their percentage of life relative to 2124-T351, averaged for both spectrums, shown in parentheses: 2124-T351 (100%), 2024-T351 (81%), 7475-T651 (76%), 2324-T39 (72%), 2020-T651 (70%), 7475-T7351 (64%), 7050-T7451 (63%), 7150-T6E189 (55%), 7075-T7351 (53%), 2124-T851 (46%), 7075-T651 (44%), and 2024-T851 (35%).
2. For each material the tension-dominated spectrum consistently resulted in longer lives than the tension-compression spectrum.

Eight of the ten alloys were spectrum fatigue tested using two independent modifications of the baseline spectrums. One modification, the racetrack method, was used to eliminate 43 percent of the low-amplitude cycles to reduce testing time. The differences in spectrum fatigue lives between the modified and baseline spectrums were small enough so that the selection of one alloy over another would not be significantly affected.

The second modification was made to determine the importance of compressive load cycles. To accomplish this, all compression load points were eliminated from the tension-compression spectrum. There were significant increases in spectrum lives compared to the baseline spectrum, but the ranking of the eight alloys for this modified spectrum was identical to that for the baseline spectrum except for 2020-T651 which changed from fifth to second.

In general, the spectrum performance rankings could not be correlated with yield strength or constant-amplitude FCP resistance. However, spectrum performance could be correlated with fracture toughness. Specifically for the testing at 145 and 169 MPa, FCP life for both spectrums generally increased with increased fracture toughness. Also the alloys that deform by planar slip generally had longer spectrum fatigue lives than those that deformed more homogeneously. The effects of deformation mode and grain structure were evaluated by producing alloys with controlled variations in chemistry, aging, and thermomechanical processing. These results are reported in Volume II of this report entitled "Spectrum Fatigue Crack-Growth Resistance of Aluminum Alloys Under Spectrum Loading-Aluminum Lithium Alloys."



Accession No.	
NTIS G7-11	
DTIC TAB	
Unclassified	
Justification	
By _____	
Distribution/	
Availability Cycles	
Dist	Avail and/or Special
A-1	

## PREFACE

This report was prepared by the Northrop Corporation, Aircraft Division, Hawthorne, California, under Naval Air Systems Command Contract N00019-82-C-0425. Ms. G. Weaver of Naval Air Systems Command (Code AIR-5304B4) was the project engineer.

Northrop Corporation, Aircraft Division, was the prime contractor, with Mr. G.V. Scarich serving as the program manager. Mr. K.M. Bresnahan was involved in the analysis of the deformation behavior, which included the correlation of fracture features with microstructure. Mr. S. Hsu was responsible for all the spectrum testing and data reduction, while Mr. P.G. Porter was responsible for spectrum selection, generation, and modification.

Aluminum Company of America, Alcoa Technical Center, was a major participant in the program. Dr. P.E. Bretz served as the Alcoa program manager and Principal Investigator. Alcoa was intimately involved in all the phases of the program and was primarily responsible for determination of baseline mechanical properties, microstructural characterization, and fracture surface/microstructure interpretation.

The contractor report number is NOR 84-141. This report covers work from 30 September 1982 through 31 March 1985, and it consists of two volumes:

- Volume I - Commercial 2XXX and 7XXX Alloys
- Volume II - Aluminum Lithium Alloys.

The authors also wish to acknowledge R. Schmidt formerly of NAVAIR; A.P. Divecha of NSWC; and B.J. Mays, A.H. Freedman, G.R. Chanani, S.W. Averill, J. Luck, D.R. Drott, J.P. Bouffard, and J.M. Wilson of Northrop; and J.T. Staley and R.R. Sawtell of Alcoa for their cooperation and support during the various phases of the program.

## CONTENTS

<u>Section</u>		<u>Page</u>
1	INTRODUCTION .....	1
2	EXPERIMENTAL PROCEDURE.....	7
3	RESULTS AND DISCUSSION .....	9
3.1	Chemistry .....	9
3.2	Microstructural Evaluation .....	9
3.3	Tensile and Fracture Toughness Results .....	13
3.4	Fatigue Crack Growth Results Under Constant-Amplitude Loading .....	13
3.5	Spectrum Test Results.....	13
3.6	Fractographic Examination of Spectrum Fatigue Specimens .....	19
3.7	Modified Spectrums .....	36
4	SUMMARY AND CONCLUSIONS.....	41
	REFERENCES .....	45

## Appendix

A	CONSTANT AMPLITUDE FATIGUE CRACK GROWTH RATE, $da/dN$ VERSUS $\Delta K$ .....	49
B	CRACK LENGTH VERSUS SIMULATED FLIGHT HOURS FOR BASELINE SPECTRUMS, $a$ VERSUS $H$ .....	53
C	SPECTRUM CRACK GROWTH RATE VERSUS MAXIMUM PEAK STRESS INTENSITY, $da/dH$ VERSUS $K_{hmax}$ .....	59
D	PREDICTION .....	65
E	EVALUATION OF SECOND HEAT OF 7475-T651.....	69

## ILLUSTRATIONS

<u>Figure</u>		<u>Page</u>
1	Program Outline .....	5
2	Optical Micrographs of Alloy 2124-T351, Longitudinal Plane .....	11
3	Optical Micrograph of Alloy 7150-T6E189, Longitudinal Plane .....	12
4	Relationship Between Yield Strength and Fracture Toughness .....	15
5	Constant Amplitude FCGR Curves.....	15
6	Stress Intensity Needed to Obtain a Given Fatigue Crack Growth Rate Under Constant Amplitude Loading.....	16
7	Spectrum FCGR Curves for TD Spectrum .....	20
8	Maximum Peak Stress Intensity Needed to Obtain a Given Spectrum FCGR for TD and TC Spectrums.....	20
9	Spectrum Fatigue Lives at 145 MPa (21 ksi) .....	23
10	Spectrum Life Versus Yield Strength .....	23
11	Spectrum Life Versus Fracture Toughness .....	24
12	Spectrum Fatigue Lives at 103 and 169 MPa .....	25
13	Fracture Surface of 2124-T351 Tested Using TD Spectrum at $a = 6.4$ mm (0.25 in.) .....	27
14	Fracture Surface of 2124-T351 Tested Using TD Spectrum at $a = 19.1$ mm (0.75 in.) .....	28
15	Fracture Surface of 2124-T351 Tested Using TC Spectrum at $a = 6.4$ mm (0.25 in.) .....	29
16	Fracture Surface of 2124-T351 Tested Using TC Spectrum at $a = 19.1$ mm (0.75 in.) .....	30
17	Fracture Surface of 7150-T6E189 Tested Using TD Spectrum at $a = 6.4$ mm (0.25 in.) .....	31

ILLUSTRATIONS (Continued)

<u>Figure</u>		<u>Page</u>
18	Fracture Surface of 7150-T6E189 Tested Using TD Spectrum at $a = 19.1$ mm (0.75 in.).....	32
19	Fracture Surface of 7150-T6E189 Tested Using TC Spectrum at $a = 6.4$ mm (0.25 in.) .....	33
20	Fracture Surface of 7150-T6E189 Tested Using TC Spectrum at $a = 19.1$ mm (0.75 in.) .....	34
21	Banded Fracture Surfaces for 2124 and 7150 Prior to Final Fracture .....	35
22	Spectrum Fatigue Lives for TCZ, TD, and TC Spectrums .....	39

## TABLES

<u>Table</u>		<u>Page</u>
1	Chemical Composition of Program Materials .....	10
2	Tensile Results - Longitudinal .....	14
3	Fracture Toughness Results, L-T Orientation .....	14
4	Ranking of Materials by Stress Intensity Range to Obtain a Given Fatigue Crack Growth Rate Under Constant-Amplitude Loading .....	17
5	Spectrum Fatigue Results - Baseline Spectrums .....	18
6	Ranking of Materials in Spectrum Fatigue by Maximum Peak Stress Intensity to Obtain a Given Fatigue Crack Growth Rate .....	21
7	Ranking of Materials Under Spectrum Loading - Baseline Spectrums .....	22
8	Spectrum Fatigue Lives at 103 MPa and 169 MPa for "a" From 6mm (0.24 in.) to Failure .....	24
9	Spectrum Fatigue Results - Modified Spectrums .....	37
10	Ranking of Materials Under Spectrum Loading - Modified Spectrums .....	38

## ABBREVIATIONS AND SYMBOLS

a	Crack-length
$a_i$	Initial crack length
$a_c$	Current crack length
$a_f$	Final crack length
B	Specimen thickness
COD	Crack opening displacement
$da/dH$	Spectrum crack growth rate
$da/dN$	Crack growth rate (constant amplitude)
F	Failure
FCGR	Fatigue crack growth rate
FCP	Fatigue crack propagation
H	Simulated flight hours or half height of compact tension specimen
K	Stress-intensity factor
$K_{eff}$	Effective stress intensity
$K_{hmax}$	Stress-intensity factor at largest (highest) peak of spectrum
$K_{hmin}$	Stress-intensity factor at smallest (lowest) valley of spectrum
$K_{max}$	Maximum stress intensity factor
$K_{Ic}$	Plane strain fracture toughness
$K_Q$	Conditional fracture toughness; test did not meet all the ASTM E399 validity criteria
L	Longitudinal
L-T	Crack growth on plane normal to the rolling direction (L) of the plate in a direction transverse (T) to the rolling direction (per ASTM E399)
N	Number of cycles
P	Load
$P_{cl}$	Crack closure load
$P_{hmax}$	Load at largest (highest) peak of a spectrum
$P_{hmin}$	Load at smallest (lowest) valley in a spectrum
$P_{max}$	Peak load
$P_{sm}$	Mean spectrum load

## ABBREVIATIONS AND SYMBOLS (Concluded)

R	Stress or load ratio = $P_{\min}/P_{\max}$
SEM	Scanning electron microscope/microscopy
SFCGR	Spectrum fatigue crack growth rate
TC	Tension-compression, horizontal hinge tail moment spectrum
TCR	Racetrack-modified, tension-compression spectrum
TC(R)	Average of TC and TCR spectrum lives
TCZ	Tension-compression-zero spectrum
TD	Tension-dominated, lower wing root spectrum
TDR	Racetrack-modified, tension-dominated spectrum
TD(R)	Average of TD and TDR spectrum lives
TEM	Transmission electron microscope/microscopy
T/2	Mid-thickness (center) location in a plate
T/4	Quarter-thickness location in a plate
3T/4	Three-quarter thickness location in a plate
W	Specimen width
YS	Yield strength
$\Delta K$	Stress-intensity range
$\Delta K_h$	Overall stress-intensity range of a spectrum
$\Delta P$	Load range
$\Delta P_h$	Overall load range of a spectrum
$\Delta \sigma$	Stress range: Algebraic difference between successive valley and peak (positive or increasing) or between successive peak and valley (negative or decreasing)
$\Delta \sigma_h$	Overall stress range in a spectrum
$\sigma$	Applied stress
$\sigma_{h\max}$	Stress at largest (highest) peak of spectrum
$\sigma_{h\min}$	Stress at smallest (lowest) valley of a spectrum
$\sigma_{sm}$	Spectrum mean stress

## 1. INTRODUCTION

Fatigue crack growth behavior under variable-amplitude loading is increasingly being used in the selection of materials for aircraft structures and their design, particularly for fatigue-critical structures. This is supplanting the selection of materials based on constant-amplitude fatigue crack growth resistance because the life of an aircraft structure cannot be predicted reliably using constant-amplitude fatigue crack growth data and existing life prediction techniques. Research in the last decade<sup>(1-12)</sup> has shown that load sequences have a considerable effect on fatigue crack propagation (FCP) behavior. In particular, the application of overloads or a few cycles at high tensile loads may cause retardation, that is, a temporary decrease in fatigue crack growth rate during subsequent lower amplitude cycles. Most of the work in the last decade was focused on understanding the effects of single overloads on fatigue crack growth rates.<sup>(1-10)</sup> Recently more emphasis is being placed upon the evaluation of fatigue crack growth under complex spectrum loading<sup>(11-14)</sup> simulating the loading experienced by aircraft structures.

The nature of a spectrum can vary widely depending on a particular component and type of aircraft. Depending on the specific details of load spectrums, FCP resistance for a given material also can vary widely. The reasons for differences in FCP resistance for the same material in different spectrums are generally unknown, since the load spectrums are complex and the interactions between alloy microstructure and variable-amplitude load histories are not well understood.

Research in the last decade<sup>(1-4,15-19)</sup> on high-strength aluminum alloys has identified several metallurgical factors which influence FCP resistance for constant-amplitude loading: alloy purity (Fe, Si content), temper, alloy content (e.g., Cu content), and dispersoid type (e.g.,  $Al_{12}Mg_2Cr$  in 7075 vs.  $Al_3Zr$  in 7050). However, the influence of these microstructural features

on crack growth is not the same at intermediate and high growth rates,  $>10^{-8}$  m/cycle ( $4 \times 10^{-7}$  in./cycle) as it is at near-threshold rates,  $<10^{-8}$  m/cycle. For example, overaging from a T6 temper to a T7 temper reduces FCP rates by a factor of two at intermediate stress intensities ( $\Delta K$ ) but can increase crack growth rates by a factor of ten at low  $\Delta K$ . These studies demonstrate that different microstructural features control constant-amplitude FCP behavior at different  $\Delta K$  values. Details of these microstructural/FCP behavior relationships will be addressed in Subsection 3.6 of this report.

The same level of understanding regarding microstructural effects on FCP under variable-amplitude loading does not exist. Whereas constant-amplitude loading characterizes the steady state FCP response of an alloy, FCP under variable-amplitude loading includes transient material responses not present in constant-amplitude FCP. Therefore, the understanding of microstructural effects on constant-amplitude FCP behavior is not sufficient to rationalize spectrum fatigue performance. In particular, the ability of an alloy to retard crack growth following a tensile overload is an important transient characteristic for assessing FCP life. However, since the present knowledge regarding the effect of microstructure on the retardation behavior of aluminum alloys is limited to studies involving simple overload spectrums, the results under complex spectrum loading at present cannot be understood.

Several mechanisms have been proposed to explain the observed retardation behavior following simple overloads. These include residual compressive stresses at the crack tip, <sup>(20,21)</sup> crack closure, <sup>(22-24)</sup> changes in the crack-tip plastic zone size, <sup>(1,20,25)</sup> crack blunting, <sup>(1,26)</sup> or combinations of these. A number of empirical models, based on either the crack closure <sup>(22,23)</sup> or plastic zone size <sup>(20,21)</sup> concepts, have been proposed that quantitatively take retardation into account in predicting FCP behavior. These models achieve satisfactory results only under certain specified conditions. However, when the test conditions are changed or broadened to include additional variables such as those existing in real spectrums, the models usually fail to predict observed crack growth lives.

The major weakness of all of these models is that they do not take into account either the metallurgical or the environmental factors that influence FCP. For instance, the Willenborg model predicts that materials with the

same yield strength will exhibit similar retardation behavior.<sup>(20)</sup> Chanani<sup>(1)</sup> found that this was not the case for 2024-T8 and 7075-T73 heat treated to the same yield strength. He concluded that metallurgical variables such as precipitate morphology, dislocation interactions, and cyclic hardening exponent, have to be taken into account to explain the differences between the crack growth rates. Sanders, et al.,<sup>(2)</sup> had identified microstructural features such as precipitate morphology, intermetallic constituent particles, and dispersoid size as influencing FCP. Improved analytical life prediction capabilities would result if microstructure/load history interactions for spectrum FCP are understood and incorporated in such models.

The objectives of the multiphase NAVAIR program (N00019-80-C-0427,<sup>(27)</sup> N00019-81-C-0550,<sup>(28)</sup> and N00019-82-C-0425) are to perform a detailed metallurgical investigation of fatigue behavior and to simplify complex load histories. These spectrums will be representative of certain classes of applications and will provide information for development of fatigue-resistant alloys. As a major part of this effort, attention will be given to identifying metallurgical factors in high-strength aluminum alloys which control FCP behavior under spectrum loading. This knowledge of load history/microstructure interactions is essential to the development of criteria by which complex load histories can be standardized and simplified for materials evaluation.

The development of standardized and/or simplified load spectrums offers several advantages in characterizing the fatigue performance of engineering materials and designing fatigue resistant alloys. It is presently not cost-effective to develop alloys for high resistance to FCP under spectrum loading, since a wide variety of load histories must be considered. If a small number of standardized spectrums existed, more meaningful tests which consider spectrum loading could be included in alloy development/selection programs. Standardized load spectrums also would provide a common data base for comparisons of fatigue performance among various materials. The two spectrums in the program were simplified by eliminating half of the cycles and by eliminating the compression cycles. Selected existing life prediction tools were evaluated, and the potential of incorporating metallurgical factors in these models were examined.

This report describes the work completed in Phase III of this program and includes pertinent results from Phases I<sup>(27)</sup> and II<sup>(28)</sup> for completeness. Twelve commercial 2XXX and 7XXX aluminum alloys (Figure 1) were chosen for analysis so that the influence of both purity and temper on FCP could be evaluated. In Phases I and II, 10 of the alloys were evaluated; and in Phase III, two additional alloys were evaluated. The results on the 12 commercial 2XXX and 7XXX aluminum alloys are presented in Volume I of this report. The 12 alloys have been characterized with respect to chemical composition, microstructure, tensile properties, and fracture toughness. FCP tests were conducted on specimens of each of the 12 alloys for both constant-amplitude loading (including the low  $\Delta K$  region) and two F-18 load spectrums. One F-18 load spectrum is a tension-dominated spectrum representing the lower wing root load history, and the other is a tension-compression spectrum representing the horizontal tail hinge moment load history. In the spectrum testing, one primary stress level was used for FCGR testing, while two other stress levels were used to obtain data at the low and high ends of the crack growth range. Fractographic examination of the spectrum fatigue specimens was used to document pertinent fracture features for each alloy. Six Al-Li alloys with systematically controlled microstructures were also evaluated in this program and the results are described in Volume II of this report.

The results of the tests performed using modified spectrums are also described in this report. Two different types of modifications were performed independently on the baseline spectrums. One modification had two goals: (1) to eliminate low-amplitude cycles to reduce testing time without changing the ranking (relative life) of the alloys, and (2) to determine the importance of low-amplitude cycles on the overall spectrum life. The second modification was made to determine the importance of compression cycles. Eight alloys (marked with + in Figure 1) were chosen for spectrum fatigue testing using the modified spectrums. These eight alloys were chosen from the 2XXX and 7XXX aluminum alloys so that the influences of purity, temper, and different alloy approaches were represented.

This report is written as an addendum to the Phase II Report.<sup>(28)</sup> In this phase two alloys were added to the original ten. The two alloys added were 2124-T351 and 7150-T6E189. The ten alloys previously evaluated were

## INVESTIGATION OF FATIGUE CRACK GROWTH OF ALUMINUM ALLOYS UNDER SPECTRUM LOADING

### MATERIALS

#### PREVIOUS PROGRAMS\*

2020-T651 +  
2024-T351 +  
2024-T851 +  
2124-T851  
2324-T39  
7050-T7451 +  
7075-T651 +  
7075-T7351 +  
7475-T651 +  
7475-T7351 +

#### CURRENT PROGRAM\*\*

2124-T351  
7150-T6E189

SPECIAL HEATS WITH SELECTED  
MICROSTRUCTURES\*\*\*

### SPECIFIC COMPARISONS

- ALLOY PURITY (FRACTURE TOUGHNESS)  
7075 vs 7475 and 2024 vs 2124
- PRECIPITATE STRUCTURE (TEMPER)  
2024-T351 vs T851, 2124-T351 vs T851, 7075-T651 vs T7351, and 7475-T651 vs T7351
- GRAIN SIZE  
RST (FINE) vs I/M (COARSE)\*\*\*\* and SYSTEMATICALLY CONTROLLED  
MICROSTRUCTURES\*\*\*
- EXISTING ALLOYS vs NEW ALLOYS and APPROACHES  
7XXX vs CW67 RST\*\*\*\* and 7150, and 2XXX vs 2324 and Al-Li (SYSTEMATICALLY  
CONTROLLED MICROSTRUCTURES)\*\*\*

### GENERAL COMPARISONS

- MICROSTRUCTURE
- TENSILE
- FRACTURE TOUGHNESS
- CONSTANT-AMPLITUDE FATIGUE-CRACK GROWTH

### LOAD HISTORY

- TWO F-18 SPECTRA (TENSION-DOMINATED and TENSION-COMPRESSION)
- THREE STRESS LEVELS
- MODIFICATIONS OF THE F-18 SPECTRUMS
- CRITICAL EXPERIMENTS\*\*\*\*

### SPECTRUM TEST SPECIMEN

- CENTER CRACKED PANEL - 6 mm THICK X 100 mm WIDE
- L-T ORIENTATION

### SPECTRUM LIFE PREDICTIONS\*\*

\*PREVIOUS PROGRAMS, CONTRACT NOS. N00019-80-C-0427 and N00019-81-C-0550

\*\*CURRENT PROGRAM, CONTRACT NO. N00019-82-C-0425

\*\*\*CURRENT PROGRAM, SEPARATE REPORT

\*\*\*\*FUTURE PLANNED EFFORT

+MATERIALS TESTED WITH MODIFIED SPECTRUMS

FIGURE 1. PROGRAM OUTLINE

2020-T651, 2024-T351, 2024-T851, 2124-T851, 2324-T39, 7050-T7451, 7075-T651, 7075-T7351, 7475-T651, and 7475-T7351.

In this report the new data are given in detail and most figures and tables from the Phase II report<sup>(28)</sup> are updated to include the new information. A limited number of copies of that report are available on request. A summary of that work is also published in "Advances in Fracture Research - Proceedings of the Sixth International Conference on Fracture."<sup>(30,31)</sup>

## **2. EXPERIMENTAL PROCEDURE**

All procedures and spectrums were identical to those used in Phase II and described in Reference 28. Note that the designation of 7050-T73651 has been changed to 7050-T7451 to reflect the change made by the Aluminum Association.

### 3. RESULTS AND DISCUSSION

The results for 2124-T351 and 7150-T6E189 are presented with summaries for all 12 alloys. Discussion is primarily limited to differences in results from those found in Phase II.

#### 3.1 CHEMISTRY

The chemical composition of all 12 alloys are listed in Table 1 along with the commercial limits for each. All 12 alloys are within the appropriate composition limits.

#### 3.2 MICROSTRUCTURAL EVALUATION

Alloys 2124-T351 and 7150-T6E189 are variants of commercial alloys examined in Phases I and II of this contract; as such, there are few microstructural distinctions between these two alloys and those studied previously. Alloy 2124-T351 is a high-purity, naturally aged variant of 2024. The as-polished microstructure (Figure 2a) indicates the distribution of constituent phases, which include insoluble  $Al_{12}(Fe,Mn)_3Si$  and  $Al_7Cu_2Fe$  particles, and partially soluble  $Mg_2Si$  and  $Al_2CuMg$  phases. The volume fraction of these constituents is substantially lower than in 2024, owing to the lower Fe plus Si content in 2124. As is the case in other 2X24 alloys, the grain morphology is a coarse, recrystallized structure (Figure 2b).

Alloy 7150 is a minor compositional variant of 7050 developed jointly by Alcoa and Boeing for maximum strength. The T6E189 temper is an Alcoa-designed practice which provides improved exfoliation resistance over the original T651 temper without sacrificing either strength or SCC resistance. Like 2124, 7150 has low Fe plus Si content and relatively small volume fractions of constituents (Figure 3a). As for other 7XXX alloys, these constituents include  $Al_7Cu_2Fe$ ,  $Mg_2Si$ , and  $Al_2CuMg$ . The grain structure of 7X50 alloys generally exhibits a low degree of recrystallization, as in Figure 3b; this

TABLE 1. CHEMICAL COMPOSITION OF PROGRAM MATERIALS

MATERIAL	SAMPLE NO.	ELEMENT, WEIGHT PERCENT											
		LIMITS	Cu	Mg	Zn	Mn	Cr	Ti	Be	Fe	Si	OTHER	
2020-T651	523713-B	4.44	—	0.03	0.52	0.00	0.02	—	0.20	0.09	—	1.09Li 0.20Cd	
2024-T351	511338	4.35	1.54	0.07	0.51	0.00	0.03	—	0.23	0.09	—	—	
-T851	511339	4.41	1.50	0.09	0.50	0.00	0.02	—	0.33	0.10	—	—	
2124-T351	554885	3.8	1.2	—	0.30	—	—	—	—	—	—	—	
-T851	511340	4.9	1.8	0.25	0.9	0.10	0.15	—	0.50	0.50	—	—	
2324-T39	492513	3.91	1.35	0.02	0.48	—	0.01	—	0.07	0.05	—	—	
-T7351	475332	4.21	1.46	0.03	0.47	0.00	0.01	—	0.10	0.05	—	—	
7075-T651	511341	3.8	1.2	—	0.30	—	—	—	—	—	—	—	
-T7351	511464	4.9	1.8	0.25	0.9	0.10	0.15	—	0.30	0.20	—	—	
7050-T73651	536031	4.23	1.52	0.01	0.51	0.00	0.01	0.002	0.08	0.05	—	—	
-T7351	511463	3.8	1.2	—	0.3	—	—	—	—	—	—	—	
7475-T651	511630	4.4	1.8	0.25	0.9	0.10	0.15	—	0.12	0.10	—	—	
-T7351	511630	3.9	1.2	—	0.30	—	—	—	0.27	0.09	—	—	
7150-T6E189	536031	2.0	2.9	6.1	0.30	0.28	0.20	—	0.50	0.40	—	—	
-T7351	511464	2.23	2.30	6.27	0.02	0.01	0.03	0.002	0.13	0.07	0.12Zr	—	
7475-T651	511463	2.0	1.9	5.7	—	—	—	—	—	—	0.08Zr	—	
-T7351	511630	2.6	2.6	6.7	0.10	0.04	0.06	0.05	0.15	0.12	0.15Zr	—	
7150-T6E189	536031	2.09	2.23	6.29	0.01	0.00	0.04	—	0.11	0.05	—	—	
-T7351	511464	1.9	2.0	5.9	—	—	—	—	—	—	—	—	
7475-T651	511463	2.5	2.7	6.9	0.10	0.04	0.06	—	0.15	0.12	—	—	
-T7351	511630	1.48	2.36	5.46	0.00	0.21	0.02	0.002	0.07	0.04	—	—	
7150-T6E189	536031	1.6	2.43	5.67	0.00	0.17	0.02	0.001	0.06	0.05	—	—	
-T7351	511464	1.2	1.9	5.2	—	0.18	—	—	—	—	—	—	
7475-T651	511463	1.9	2.6	6.2	0.06	0.25	0.06	0.05	0.12	0.1	—	—	

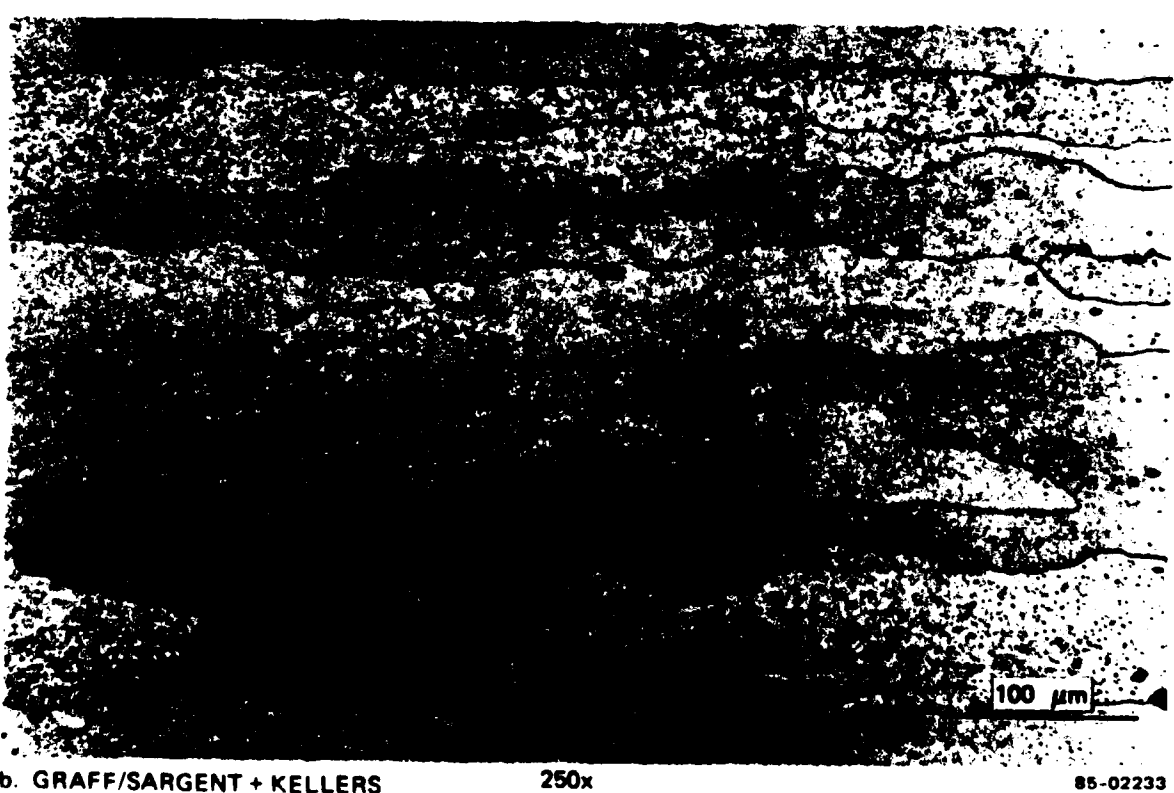
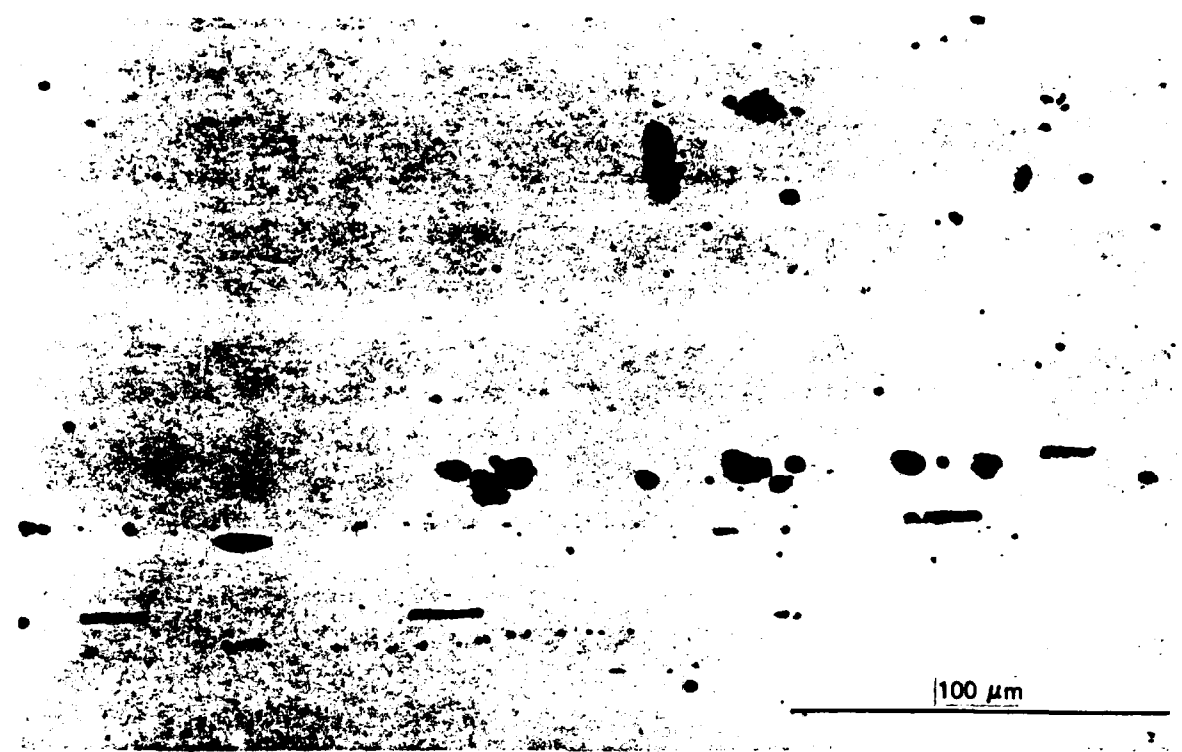


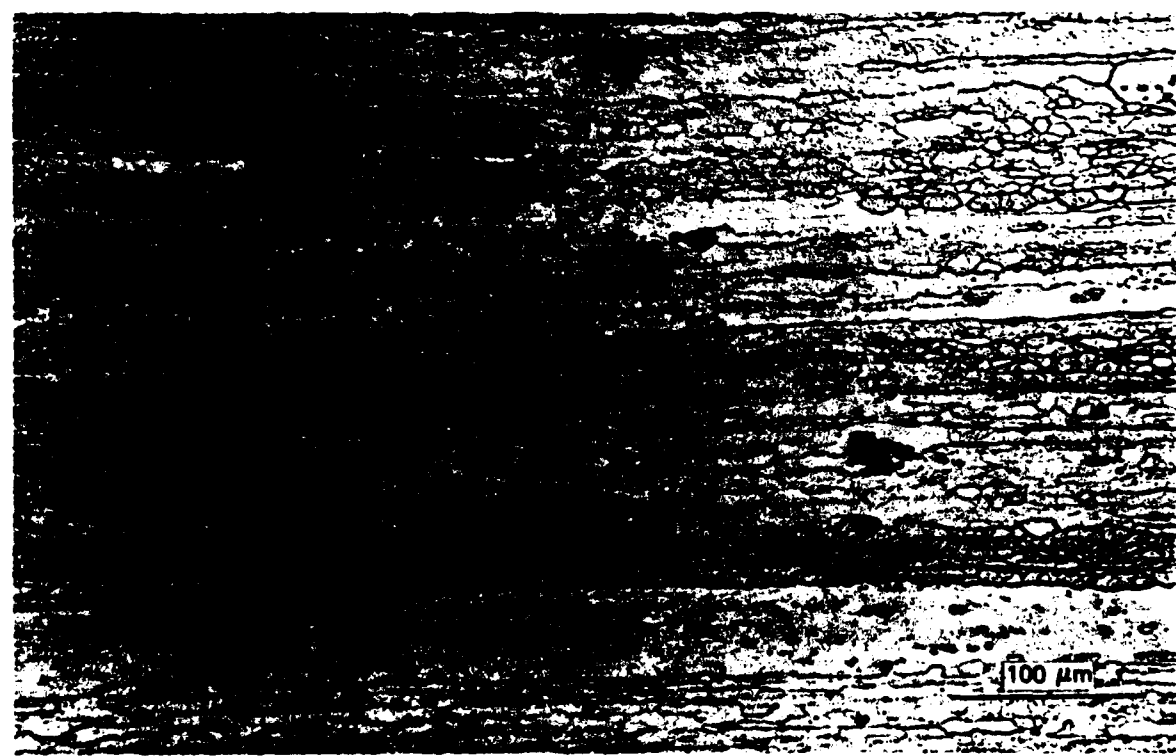
FIGURE 2. OPTICAL MICROGRAPHS OF ALLOY 2124-T351,  
LONGITUDINAL PLANE



a. AS POLISHED

500x

85-02219-1



b. KELLER'S ETCH

250x

85-02219-2

FIGURE 3. OPTICAL MICROGRAPHS OF ALLOY 7150-T6E189,  
LONGITUDINAL PLANE

structure is maintained by  $\text{Al}_3\text{Zr}$  dispersoids, which are finely distributed throughout the microstructure and are too small to be seen optically.

The fine microstructural features (optically unresolvable) of 2124-T351 and 7150-T6E189 are analogous, respectively, to those of 2124-T351 and 7050-T7451; these were discussed in the previous reports.<sup>(27, 28)</sup>

### 3.3 TENSILE AND FRACTURE TOUGHNESS RESULTS

The tensile and fracture toughness results for 2124-T351 and 7150-T6E189 are given in Tables 2 and 3. Alloy 7150-T6E189 is the strongest alloy evaluated in the program with both the highest ultimate and yield strengths. The 12 alloys are compared in Figure 4. Note that the toughness value for 2124-T351 is not valid per ASTM E399 nor meaningful per ASTM B646.

### 3.4 FATIGUE CRACK GROWTH RESULTS UNDER CONSTANT-AMPLITUDE LOADING

Fatigue crack growth data were generated for all alloys from near-threshold ( $\Delta K_{th}$ ) through intermediate  $\Delta K$  values, with measured near-threshold FCG rates approaching  $10^{-10}$  m/cycle ( $4 \times 10^{-9}$  in./cycle). The FCGR data for the two alloys evaluated in this phase are presented in Figures A-1 and A-2 in Appendix A. In Figure 5, the  $da/dN$  versus  $\Delta K$  curves for all 12 alloys are shown. In addition, the FCGR data are shown in Figure 6 and Table 4 as the stress intensity required to drive a fatigue crack at a specified rate. In Figure 6 the results are grouped into 2000 and 7000 series and, within the groups, are in descending order of their spectrum fatigue lives (Subsection 3.5).

### 3.5 SPECTRUM TEST RESULTS

The spectrum life results for each test are presented in Table 5. Overall, the results were reproducible, with the maximum difference between the lives of duplicate tests being 22 percent. Crack length versus simulated flight hour data ( $a$  versus  $H$ ) are shown graphically in Appendix B, while results for spectrum crack growth rate versus maximum peak stress intensity ( $da/dH$  versus  $K_{hmax}$ ) are shown in Appendix C. For comparison, spectrum crack growth rate curves ( $da/dH$  versus  $K_{hmax}$ ) for all 12 materials are

TABLE 2. TENSILE RESULTS – LONGITUDINAL

MATERIAL PLATE THICKNESS mm (in.)	SPECIMEN LOCATION <sup>ab</sup>	ULTIMATE STRENGTH MPa (ksi)	YIELD STRENGTH MPa (ksi)	ELONGATION IN 4D % <sup>b</sup>	REDUCTION OF AREA % <sup>b</sup>
2124-T351 25.4(1.0)	T/4	471(68)	370(54)	23	26
	T/2	462(67)	359(52)	22	26
	T/2	462(67)	358(52)	23	30
	3T/4	469(68)	369(54)	23	25
	AVERAGE	466(68)	364(53)	22	27
	AVG T/4, 3T/4	470(68)	369(54)	23	26
7150-T6E189 25.4 (1.0)	T/4	631(91)	585(85)	12	22
	T/2	628(91)	581(84)	11	18
	T/2	628(91)	581(84)	11	18
	3T/4	635(92)	585(85)	12	18
	AVERAGE	631(91)	584(85)	12	20
	AVG T/4, 3T/4	633(92)	585(85)	12	20

a SPECIMENS TAKEN FROM THE T/2 LOCATION ARE FROM THE CENTER OF THE PLATE THICKNESS AND THOSE FROM THE T/4 AND 3T/4 ARE FROM MIDWAY BETWEEN THE CENTER AND THE TOP SURFACE OR BOTTOM SURFACE, RESPECTIVELY

b THE NOMINAL DIAMETER OF THE REDUCED-SECTION OF T/2 SPECIMENS WAS 12.7MM AND T/4 AND 3T/4 SPECIMENS WAS 6.4MM

TABLE 3. FRACTURE TOUGHNESS RESULTS, L-T ORIENTATION

ALLOY AND TEMPER	PLATE THICKNESS mm (in.)	SPECIMEN THICKNESS mm	K <sub>Q</sub> MPa $\sqrt{m}$ (ksi $\sqrt{in.}$ )	VALID K <sub>IC</sub> PER ASTM E399	AVERAGE VALID K <sub>IC</sub> OR MEANINGFUL K <sub>Q</sub> MPa $\sqrt{m}$ (ksi $\sqrt{in.}$ )
2124-T351	25.4(1.0)	25.4	50(46) 45(41)	NO <sup>a</sup> NO <sup>a</sup>	— —
7150-T6E189	25.4(1.0)	25.4	30(27) 32(29)	YES YES	31(28)

a TEST INVALID PER ASTM E399 DUE TO INSUFFICIENT THICKNESS AND FATIGUE CRACK LENGTH, AND P<sub>MAX</sub>/P<sub>Q</sub> > 1.10

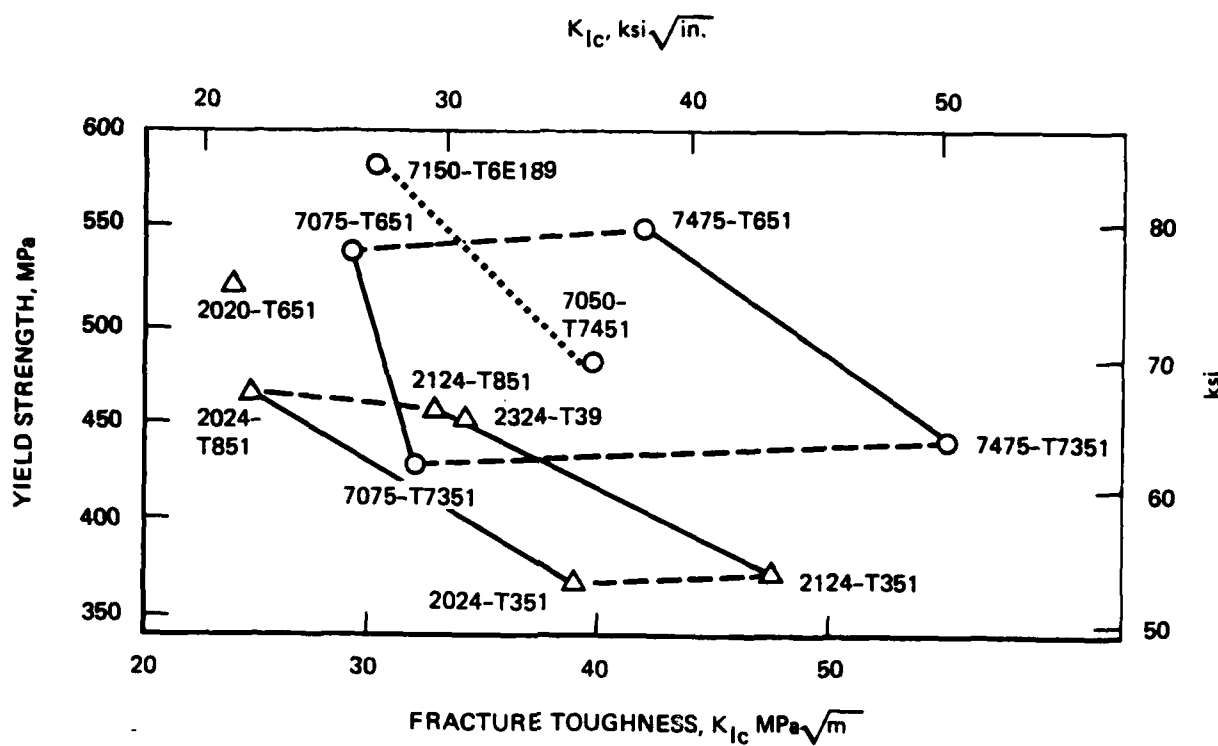


FIGURE 4. RELATIONSHIP BETWEEN YIELD STRENGTH AND FRACTURE TOUGHNESS

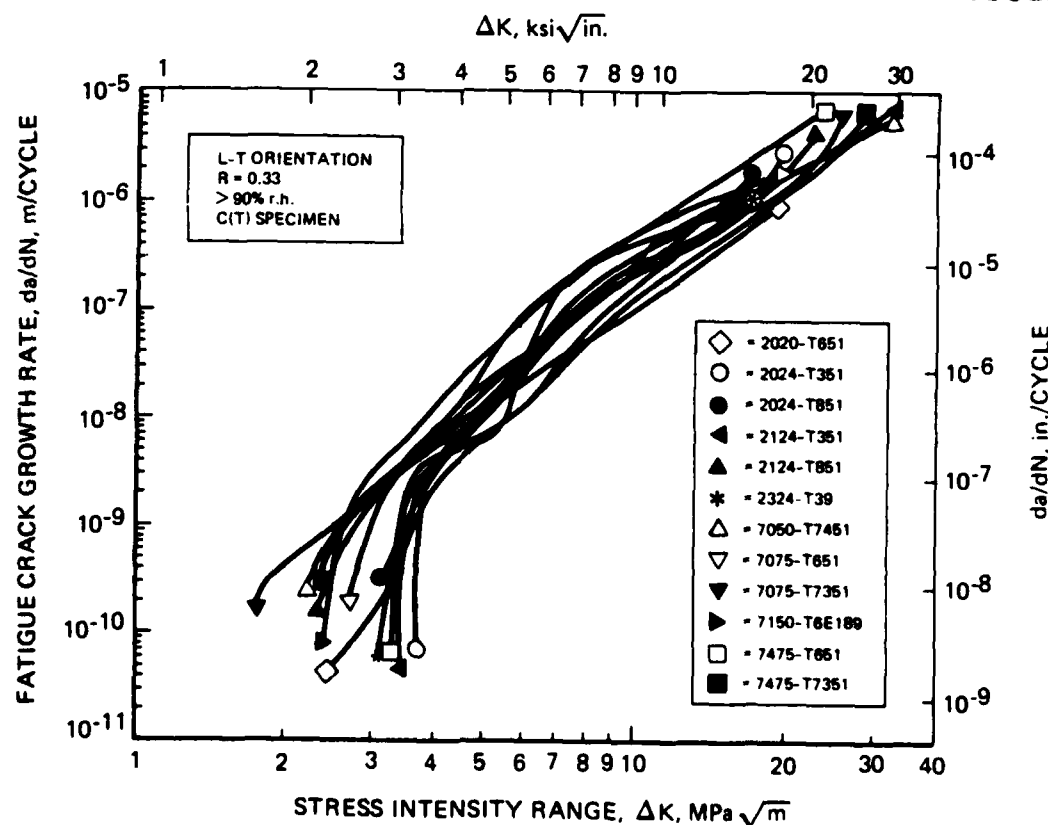
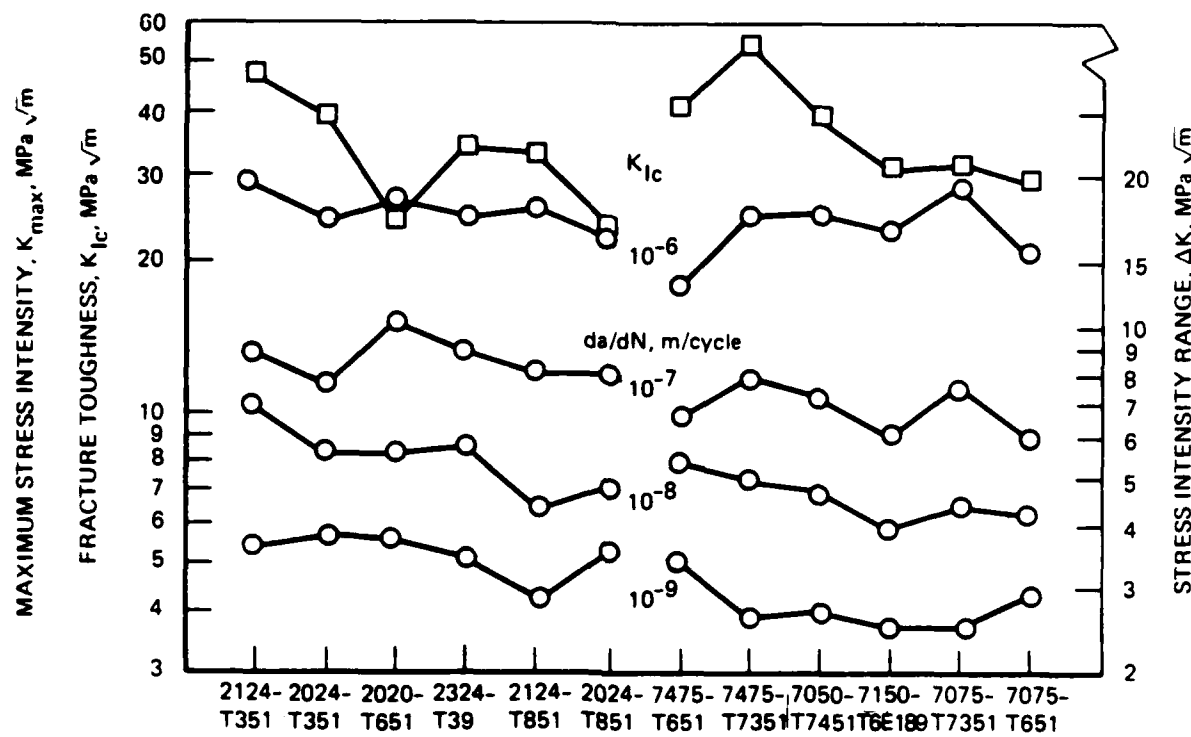


FIGURE 5. CONSTANT AMPLITUDE FCGR CURVES



**FIGURE 6. STRESS INTENSITY NEEDED TO OBTAIN A GIVEN FATIGUE CRACK GROWTH RATE UNDER CONSTANT-AMPLITUDE LOADING. ( $R = 0.33, > 90\% rh$ , L-T ORIENTATION)**

TABLE 4. RANKING OF MATERIALS BY STRESS INTENSITY RANGE TO OBTAIN A GIVEN FATIGUE CRACK GROWTH RATE UNDER CONSTANT-AMPLITUDE LOADING

FCGR	RANK	ΔK, MPa $\sqrt{\text{m}}$ (ksi $\sqrt{\text{in.}}$ ) TO OBTAIN A GIVEN FCGR				RANK	$10^{-7}$ m/CYCLE ( $4 \times 10^{-6}$ in/CYCLE)	RANK	$10^{-6}$ m/CYCLE ( $4 \times 10^{-5}$ in/CYCLE)	
		$10^{-10}$ m/CYCLE ( $4 \times 10^{-9}$ in/CYCLE)	RANK	$10^{-9}$ m/CYCLE ( $4 \times 10^{-8}$ in/CYCLE)	RANK					
MATERIAL 2020-T651	5	2.9 (2.7)	2	3.7 (3.4)	3	5.5 (5.0)	1	10.2 (9.3)	3	18.0 (16.4)
2024-T351	1	3.7 (3.4)	1	3.8 (3.5)	3	5.5 (5.0)	7	7.6 (6.9)	8	16.2 (14.7)
2024-T851	6	2.7 (2.5) <sup>a</sup>	4	3.5 (3.2)	7	4.8 (4.4)	4	8.0 (7.3)	10	15.0 (13.7)
2124-T351	2	3.5 (3.2)	3	3.6 (3.3)	1	6.8 (6.2)	3	8.8 (8.0)	1	19.1 (17.4)
2124-T851	9	2.2 (2.0) <sup>a</sup>	8	2.8 (2.5)	10	4.3 (3.9)	4	8.0 (7.3)	4	17.2 (15.7)
2324-T39	4	3.2 (2.9)	6	3.4 (3.1)	2	5.7 (5.2)	2	8.9 (8.1)	7	16.4 (14.9)
7050-T73651	10	2.1 (1.9) <sup>a</sup>	9	2.7 (2.5)	8	4.7 (4.3)	8	7.2 (6.6)	5	16.9 (15.4)
7075-T651	7	2.6 (2.3) <sup>a</sup>	7	2.9 (2.7)	11	4.2 (3.9)	11	6.0 (5.5)	11	14.0 (12.7)
7075-T7351	12	1.7 (1.6) <sup>a</sup>	11	2.5 (2.3)	9	4.4 (4.0)	7	7.6 (6.9)	2	19.0 (17.3)
7150-T6E189	8	2.4 (2.2)	11	2.5 (2.3)	12	3.9 (3.5)	11	6.0 (5.5)	9	15.5 (14.1)
7475-T651	3	3.3 (3.0)	5	3.4 (3.1)	5	5.4 (4.9)	10	6.6 (6.0)	12	12.1 (11.0)
7475-T7351	11	2.0 (1.8) <sup>a</sup>	10	2.6 (2.4)	6	4.9 (4.5)	4	8.0 (7.3)	6	16.6 (15.1)

<sup>a</sup> EXTRAPOLATED

TABLE 5. SPECTRUM FATIGUE RESULTS - BASELINE SPECTRUMS

MAXIMUM PEAK STRESS $\sigma_{hmax}$	SPECTRUM	SIMULATED FLIGHT HOURS, H					
		103 MPa (15 ksi)		145 MPa (21 ksi)		169 MPa (24.5 ksi)	
CRACK-GROWTH REGIME, $a_i$ to $a_f$	TD	TC	TD	TC	TD	TC	
MATERIAL <sup>b</sup>			6 mm-F 0.24 in.-F	6 mm-F 0.24 in.-F	6 mm-F 0.24 in.-F	18 mm-F 0.71 in.-F	18 mm-F 0.71 in.-F
2020-T651	78,416	54,895	17,188	14,575	0 <sup>c</sup>	0 <sup>c</sup>	0 <sup>c</sup>
2024-T351	—	—	20,020	11,717	—	—	—
2024-T851	26,412	24,633	21,719	15,375	2,451	1,092	1,192
2124-T351	28,027	24,035	22,565	15,389	2,363	—	—
2124-T851	18,297	18,299	8,505	7,031	196	0 <sup>c</sup>	0 <sup>c</sup>
2324-T39	19,258	17,824	8,557	7,132	184	184	184
7050-T7451	33,132	25,536	25,642	18,800	4,329	2,165	2,165
7075-T7351	—	—	25,459	19,664	—	—	—
7150-T6E189	17,274	15,787	11,244	8,853	851	1,085	1,085
7475-T651	16,769	15,563	11,096	9,314	828	1,245	1,245
7475-T7351	29,057	24,616	18,148	15,338	2,443	1,159	1,159
7050-T7451	—	—	17,547	13,529	—	—	—
7075-T7351	18,741	19,467	14,496	13,340	2,260	1,638	1,638
7075-T651	18,930	16,217	15,223	12,962	2,455	1,837	1,837
7075-T7351	14,775	13,886	9,820	8,617	651	380	380
7075-T7351	—	—	11,945	9,181	—	—	—
7150-T6E189	17,642	16,666	13,517	10,392	1,300	740	740
7475-T651	16,910	16,529	12,314	10,934	1,601	781	781
7475-T7351	13,299	13,329	12,857	11,179	1,079	585	585
7475-T7351	—	—	13,234	11,574	—	—	—
7475-T651	15,387	15,522	18,303	14,744	3,777	2,661	2,661
7475-T7351	15,384	16,624	19,792	15,141	3,197	2,608	2,608
7475-T7351	18,241	16,578	15,417	13,410	2,714	2,152	2,152
7475-T7351	18,873	17,332	14,661	13,345	2,852	2,256	2,256

<sup>a</sup> F = FAILURE<sup>b</sup> RESULTS FOR 2124-T351 AND 7150-T6E189 ARE FOR PRESENT EFFORT, OTHER RESULTS FROM PHASES I AND II<sup>c</sup> SPECIMEN FRACTURED BEFORE REACHING INITIAL CRACK LENGTH,  $a_i$ , OF 18mm, FOR THESE 169 MPa (24.5 ksi) TESTS, IN FATIGUE

shown in Figure 7. For easier comparison of resistance to spectrum crack growth among all 12 materials for both spectrums, the maximum peak stress intensities to obtain a given crack-growth rate are shown in Figure 8 and Table 6 in presentations similar to those for the constant-amplitude data in Figure 6 and Table 4.

The alloys are ranked by their spectrum fatigue lives for each spectrum (average of the two duplicate tests) in Table 7 and in Figure 9.

The relationship between spectrum fatigue lives and yield strength and fracture toughness is shown in Figures 10 and 11, respectively.

All alloys were evaluated at two other maximum peak stresses, 103 MPa (15 ksi) and 169 MPa (24.5 ksi). As described in the Phase II report,<sup>(28)</sup> two test procedures were used. Results are presented in Table 8 and Figure 12 for the five alloys evaluated in Phases II and III from a crack length of 6 mm to failure.

The spectrum fatigue results for 7475-T651 were unusual in comparison to the other alloys. The notable differences were that (1) the life for the 7475-T651 with lower toughness was longer than for 7475-T351, and (2) that the spectrum FCG rates were faster than all other alloys at the lowest maximum peak stress intensities (Figure 7) and were slower at the higher maximum peak stress intensities. To evaluate a second lot of material was beyond the scope of the program. Therefore, at their own expense, Northrop and Alcoa evaluated a second lot of 7475-T651 to determine whether this behavior was repeatable. The results and discussion of this evaluation are presented in Appendix E. The behavior of the second lot confirmed the results for the first lot evaluated in Phase I.

### 3.6 FRACTOGRAPHIC EXAMINATION OF SPECTRUM FATIGUE SPECIMENS

As noted in Subsection 3.2, the microstructures of 2124-T351 and 7150-T6E189 are similar to those of 2024-T351 and 7050-T7451, respectively. The spectrum fatigue data also show a great deal of similarity between 2024 and 2124, and between 7050 and 7150. It would be expected, therefore, that the fatigue fracture surfaces for these pairs of alloys should be similar as well; this is, in fact, what is observed. As has been done in Phases I and II, the specimens were examined primarily at crack lengths of 6 and 19 mm (0.25 and

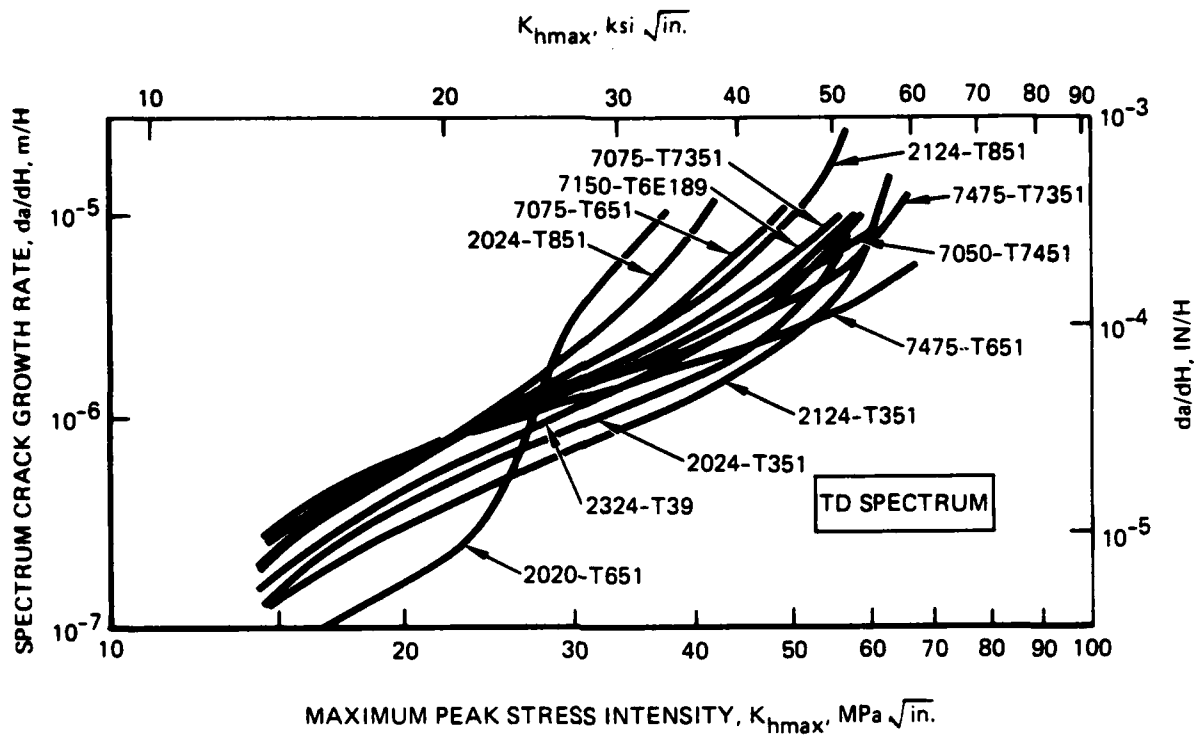


FIGURE 7. SPECTRUM FCGR CURVES FOR TD SPECTRUM

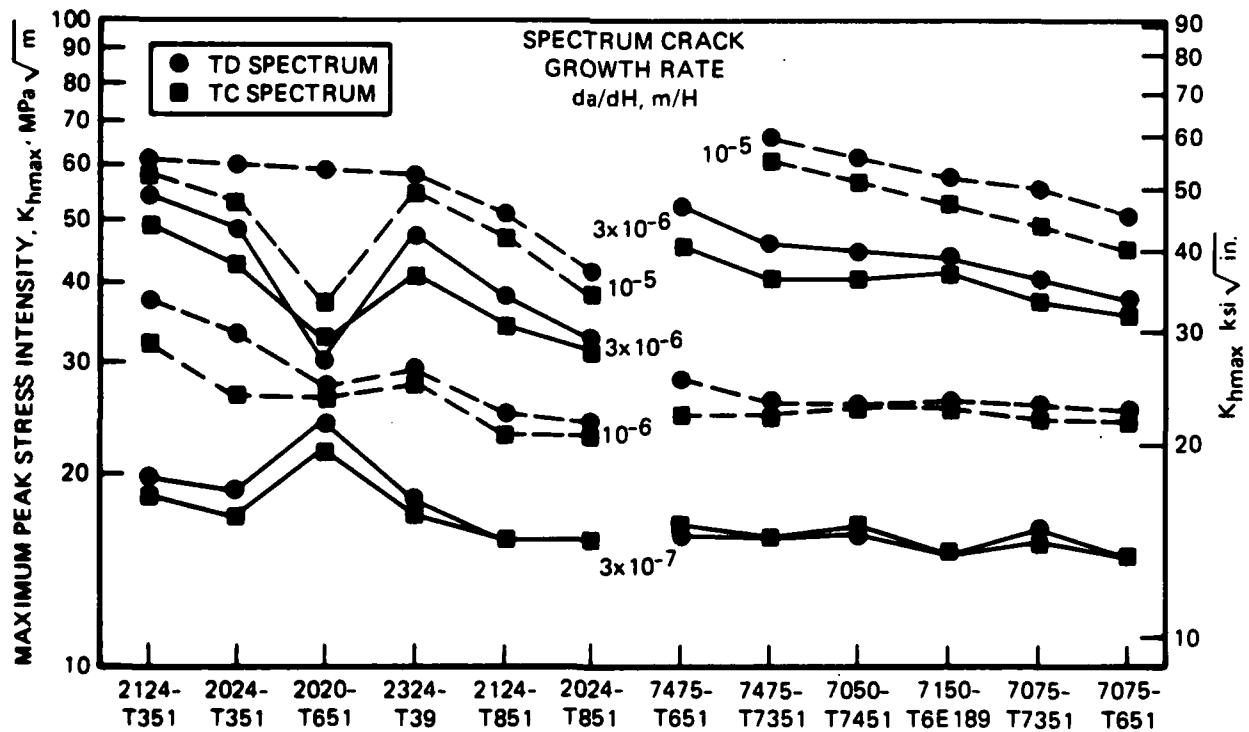


FIGURE 8. MAXIMUM PEAK STRESS INTENSITY NEEDED TO OBTAIN A GIVEN SPECTRUM FCGR FOR TD AND TC SPECTRUMS

TABLE 6. RANKING OF MATERIALS IN SPECTRUM FATIGUE BY MAXIMUM PEAK STRESS INTENSITY TO OBTAIN A GIVEN FATIGUE CRACK GROWTH RATE

SPECTRUM	FCGR	K <sub>hmax</sub> , MPa $\sqrt{m}$ (ksi $\sqrt{in.}$ ) TO OBTAIN A GIVEN SPECTRUM FCGR							
		3X10 <sup>-7</sup> m/H <sup>a</sup> (1.2X10 <sup>-5</sup> in./H)	10 <sup>-6</sup> m/H (4X10 <sup>-5</sup> in./H) <sup>b</sup>	3X10 <sup>-6</sup> m/H (1.2X10 <sup>-4</sup> in./H) <sup>c</sup>	TD	TC	TD	TC	TD
MATERIAL	TD	RANK <sup>e</sup>	TC	TD	RANK <sup>e</sup>	TC	TD	RANK <sup>e</sup>	TC
2020-T651	24.1 (21.9)	1 (19.9)	21.9 (24.9)	27.1 (23.9)	4 (28)	26.3 (28)	30 (29)	11 (29)	32 (34)
2024-T351	18.8 (17.1)	3 (15.5)	17.0 (30.0)	33.0 (24.1)	2 (44)	26.5 (44)	48 (38)	3 (38)	42 (34)
2024-T851	16.0 (14.6)	9 (14.5)	15.9 (21.8)	24.0 (20.9)	12 (29)	23.0 (28)	32 (28)	11 (28)	31 (37)
2124-T351	19.8 (18.0)	2 (16.7)	18.4 (33.7)	37.0 (29.1)	1 (49)	32.0 (49)	54 (45)	1 (45)	49 (56)
2124-T851	15.8 (14.4)	10 (14.3)	15.7 (22.6)	24.8 (20.9)	11 (35)	23.0 (35)	38 (31)	9 (31)	34 (46)
2324-T39	18.1 (16.5)	4 (15.9)	17.5 (26.4)	29.0 (25.6)	3 (43)	28.1 (43)	47 (41)	4 (41)	51 (56)
7050-T7351	16.2 (14.7)	5 (15.0)	16.5 (23.2)	25.5 (23.2)	6 (40)	25.5 (40)	44 (36)	6 (36)	40 (36)
7075-T651	14.8 (13.5)	12 (13.5)	14.8 (22.7)	24.9 (21.7)	10 (34)	23.8 (34)	37 (32)	10 (32)	35 (46)
7075-T7351	16.4 (14.9)	7 (14.5)	15.9 (23.2)	25.5 (22.0)	9 (36)	24.2 (36)	40 (34)	8 (34)	37 (50)
7150-T6E189	14.8 (13.5)	11 (13.7)	15.0 (23.7)	26.0 (23.3)	8 (39)	25.6 (39)	43 (37)	6 (37)	50 (52)
7475-T651	16.2 (14.7)	5 (15.0)	16.5 (25.5)	28.0 (22.5)	5 (47)	24.7 (47)	52 (41)	2 (41)	45 (52)
7475-T7351	16.0 (14.7)	8 (14.5)	15.9 (23.2)	25.5 (22.3)	7 (41)	24.5 (41)	45 (36)	5 (36)	40 (59)

a "hmax = 103 MPa (15 ksi)

b "hmax = 103 MPa (15 ksi) and 145 MPa (21 ksi)

c "hmax = 145 MPa (21 ksi)

d "hmax = 145 MPa (21 ksi) and 169 MPa (24.5 ksi)

e BASED ON AVERAGE TD AND TC SPECTRUM

f BASED ON EXTRAPOLATION

TABLE 7. RANKING OF MATERIALS UNDER SPECTRUM LOADING – BASELINE SPECTRUMS  
AVERAGES OF TWO TESTS ROUNDED TO NEAREST HUNDRED HOURS

a.  $\sigma_{hmax} = 103 \text{ MPa}$  FROM  $a = 6$  TO 13 mm

TD SPECTRUM	
MATERIAL	SIMULATED FLIGHT HOURS
2020-T651	78,400 <sup>a</sup>
2124-T351	33,100 <sup>a</sup>
2324-T39	29,100 <sup>a</sup>
2024-T351	27,200
7050-T7451	18,800
2024-T851	18,800
7475-T7351	18,600
7075-T7351	17,300
2124-T851	17,300
7475-T651	15,400
7075-T651	14,800 <sup>a</sup>
7150-T6E189	13,300 <sup>a</sup>

TC SPECTRUM	
MATERIAL	SIMULATED FLIGHT HOURS
2020-T651	54,900 <sup>a</sup>
2124-T351	25,500 <sup>a</sup>
2324-T39	24,600
2024-T351	24,300 <sup>a</sup>
2024-T851	18,100
7050-T7451	17,800
7475-T7351	17,000
7075-T7351	16,600
7475-T651	16,100
2124-T851	15,700
7075-T651	13,900 <sup>a</sup>
7150-T6E189	13,300 <sup>a</sup>

b.  $\sigma_{hmax} = 145 \text{ MPa}$  FROM  $a = 6$  mm TO FAILURE

TD SPECTRUM	
MATERIAL	SIMULATED FLIGHT HOURS
2124-T351	25,600
2024-T351	22,100
7475-T651	19,000
2020-T651	18,500
2324-T39	17,800
7475-T7351	15,000
7050-T7451	14,900
7150-T6E189	13,000
7075-T7351	12,900
2124-T851	11,200
7075-T651	10,800
2024-T851	8,500

TC SPECTRUM	
MATERIAL	SIMULATED FLIGHT HOURS
2124-T351	19,200
2024-T351	15,400
7475-T651	14,900
2324-T39	14,400
7475-T7351	13,400
7050-T7451	13,200
2020-T651	13,100
7150-T6E189	11,300
7075-T7351	10,700
2124-T851	9,100
7075-T651	8,900
2024-T851	7,100

c.  $\sigma_{hmax} = 169 \text{ MPa}$  FROM  $a = 18$  mm TO FAILURE

TD SPECTRUM	
MATERIAL	SIMULATED FLIGHT HOURS
2124-T351	4,300 <sup>a</sup>
7475-T651	3,400
7475-T7351	2,800
2324-T39	2,400 <sup>a</sup>
2024-T351	2,400
7050-T7451	2,400
7075-T7351	1,400
7150-T6E189	1,100 <sup>a</sup>
2124-T851	800
7075-T651	700 <sup>a</sup>
2024-T851	200
2020-T651	0 <sup>a,b</sup>

TC SPECTRUM	
MATERIAL	SIMULATED FLIGHT HOURS
7475-T651	2,600
7475-T7351	2,200
2124-T351	2,200 <sup>a</sup>
7050-T7451	1,700
2124-T851	1,200
2324-T39	1,200 <sup>a</sup>
2024-T351	1,100
7075-T7351	800
7150-T6E189	600 <sup>a</sup>
7075-T651	400 <sup>a</sup>
2024-T851	0 <sup>b</sup>
2020-T651	0 <sup>a,b</sup>

a ONE TEST RESULT

b SPECIMEN FRACTURED BEFORE REACHING INITIAL CRACK LENGTH

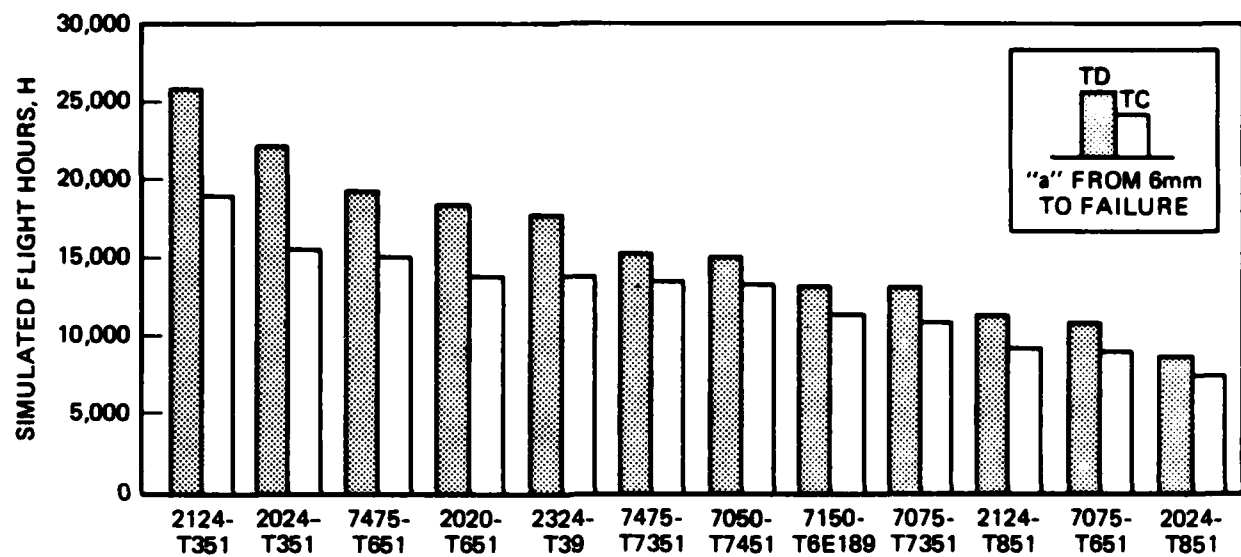


FIGURE 9. SPECTRUM FATIGUE LIVES AT 145 MPa (21 ksi)

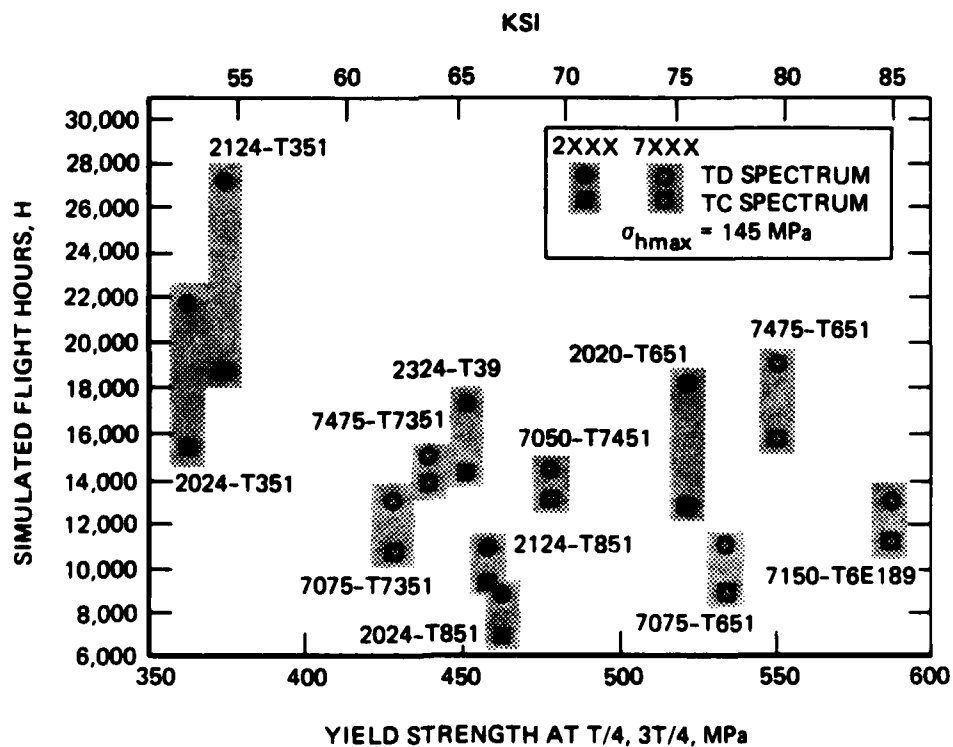


FIGURE 10. SPECTRUM LIFE VERSUS YIELD STRENGTH

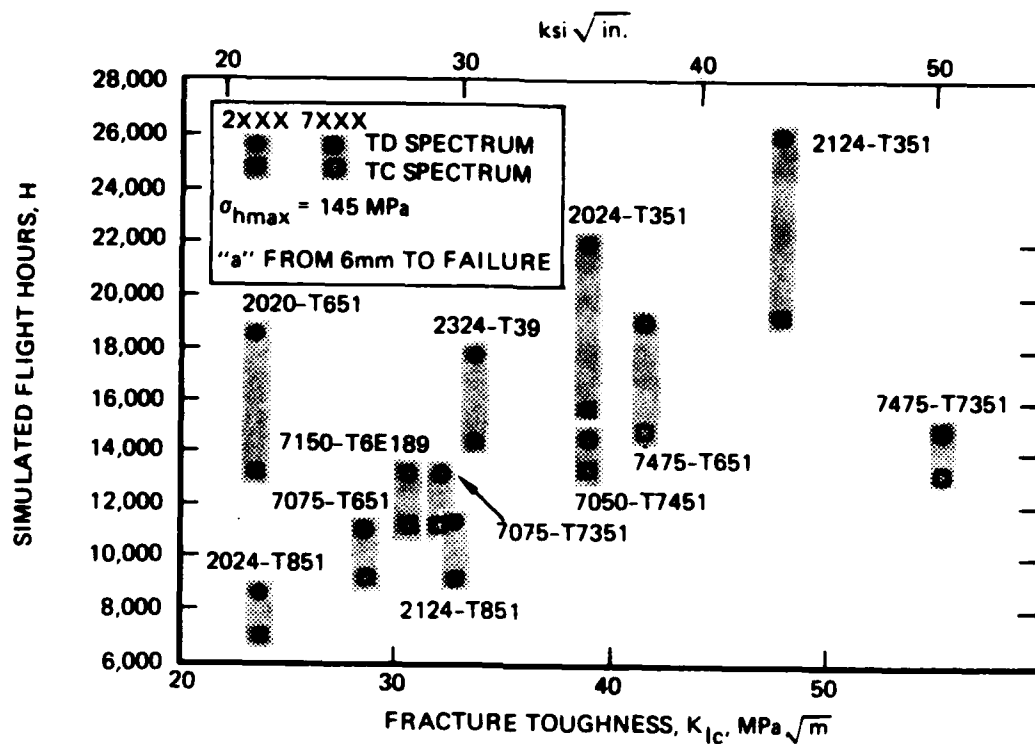
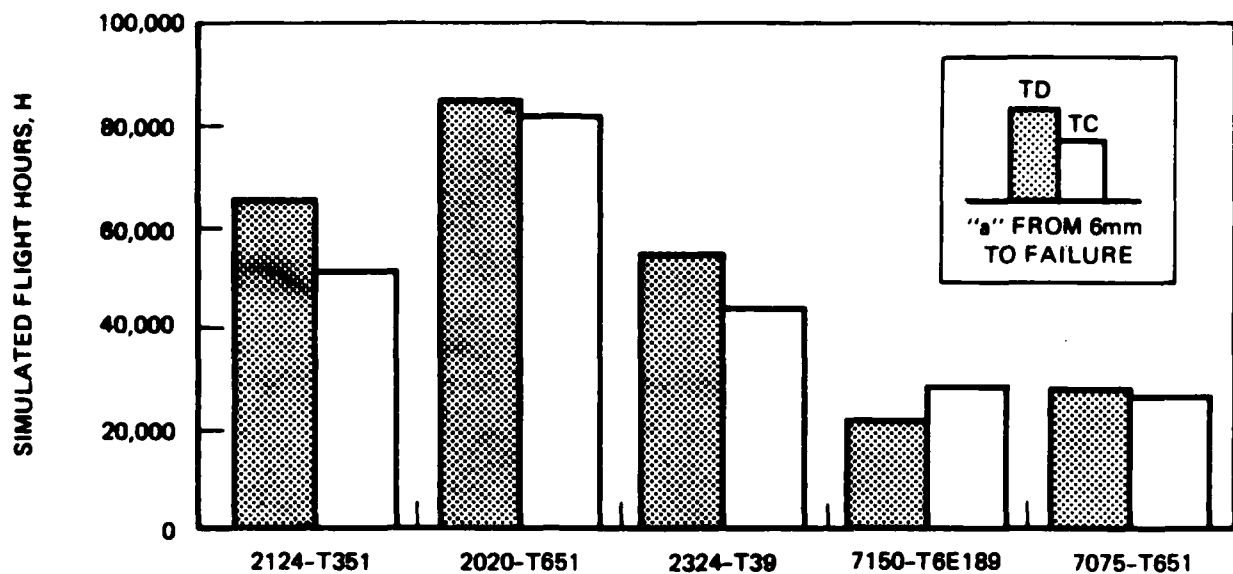


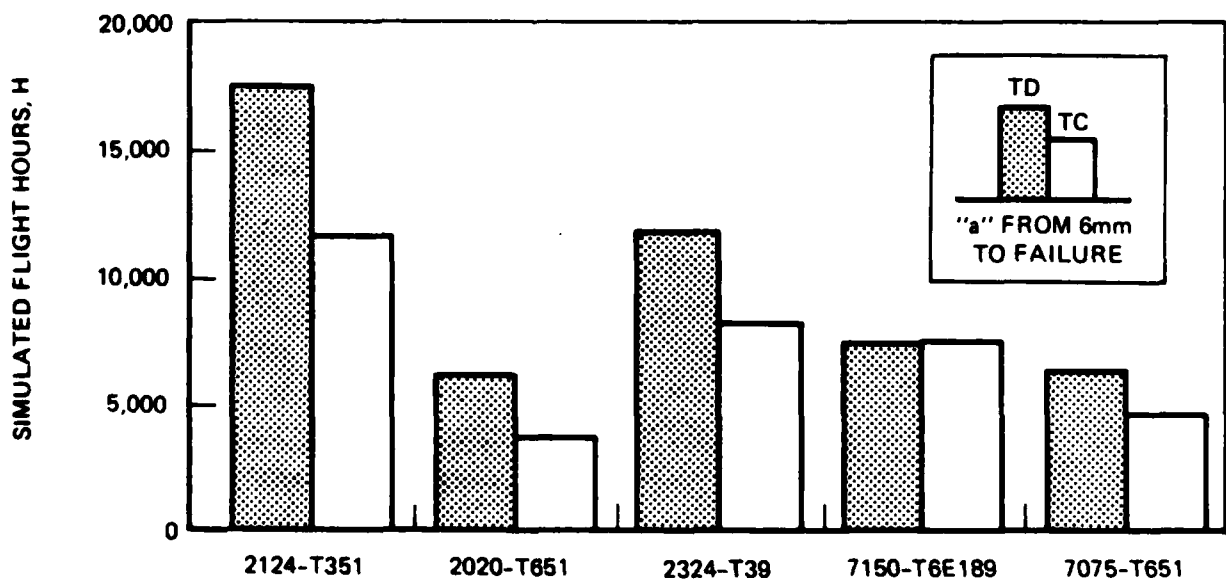
FIGURE 11. SPECTRUM LIFE VERSUS FRACTURE TOUGHNESS

TABLE 8. SPECTRUM FATIGUE LIVES AT 103 MPa AND 169 MPa  
FOR "a" FROM 6MM (0.24 IN.) TO FAILURE

MAXIMUM PEAK STRESS $\sigma_{hmax}$	SIMULATED FLIGHT HOURS, H			
	103 MPa (15 ksi)		169 MPa (24.5 ksi)	
SPECTRUM	TD	TC	TD	TC
<b>MATERIAL</b>				
2020-T651	83,910	80,953	6,217	3,636
2124-T351	64,275	50,607	17,530	11,662
2324-T39	53,738	42,939	11,862	8,261
7075-T651	27,341	25,268	6,333	4,612
7150-T6E189	21,281	27,760	7,349	7,520



a. SPECTRUM LIFE AT 103 MPa. THE MATERIALS ARE LISTED IN DESCENDING ORDER FOR LIFE AT 145 MPa



b. SPECTRUM LIFE AT 169 MPa. THE MATERIALS ARE LISTED IN DESCENDING ORDER FOR LIFE AT 145 MPa

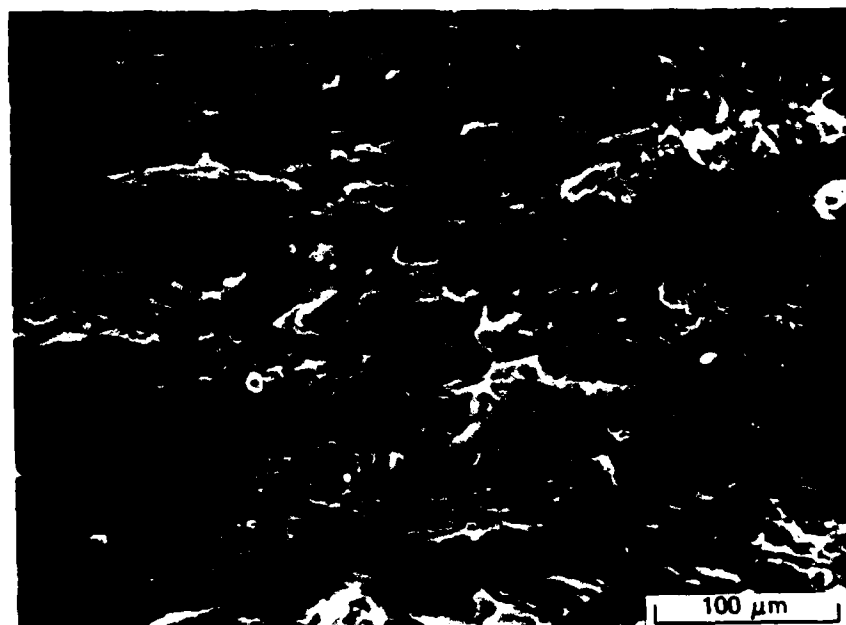
FIGURE 12. SPECTRUM FATIGUE LIVES AT 103 AND 169 MPa

0.75 in.). The shorter position represents the very lowest  $K_{hmax}$  value in the spectrum test, while the other position is the longest crack length (highest  $K_{hmax}$ ) consistently attained for all alloys, regardless of toughness.

For 2124-T351, the fatigue fracture mechanism for both the TD and TC spectrums at all crack lengths consists predominantly of ductile "striation" formation, though it is not clear that these striations correspond to individual load excursions in the spectrums (Figures 13 through 16). Very little evidence of void coalescence at constituent particles is seen for the TD spectrum, even at 19 mm, as shown in Figures 13 and 14. Limited void growth is evident for the TC spectrum at the longer crack length, Figure 16, but the fracture mechanism remains predominantly ductile striation formation. There is some evidence of abrasion on the TC fractures (Figure 15 especially), as suggested by the smooth areas where the striations have been rubbed away. Such abrasion was observed in Phase I on TC fractures, and is consistent with the extensive compressive loading in this spectrum.

Striation formation is not as evident for 7150 (Figures 17 through 20). In this high strength, lower ductility alloy it is more difficult to achieve the high degree of crack tip plasticity and blunting which is necessary to form well-defined striations. Rather, the general fracture topography is banded in the direction of crack growth, reflecting the "pancaked" grain structure of this alloy (Figures 17 and 19, especially). Fracture of constituent particles occurs at higher  $K_{hmax}$  levels (Figure 18), along with some striated growth which is better seen in the TC spectrum, Figure 20. The presence of striations at high  $K_{hmax}$  levels shows that extensive crack-tip plasticity can be developed, but only at the higher strains which occur at these stress intensity levels. As was the case with 2124, some fracture surface abrasion is evident on the TC specimen of 7150, Figure 19, along with some debris believed to be the result of fretting between the mating fracture surfaces.

Figure 18 shows an abrupt transition from stable fatigue crack growth (characterized by indistinct striation formation) to unstable tearing (denoted by void coalescence); this does not correspond, however, to the onset of rapid fracture at the end of the fatigue test. Rather, this tear is one of a series of "pop-in" fractures which occur as the crack approaches a critical flaw size. Figure 21 shows a series of bands for both 2124 and 7150 at crack lengths approaching final fracture; the darker bands are stable growth,



a.

250x

85-02224-1

—→  
CRACK GROWTH DIRECTION



b.

1500x

85-02224-2

**FIGURE 13. FRACTURE SURFACE OF 2124-T351 TESTED USING TD SPECTRUM AT  $a = 6.4$  mm (0.25 IN.)**

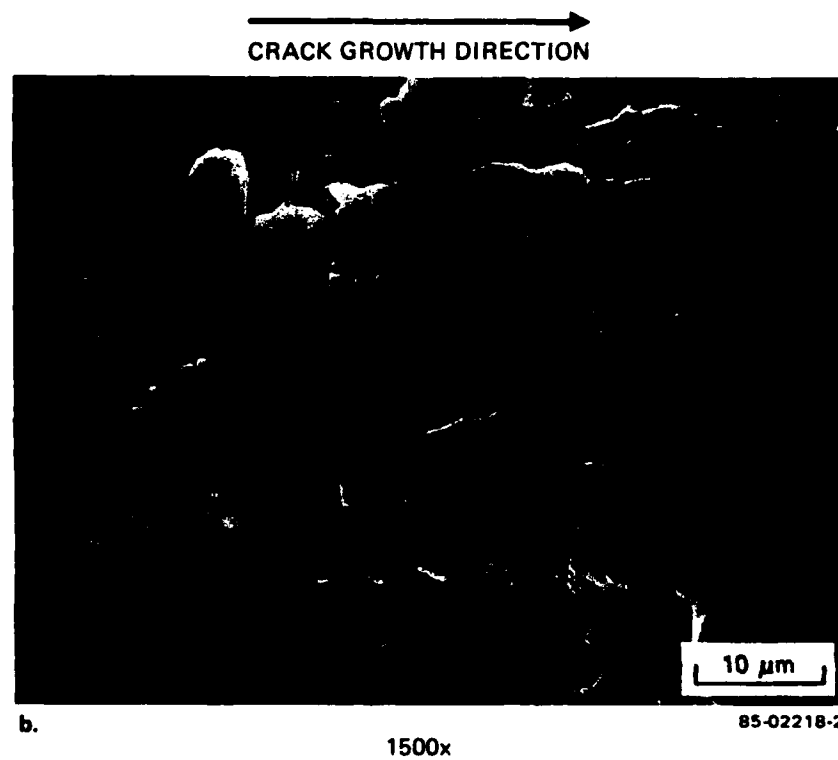
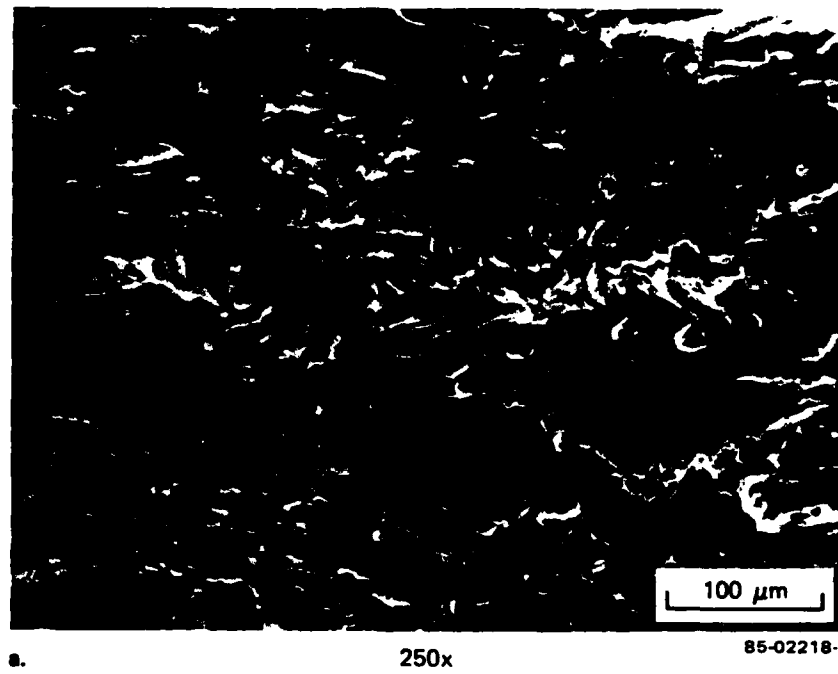
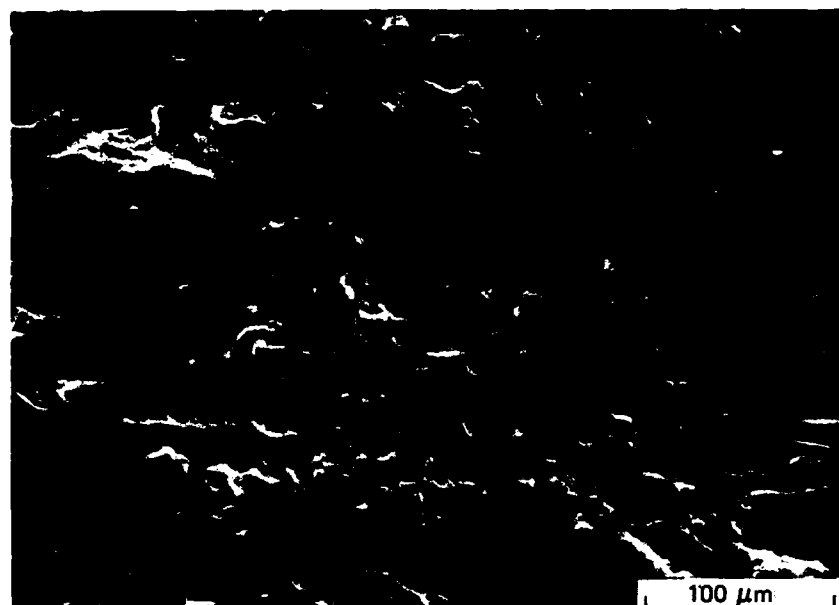


**FIGURE 14. FRACTURE SURFACE OF 2124-T351 TESTED USING TD SPECTRUM AT  $a = 19.1$  mm (0.75 IN.)**

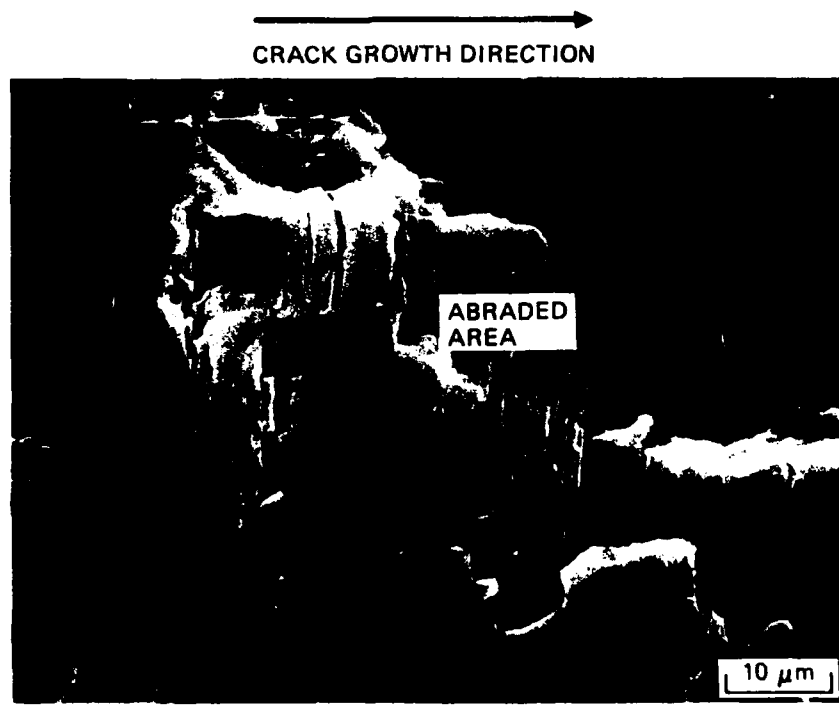


a.

250x

100  $\mu$ m

85-02220-1



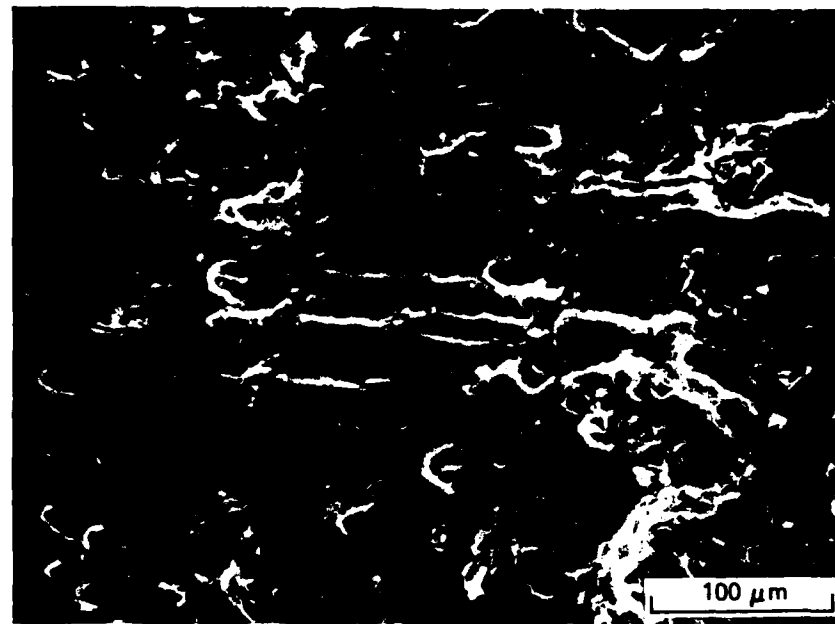
b.

1500x

10  $\mu$ m

85-02220-2

**FIGURE 15. FRACTURE SURFACE OF 2124-T351 TESTED USING TC SPECTRUM AT  $a = 6.4$  mm (0.25 IN.)**



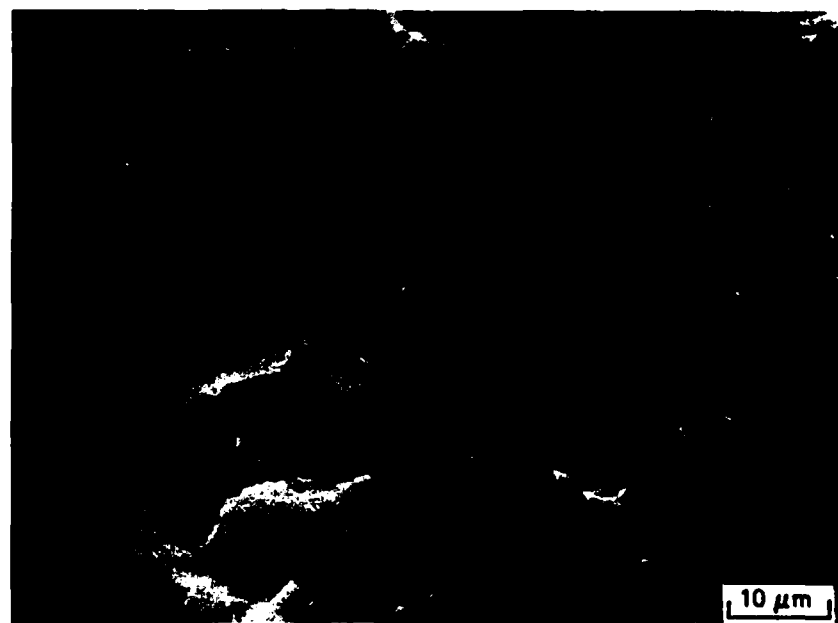
a.

250x

100  $\mu\text{m}$

85-02217-1

CRACK GROWTH DIRECTION 



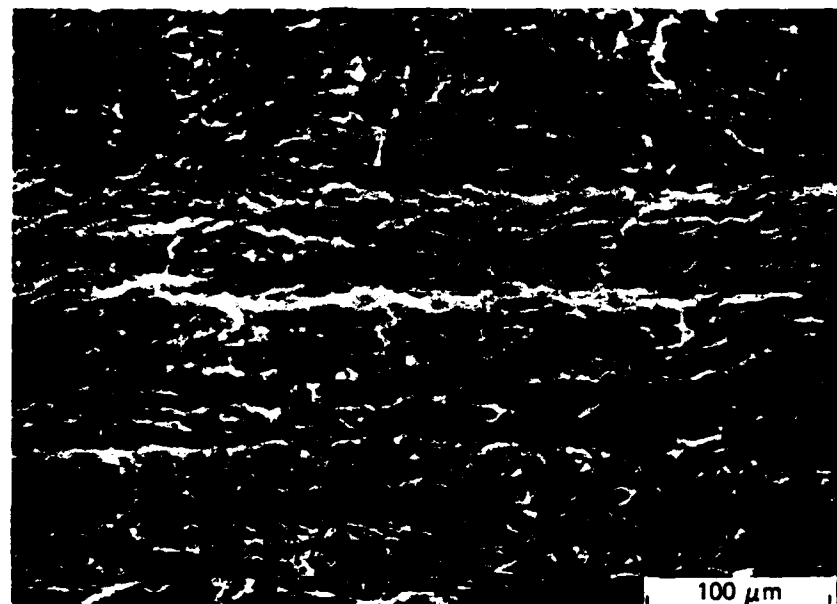
b.

1500x

10  $\mu\text{m}$

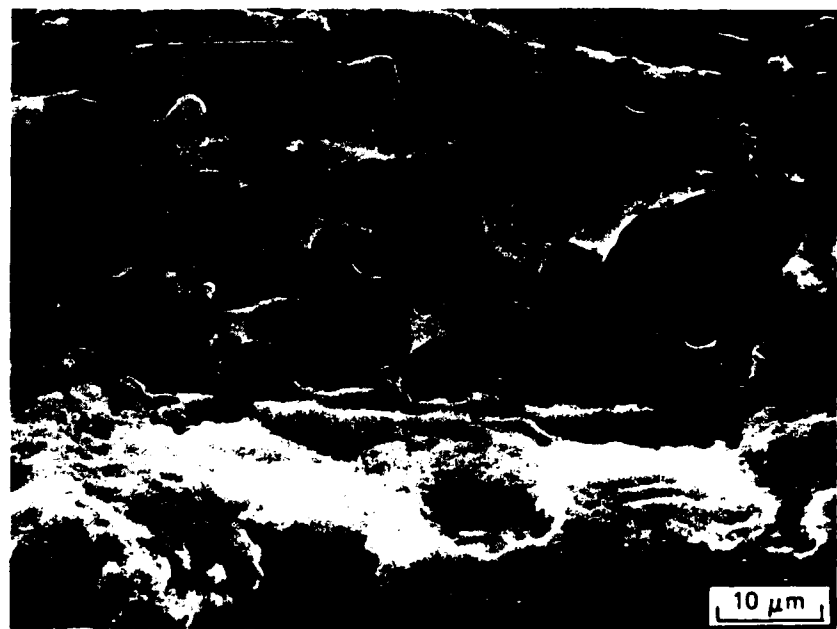
85-02217-2

**FIGURE 16. FRACTURE SURFACE OF 2124-T351 TESTED USING TC SPECTRUM AT  $a = 19.1 \text{ mm (0.75 in.)}$**



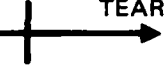
a. 250x 86-02222-1

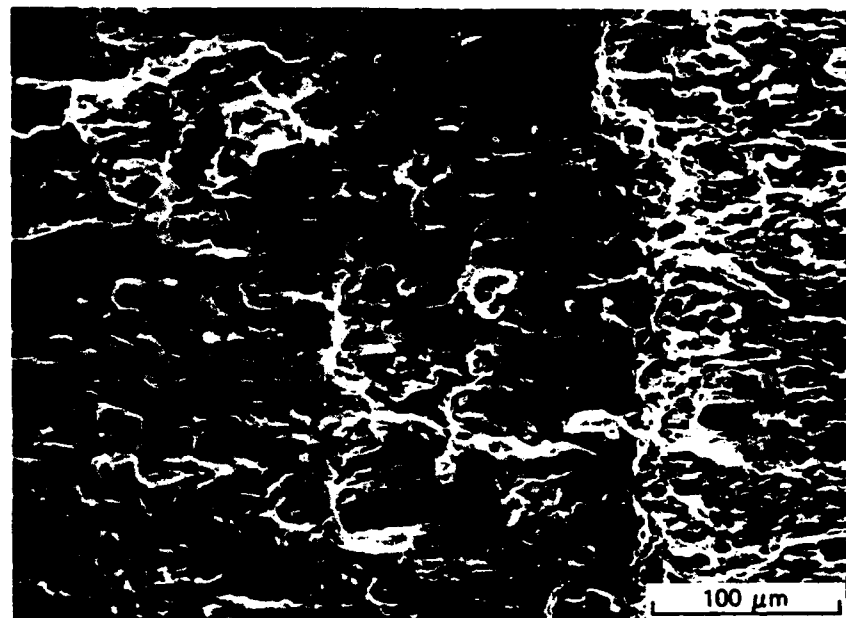
CRACK GROWTH DIRECTION 



b. 1500x 86-02222-2

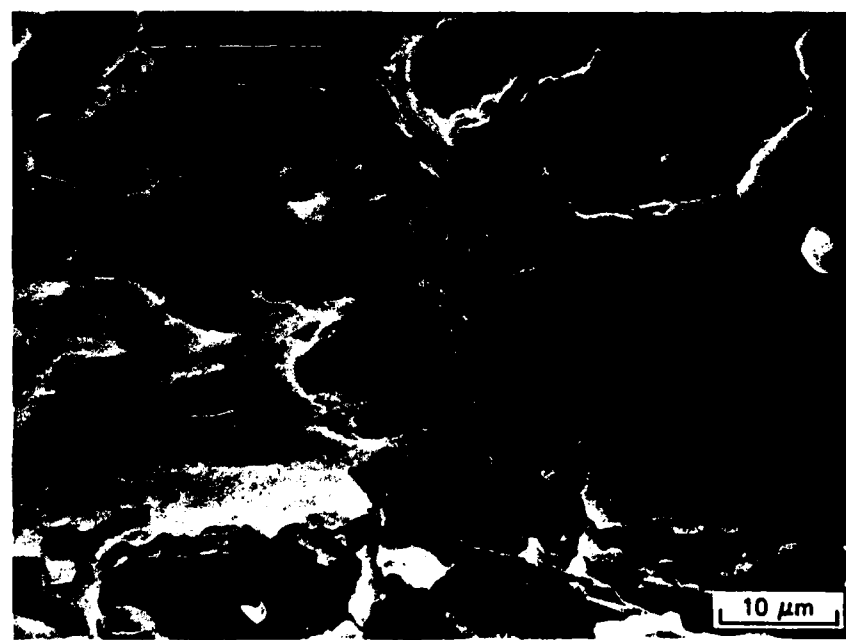
**FIGURE 17. FRACTURE SURFACE OF 7150-T6E189 TESTED USING TD SPECTRUM AT  $a = 6.4$  mm (0.25 IN.)**

FATIGUE  TEARING



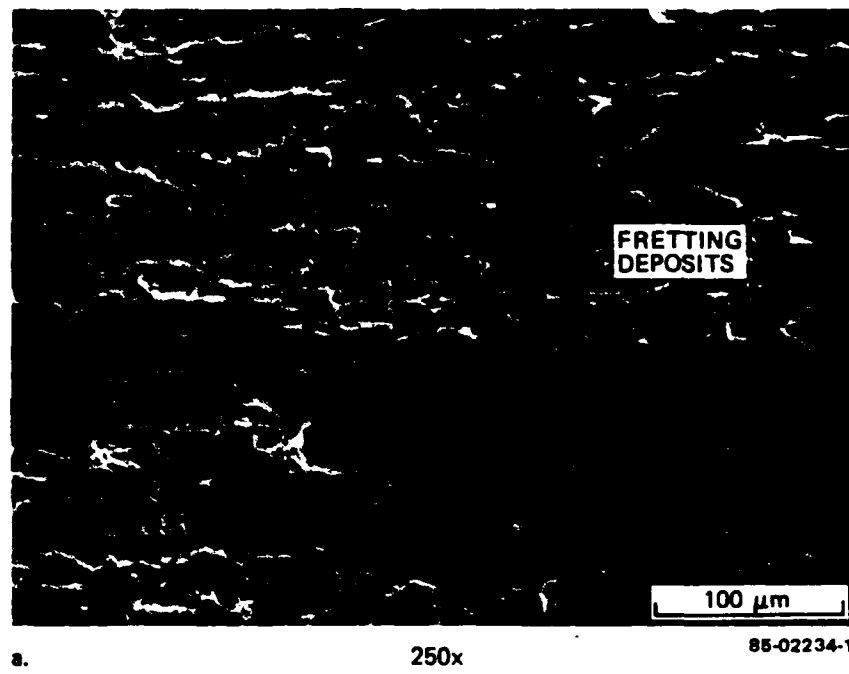
a. 250x 85-02225-1

 CRACK GROWTH DIRECTION

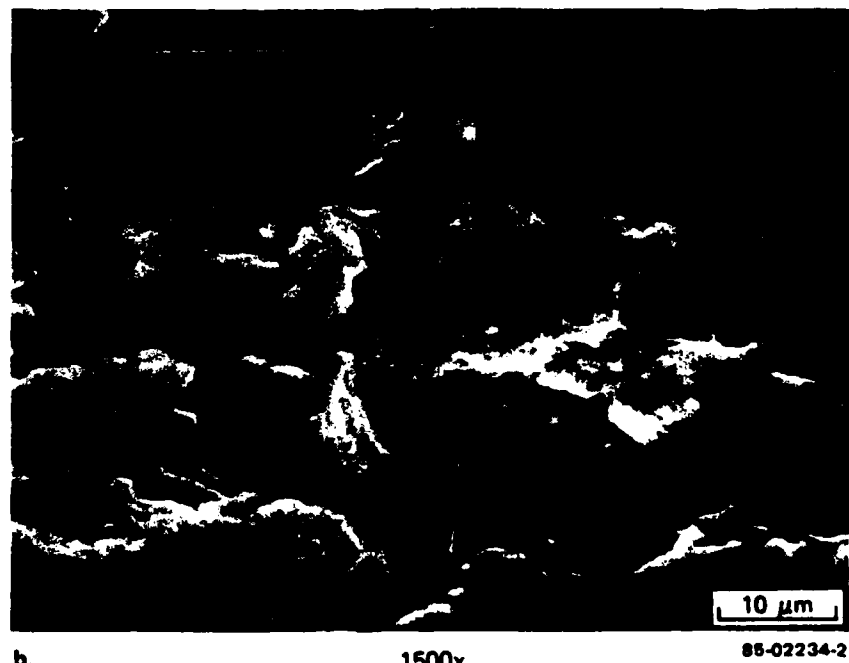


b. 1500x 85-02225-2

**FIGURE 18. FRACTURE SURFACE OF 7150-T6E189 TESTED USING TD SPECTRUM AT  $a = 19.1 \text{ mm (0.75 in.)}$  AREA IN b FROM STABLE FATIGUE REGION IN a**

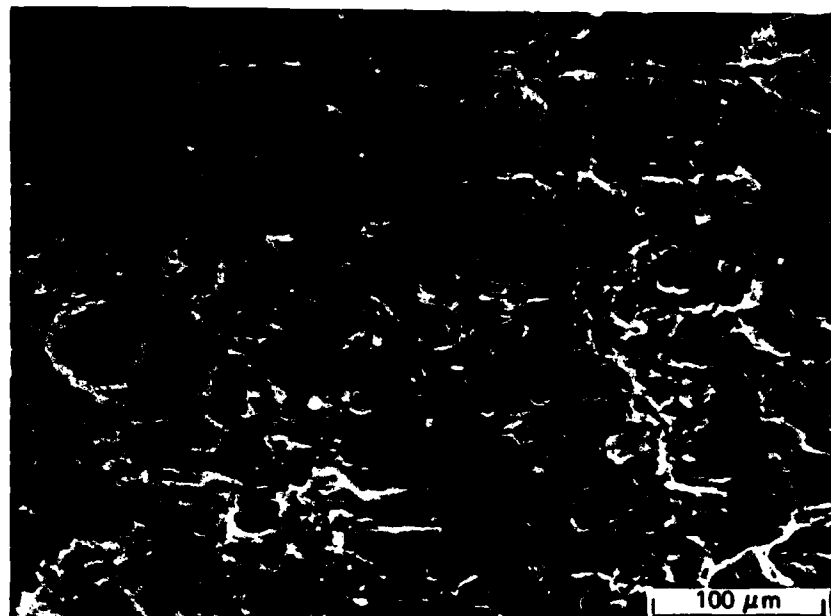


a. 250x



b. 1500x

**FIGURE 19. FRACTURE SURFACE OF 7150-T6E189 TESTED USING TC SPECTRUM AT  $a = 6.4 \text{ mm (0.25 in.)}$**



a.

250x

85-02221-1

—→  
CRACK GROWTH DIRECTION



b.

1500x

85-02221-2

**FIGURE 20. FRACTURE SURFACE OF 7150-T6E189 TESTED USING TC SPECTRUM AT  $a = 19.1$  mm (0.75 IN.)**

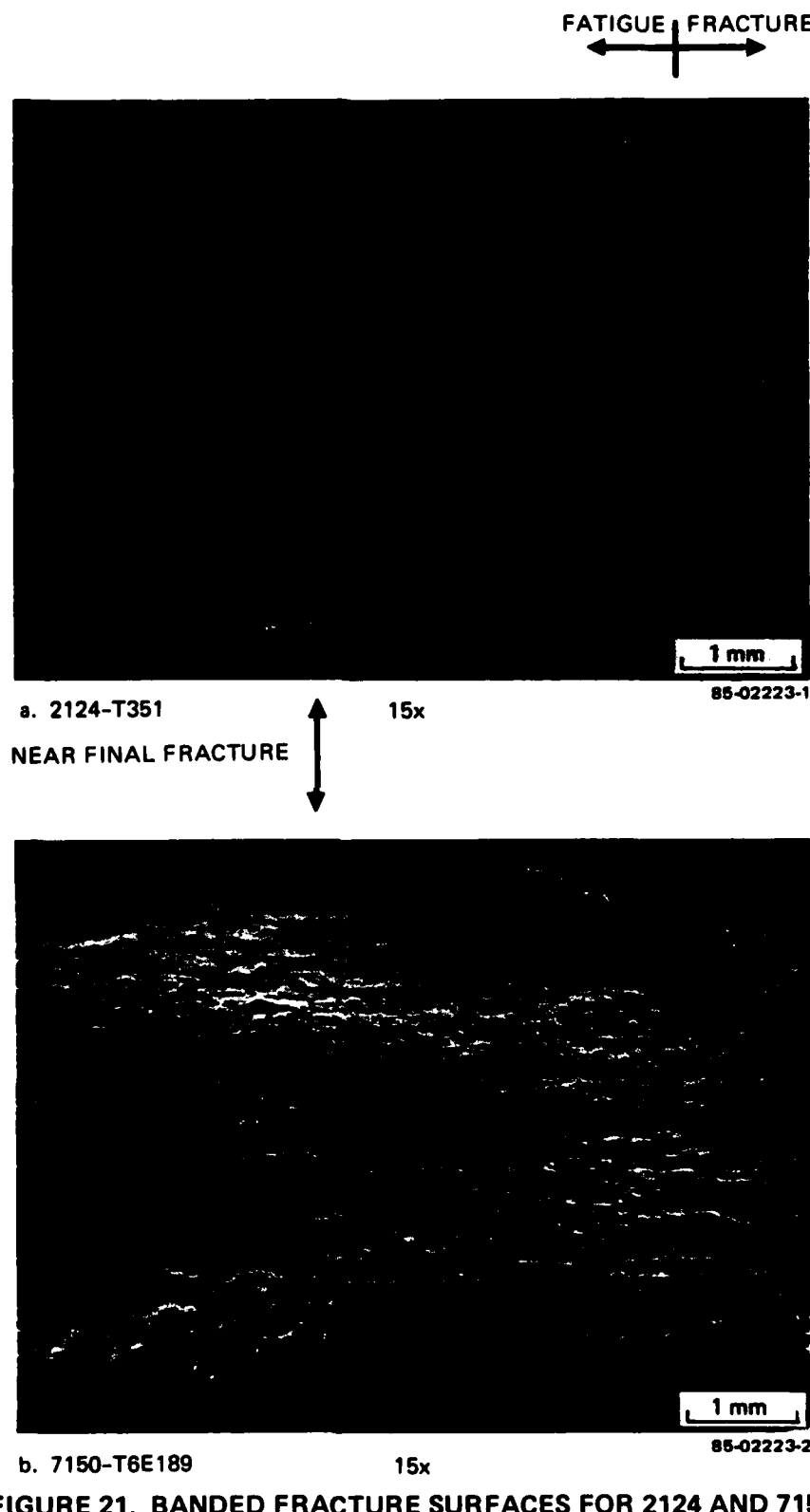


**FIGURE 21. BANDED FRACTURE SURFACES FOR 2124 AND 7150 PRIOR TO FINAL FRACTURE, INDICATING LOCAL TEARING DURING HIGH-SPECTRUM LOAD EXCURSIONS, BOTH TESTED USING TD SPECTRUM**

while the lighter regions indicate local tearing instability. Presumably, these local tears correspond with the highest load excursions in the spectrum.

### 3.7 MODIFIED SPECTRUMS

One of the goals of this overall program was to develop a simplified spectrum that would reduce the testing required to evaluate materials for their resistance to spectrum fatigue crack growth. Several evaluations in this program were performed wholly or in part to satisfy that goal - the racetrack spectrums, which eliminated the smaller amplitude cycles, and the TCZ spectrum, which determined the importance of compression cycles. Eight alloys were evaluated using these three modified spectrums. Seven of the alloys were evaluated in Phase II and the eighth, 2020-T651, was evaluated in this phase. The results are presented in Tables 9 and 10 and Figure 22. Another effort was analytic. This analysis was a modified Willenborg prediction method which used the yield strength and constant-amplitude FCG behavior to predict the spectrum life of the specimens used in this program and correlate those results to the actual lives. This has never before been possible for such a variety of aluminum alloys evaluated under the same conditions. Although high correlation was not expected, trends may have existed that would have suggested those aspects of the spectrum that were more significant to the life, those changes that were needed in the models or indicated indirectly, and those metallurgical features that were significant to spectrum fatigue crack growth. The techniques used and the results are presented in Appendix D. Overall, the correlation was good; however, the life predictions for one alloy, 7475-T651, were grossly underestimated. This alloy later had the longest life of all the 7000 series alloys evaluated but it was predicted to have the shortest life. This indicated that using this model to determine the significant metallurgical variables was not likely to succeed at this time.

**TABLE 9. SPECTRUM FATIGUE RESULTS – MODIFIED SPECTRUMS**

MAXIMUM PEAK STRESS,  $\sigma_{hmax}$  = 145 MPa (21 ksi)  
CRACK GROWTH FROM 6mm (0.24 in.) TO FAILURE

SPECTRUM	SIMULATED FLIGHT HOURS, H		
	TDR	TCR	TCZ
<b>MATERIAL</b>			
2020-T651	26,315	11,867	22,552 31,168
2024-T351	24,899	15,738	34,205 31,090
2024-T851	9,410	7,403	10,258 12,175
7050-T7451	16,787	13,501	19,096 19,346
7075-T651	12,600	9,526	13,039 14,975
7075-T7351	14,179	11,446	17,502 17,595
7475-T651	21,259	19,387	22,630 23,364
7475-T7351	13,785	13,011	19,140 20,268

TABLE 10. RANKING OF MATERIALS UNDER SPECTRUM  
LOADING - MODIFIED SPECTRUMS

a.  $\sigma_{hmax} = 145\text{ MPa}$  FROM  $\sigma = 6\text{ mm}$  TO FAILURE

TDR SPECTRUM		
MATERIAL	SIMULATED FLIGHT HOURS <sup>a</sup>	RANKING UNDER TD SPECTRUM <sup>b</sup>
2020-T651	26,300	3
2024-T351	24,900	1
7475-T651	21,300	2
7050-T7451	16,800	5
7075-T7351	14,200	6
7475-T7351	13,800	4
7075-T651	12,600	7
2024-T851	9,400	8

b. TCR SPECTRUM		
MATERIAL	SIMULATED FLIGHT HOURS <sup>a</sup>	RANKING UNDER TC SPECTRUM <sup>b</sup>
7475-T651	19,400	2
2024-T351	15,700	1
7050-T7451	13,500	4
7475-T7351	13,000	3
2020-T651	11,900	5
7075-T7351	11,400	6
7075-T651	9,500	7
2024-T851	7,400	8

c. TCZ SPECTRUM		
MATERIAL	SIMULATED FLIGHT HOURS <sup>c</sup>	RANKING UNDER TC SPECTRUM <sup>b</sup>
2024-T351	32,600	1
2020-T651	26,500	5
7475-T651	23,000	2
7475-T7351	19,700	3
7050-T7451	19,200	4
7075-T7351	17,500	6
7075-T651	14,000	7
2024-T851	11,200	8

a ONE TEST RESULT ROUNDED TO NEAREST HUNDRED HOURS

b CONSIDERING THESE EIGHT ALLOYS

c AVERAGE OF TWO TEST RESULTS ROUNDED TO NEAREST HUNDRED HOURS

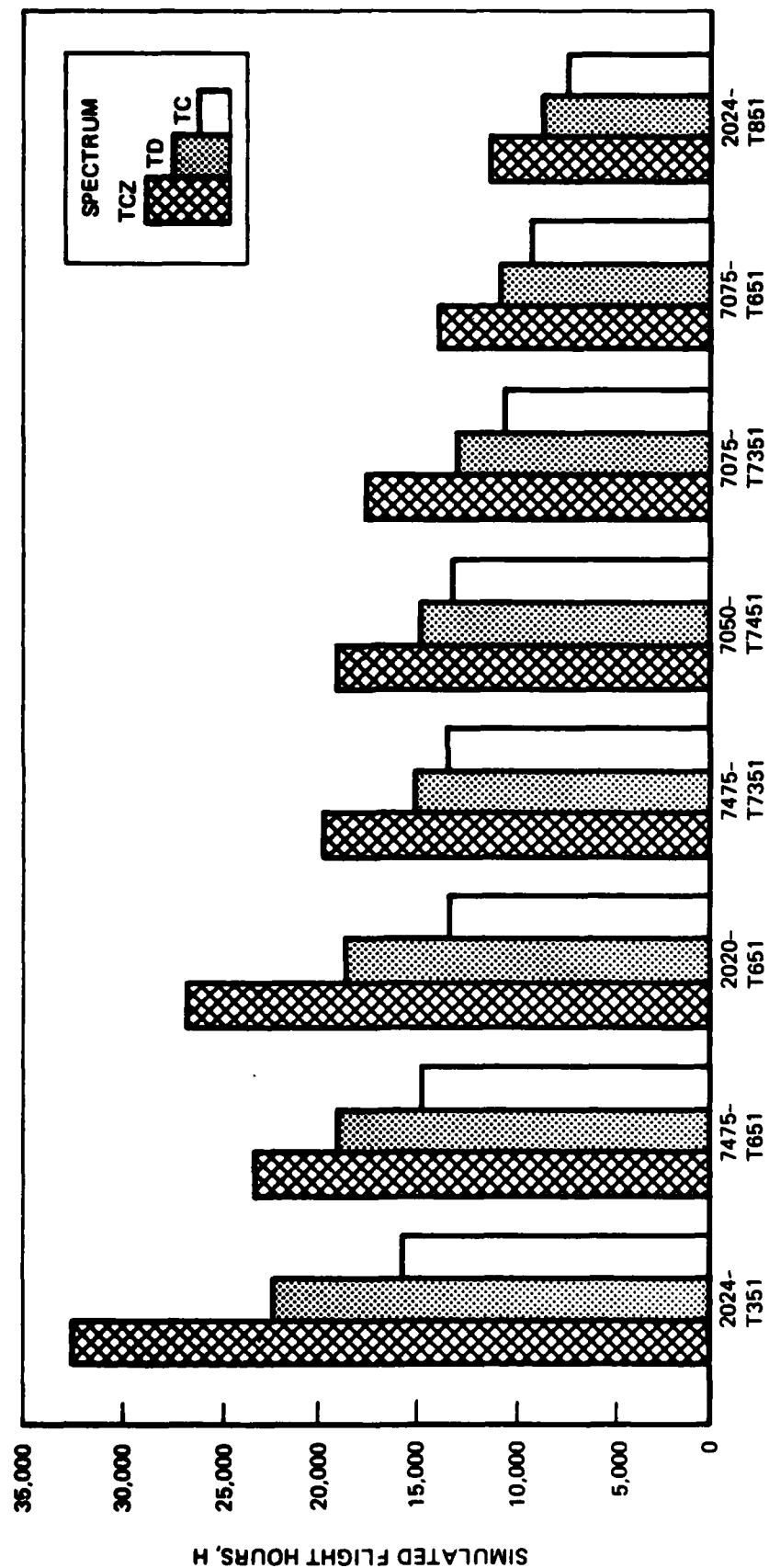


FIGURE 22. SPECTRUM FATIGUE LIVES FOR TCZ, TD, AND TC SPECTRUMS

#### 4. SUMMARY AND CONCLUSIONS

An investigation to determine the important metallurgical factors that influence spectrum fatigue crack propagation (FCP) in selected high-strength aluminum alloys is being performed. This program was also designed to simplify complex load histories into generic simple spectrums and provide information for development and selection of fatigue resistant alloys. Most of the results on which this summary was based are discussed in the Phase II final report.<sup>(28)</sup> The results summarized herein represent a baseline characterization of a number of high-strength aluminum alloys, from which the selection, fabrication, and critical evaluation of alloys with systematically controlled microstructures followed - the results of which are described in a companion report.<sup>(29)</sup>

Twelve commercial 2XXX and 7XXX aluminum alloys were chosen for analysis so that the influence of both purity and temper on FCP could be evaluated. The alloys evaluated were 2020-T651, 2024-T351, 2024-T851, 2124-T351, 2124-T851, 2324-T39, 7050-T7451, 7075-T651, 7075-T7351, 7150-T6E189, 7475-T651, and 7475-T7351. All 12 alloys (seven in Phase I, three in Phase II, and two in Phase III) have been characterized with respect to chemical composition, microstructure, tensile properties, and fracture toughness. FCP tests were conducted on specimens of each alloy for both constant-amplitude loading (including the low  $\Delta K$  region) and two F-18 load spectrums. The spectrum FCP testing was performed at a maximum peak stress of 145 MPa (21 ksi) as well as limited testing at 103 and 169 MPa (15 and 24.5 ksi) to obtain additional data at the low and high end of the crack growth range. Eight of the alloys were evaluated using three simplified spectrums. Pertinent fracture surface features were documented on the spectrum fatigue specimens.

The constant-load-amplitude FCP tests were performed on each material to provide a baseline characterization of steady-state FCP response. These data are necessary as inputs to life-prediction models. Fractographic analyses of these specimens are used to help explain the spectrum fatigue results.

The following observations can be made about the constant-load-amplitude FCP behavior of these alloys:

1. Rankings of constant-load-amplitude FCP resistance among the 12 materials are  $\Delta K$  dependent
2. At near-threshold  $\Delta K$  levels ( $\leq 4 \text{ MPa}\sqrt{\text{m}}$ ):
  - a. Fatigue crack growth resistance varies more than that at higher  $\Delta K$  levels
  - b. 2124-T351 has greater crack growth resistance than the other 11 alloy-temper combinations
  - c. FCP resistance of 7475-T651 exceeds that of the other five 7XXX alloys: 7075-T651, 7075-T7351, 7050-T7451, 7150-T6E189 and 7475-T7351
  - d. These data confirm that:
    - (1) Increased aging reduces near-threshold FCP resistance
    - (2) Purity (Fe, Si content) has little or no effect on near-threshold crack growth rates
3. At intermediate  $\Delta K$  levels (4 to 15  $\text{MPa}\sqrt{\text{m}}$ ):
  - a. The 2XXX alloys, 2020-T651, 2124-T351, and 2324-T39, have lower FCG rates than the other alloys
  - b. The peak aged 7XXX alloys, 7075-T651, 7150-T6E189, and 7475-T651, have faster FCG rates than the other alloys.

Spectrum FCP tests were conducted on each of the 12 alloys, using two complex F-18 load histories. The performance of each alloy in these spectrum tests and the relative rankings of the alloys represent valuable engineering information resulting in the selection of metallurgical variables that were systematically evaluated for their effects on fatigue crack growth as reported in Volume II of this report. Secondly, these results are baseline information for spectrum analyses and spectrum modifications. Several observations can

be made based on the results for testing at the maximum peak stress of 145 MPa (21 ksi):

1. The ranking of the 12 alloys is the same for the two spectrums, except for 2020-T651 for which the ranking under the tension-compression (TC) spectrum is considerably lower than the tension-dominated (TD) spectrum.
2. For each material the TD spectrum consistently results in longer lives.
3. The differences in life between the two spectrums for the same alloy were relatively small – not more than 35 percent.
4. There were larger differences in lives among the 2XXX alloys than the 7XXX alloys; for example, a 100-percent difference for the TD spectrum between the two extremes for the 2XXX alloys – 2024-T851 and 2124-T351 – compared to a 55-percent difference between the extremes for the 7XXX alloys, 7475-T651, and 7075-T651.
5. A comparison of the spectrum lives and fatigue crack growth rates indicates that the overall spectrum life does not appear to be controlled by any particular regime of spectrum crack growth (or stress intensity).

In general, the spectrum performance rankings could not be correlated with yield strength or constant-amplitude FCP resistance at any  $\Delta K$  level. However, spectrum performance could be correlated with fracture toughness; FCP life for both spectrums generally increased with increasing fracture toughness. Perhaps more significantly, the alloys that deform by planar slip generally had longer spectrum fatigue lives than those that deform more homogeneously.

Eight of the 12 alloys were spectrum fatigue tested using modifications of the baseline spectrums. Two different types of modifications were performed independently on the baseline spectrums. One modification had two goals:

1. Eliminate low-amplitude cycles to reduce testing time without changing the ranking (relative life) of the alloys

2. Determine the importance of low-amplitude cycles on the overall spectrum life.

The racetrack method was used to eliminate 43 percent of the low-amplitude cycles. Although the goal of preserving the same ranking as the baseline spectrums was not met, the differences in spectrum fatigue lives between the modified and baseline spectrums are small enough so that the selection of one alloy over another would not be significantly affected.

The second modification was made to determine the importance of compressive load cycles. To accomplish this, all compression load points were eliminated from the TC spectrum. There were significant increases in spectrum lives compared to the baseline spectrum; but surprisingly, the rankings of the eight alloys for this modified spectrum were the same as those for the two baseline spectrums except for 2020-T651 which performed relatively better under the TCZ spectrum.

A limited evaluation of a spectrum life prediction model indicated the inability of the model to predict the relative behavior these materials compared to their actual performance.

## REFERENCES

1. Chanani, G.R., "Fundamental Investigation of Fatigue Crack Growth Retardation in Aluminum Alloys," AFML-TR-76-156, 1976.
2. Sanders, T.H., Sawtell, R.R., Staley, J.T., Bucci, R.J., and Thakker, A.B., "The Effect of Microstructure on Fatigue Crack Growth of 7XXX Aluminum Alloys Under Constant Amplitude and Spectrum Loading," NADC Contract No. N00019-76-C-0482, 1978.
3. Bucci, R.J., Thakker, A.B., Sanders, T.H., Sawtell, R.R., and Staley, J.T., "Ranking 7XXX Aluminum Alloy Fatigue Crack Growth Resistance Under Constant Amplitude and Spectrum Loading," ASTM STP 714, 1980.
4. Bucci, R.J., "Spectrum Loading - A Useful Tool to Screen Effects of Microstructure on Fatigue Crack Growth Resistance," ASTM STP 631, 1977.
5. Jonas, O., and Wei, R.P., "An Exploratory Study of Delay in Fatigue-Crack Growth," Int. J. of Fracture Mechanics, Vol 7, 1971, p. 116.
6. Schijve, J., "Effect of Load Sequences on Crack Propagation Under Random and Program Loading," Eng. Frac. Mech., Vol. 5, 1973, p. 269.
7. Stephens, R.I., Chen D.K., and Hom, B.W., "Fatigue Crack Growth With Negative Stress Ratio Following Single Overloads in 2024-T3 and 7075-T6 Aluminum Alloys," ASTM STP 595, 1976.
8. Alzos, W.X., Skat, A.C., Jr., and Hillberry, B.M., "Effect of Single Overload/Underload Cycles on Fatigue Crack Propagation," ASTM STP 595, 1976.
9. Chanani, G.R., "Effect of Thickness on Retardation Behavior of 7075 and 2024 Aluminum Alloys," ASTM STP 631, 1977.

10. Chanani, G.R., "Investigation of Effects of Saltwater on Retardation Behavior of Aluminum Alloys," ASTM STP 642, 1977.
11. Schijve, J., "Observations on the Prediction of Fatigue Crack Growth Propagation Under Variable-Amplitude Loading," ASTM STP 595, 1976.
12. Wanhill, R.J.H., "Maneuver Spectrum Fatigue Crack Propagation in Aluminum Alloy Sheet Materials," NLR-TR-78091-U, May 1980.
13. Dill, H.D., Saff, C.R., and Potter, J.M., "Effects of Fighter Attack Spectrum on Crack Growth," ASTM STP 714, 1980.
14. Abelkis, P.R., "Effect of Transport Aircraft Wing Loads Spectrum Variation on Crack Growth," ASTM STP 714, 1980.
15. Staley, J.T., "Microstructure and Toughness of High Strength Aluminum Alloys," ASTM STP 605, 1976.
16. Truckner, W.G., Staley, J.T., Bucci, R.J., and Thakker, A.B., "Effects of Microstructure on Fatigue Crack Growth of High Strength Aluminum Alloys," AFML-TR-76-169, 1976.
17. Staley, J.T., Truckner, W.G., Bucci, R.J., and Thakker, A.B., "Improving Fatigue Resistance of Aluminum Aircraft Alloys," Aluminum, 11, 1977, p. 53.
18. Sanders, T.H., Jr., and Staley, J.T., "Review of Fatigue and Fracture Research on High-Strength Aluminum Alloys," Fatigue and Microstructure, Metals Park: American Society for Metals, 1979.
19. Bretz, P.E., Vasudevan, A.K., Bucci, R.J., and Malcolm, R.C., "Effect of Microstructure on 7XXX Aluminum Alloy Fatigue Crack Growth Behavior Down to Near-Threshold Rates," Final Report, Naval Air Systems Command, Contract N00019-79-C-0258, 1981.
20. Willenborg, J., Engle, R.M., and Wood, H.A., "A Crack Growth Retardation Model Using an Effective Stress Concept," TM-71-1-FBR, WPAFB, Ohio, 1971.
21. Wheeler, O.E., "Crack Growth Under Spectrum Loading," J. of Basic Eng., Trans. ASME, March 1972, p. 181.
22. Elber, W., "The Significance of Fatigue Crack Closure," ASTM STP 1971, p. 486.

23. Dill, H.D., and Saff, C.R., "Effects of Fighter Attack Spectrum on Crack Growth," AFFDL-TR-76-112, March 1977.
24. Chanani, G.R., and Mays, B.J., "Observation of Crack-Closure Behavior After Single Overload Cycles in 7075-T6 SEN Specimens," Eng. Fract. Mech., Vol. 9, 1977, p. 65.
25. Chanani, G.R., "Determination of Plastic-Zone Sites at Fatigue Cracks by Optical Interference Technique," Int. J. of Fracture, Vol. 13, 1977, p. 394.
26. Jones, R.L., and Cagle, T.E., "The Mechanical Stress-Corrosion, Fracture Mechanics, and Fatigue Properties of 7050, 7475, and Ti-8Mo-8V-2Fe-3Al Plate and Sheet Alloys," Report FGT-5791, General Dynamics, 1976.
27. Chanani, G.R., Telesman, I., Bretz, P.E., and Scarich, G.V., "Methodology for Evaluation of Fatigue Crack-Growth Resistance of Aluminum Alloys Under Spectrum Loading," Technical Report (Phase I, Final Report), Naval Air Systems Command, Contract N00019-80-C-0427, April 1982.
28. Scarich, G.V., and Bretz, P.E., "Investigation of Fatigue Crack Growth Resistance of Aluminum Alloys Under Spectrum Loading," Technical Report (Phase II, Final Report). Naval Air Systems Command, Contract N00019-81-C-0550, April 1983.
29. Scarich, G.V., Bresnahan, K.M., and Bretz, P.E., "Fatigue Crack-Growth Resistance of Aluminum Alloys Under Spectrum Loading, Volume II - Aluminum Lithium Alloys," Technical Report, Naval Air System Command, Contract N00019-82-C-0425, December 1985.
30. Chanani, G.R., Scarich, G.V., Bretz, P.E., and Sheinker, A.A., "Spectrum Fatigue Crack Growth Behavior of Aluminum Alloys," Proceedings of the Sixth International Conference on Fracture (ICF6), New Delhi, India, Vol. 3, 1984, p. 1609.
31. Scarich, G.V., Gambone, M.J., Chanani, G.R., and Bretz, P.E., "Correlation of Fatigue Behavior With Microstructure of 2XXX and 7XXX Aluminum Alloys," Proceedings of the Sixth International Conference on Fracture (ICF6), New Delhi, India, Vol. 3, 1984, p. 2015.

APPENDIX A  
CONSTANT AMPLITUDE FATIGUE CRACK-GROWTH RATE,  
 $da/dN$  VERSUS  $\Delta K$

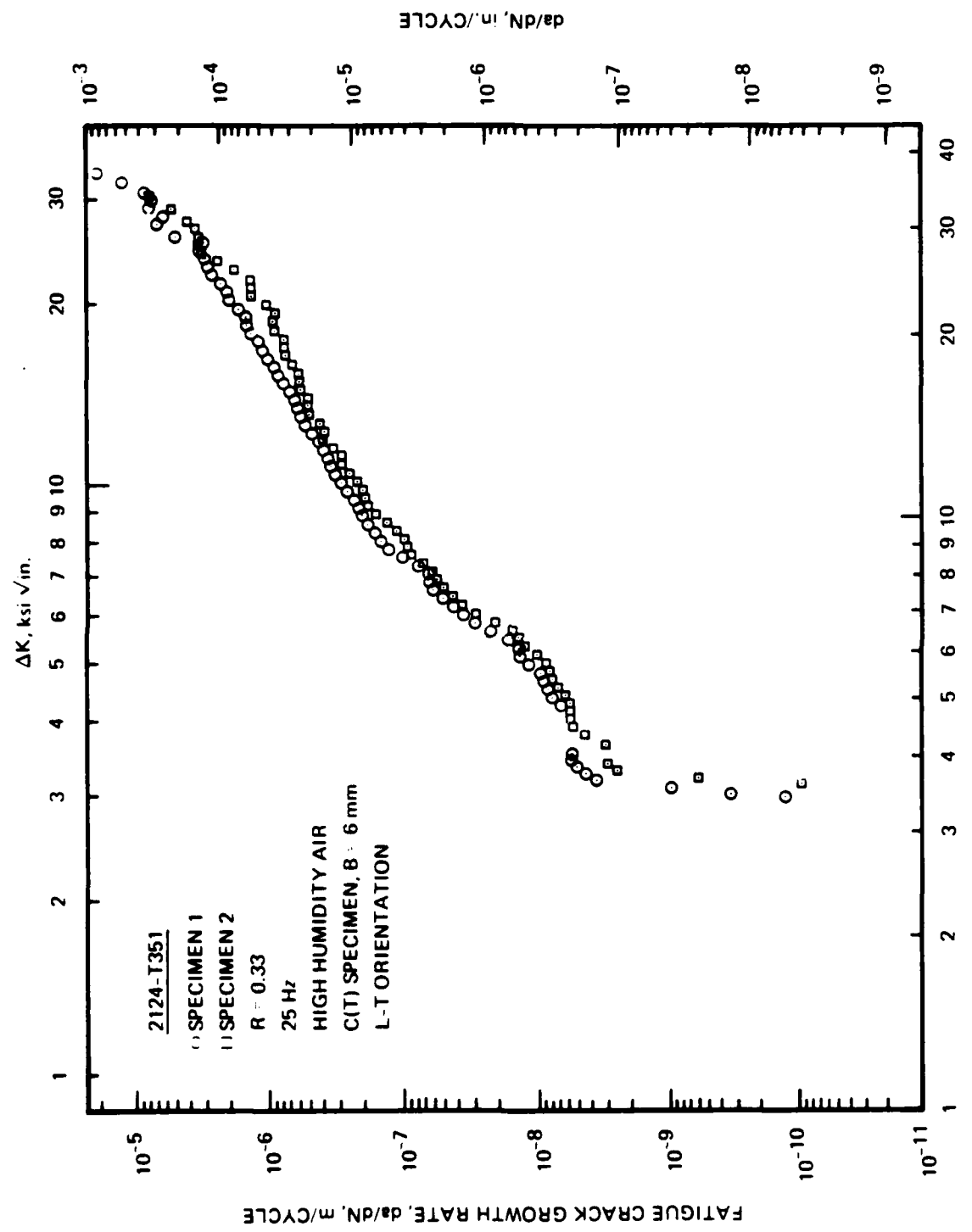


FIGURE A-1. CONSTANT-LOAD-AMPLITUDE FATIGUE CRACK GROWTH RATE DATA FOR 2124-T351

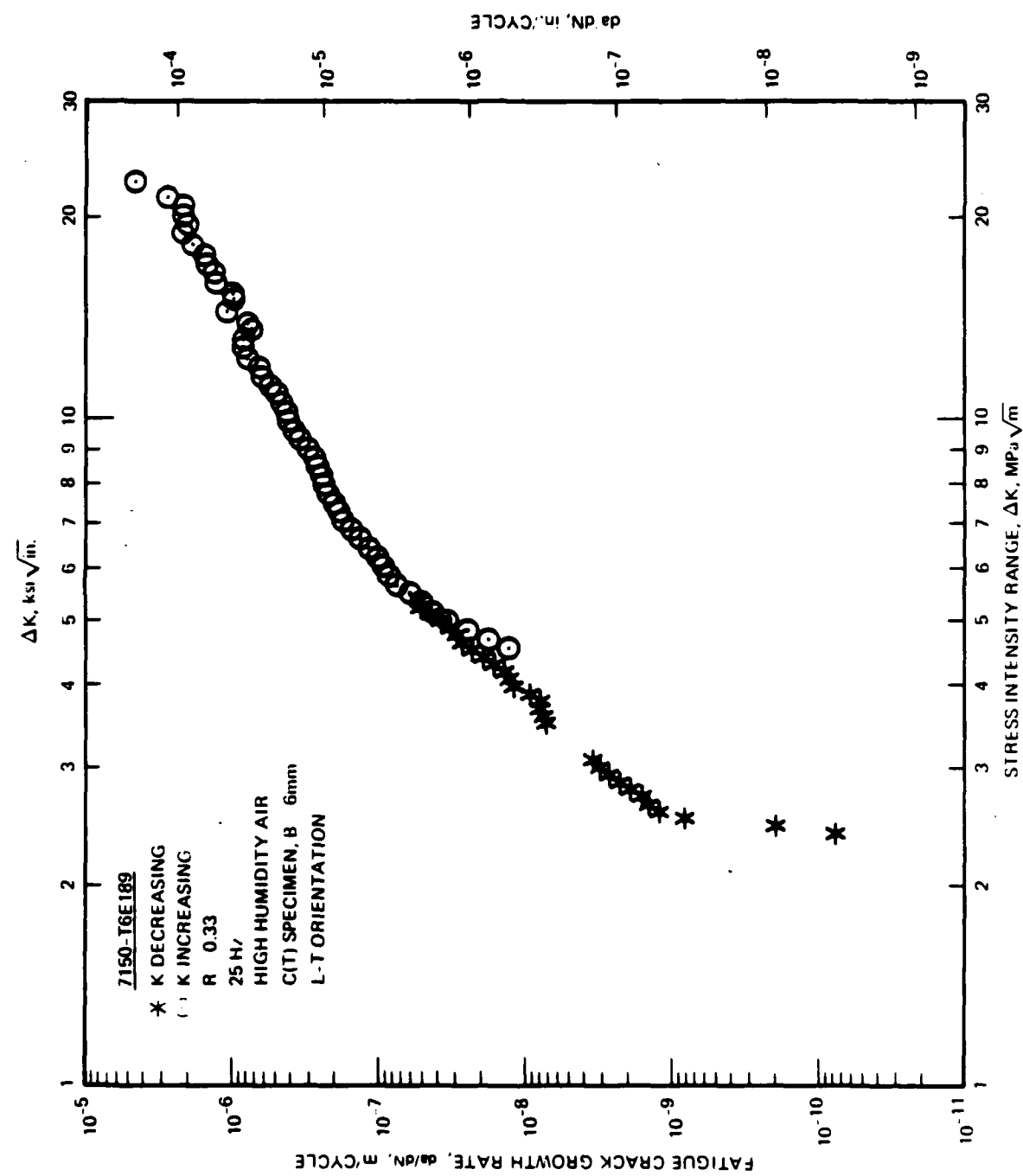
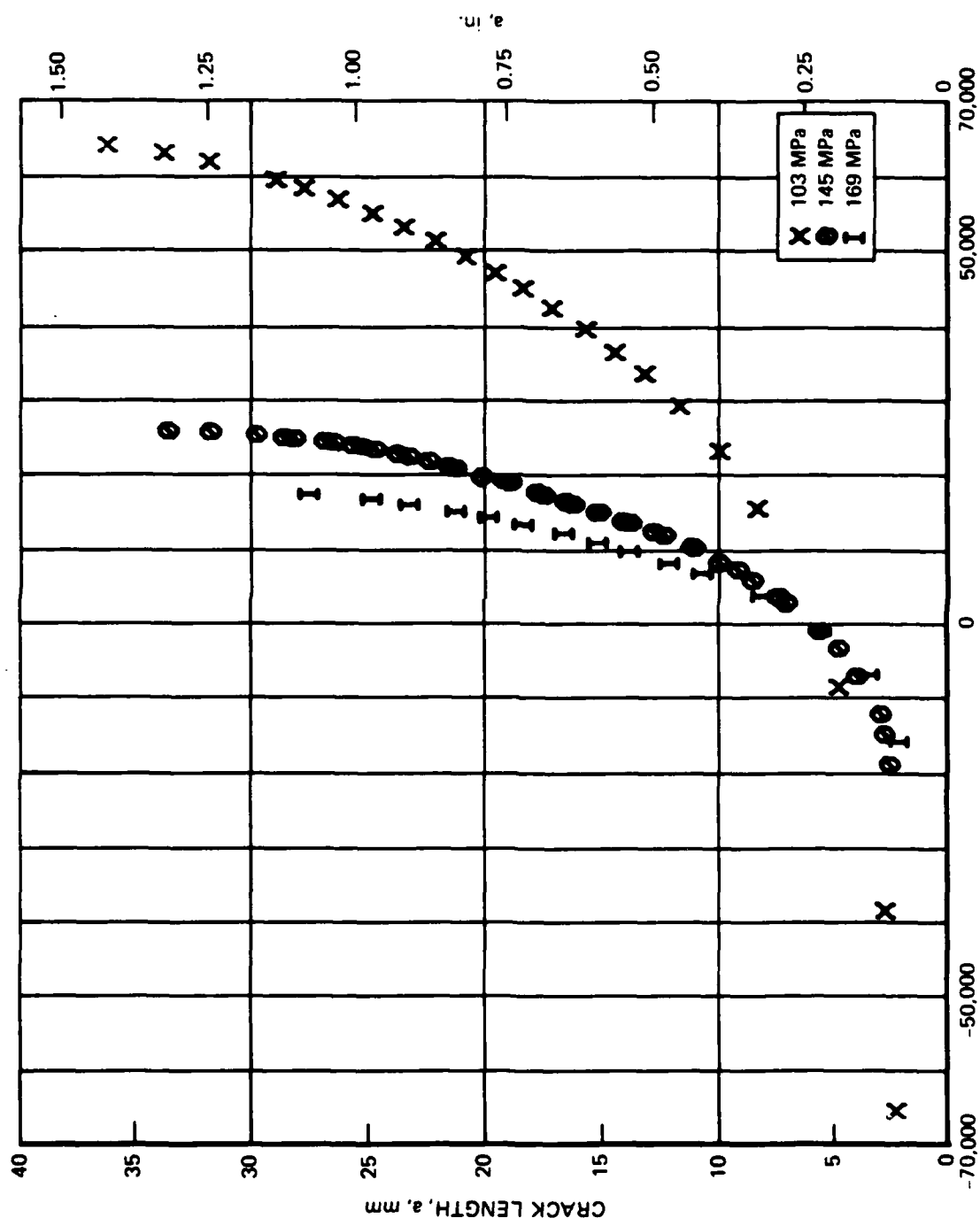


FIGURE A-2. CONSTANT-LOAD-AMPLITUDE FATIGUE CRACK GROWTH RATE DATA FOR 7150-T6E189

## APPENDIX B

### CRACK LENGTH VERSUS SIMULATED FLIGHT HOURS FOR BASELINE SPECTRUMS, a VERSUS H

1. The scale for the ordinate (a) is the same for each graph; the scale for the abscissa (H) varies, and to make comparisons easier, the abscissa was adjusted so that a crack length of 6 mm corresponded to zero simulated flight hours.
2. Two specimens each were tested at 145 MPa, and one each at 103 and 169 MPa.
3. Data are in numerical order by alloy designation with TD spectrum first, then TC spectrum.
4. The tension-dominated (TD) spectrum representing the lower wing root load history of the F-18 is coded C2 at Northrop and the tension-compression (TC) spectrum representing the horizontal hinge tail moment load history is coded E3.
5. Crack length was measured at the end of one or more passes (300 simulated flight hours per pass) of the spectrum, which at the beginning of the 103 and 145 MPa tests resulted in the crack growth increment being less than 0.25 mm which is required by ASTM E647. (Note that ASTM E647 is a method for constant amplitude fatigue crack-growth.) However, in calculating crack growth rates, the 0.25 mm increment requirement was observed. At the higher crack-growth rates, the one-per-pass crack measurement resulted in larger crack-growth increments than required by ASTM E647.
6. Graphs were plotted using a Northrop Support Services Laboratory computer program designated \$DDNPT1 from data on files designated .DDN, created from crack length measurement versus pass raw data.



SIMULATED FLIGHT HOURS,  $H$  (ZERO AT  $a = 6\text{mm}$ )

FIGURE B-1. 2124-T351, TD SPECTRUM

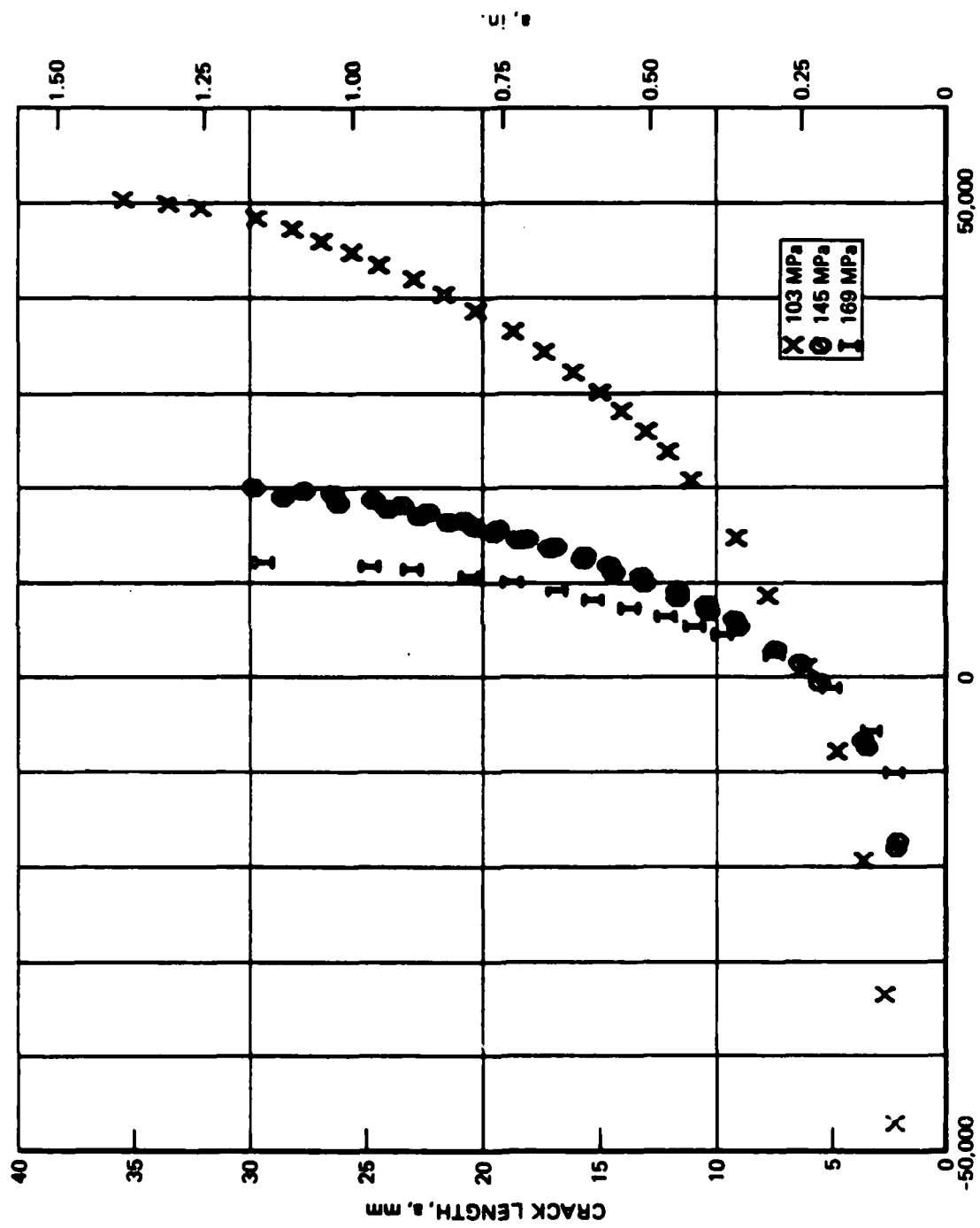


FIGURE B-2. 2124-T361 TC SPECTRUM  
SIMULATED FLIGHT HOURS, H (ZERO AT  $a = 6$ mm)

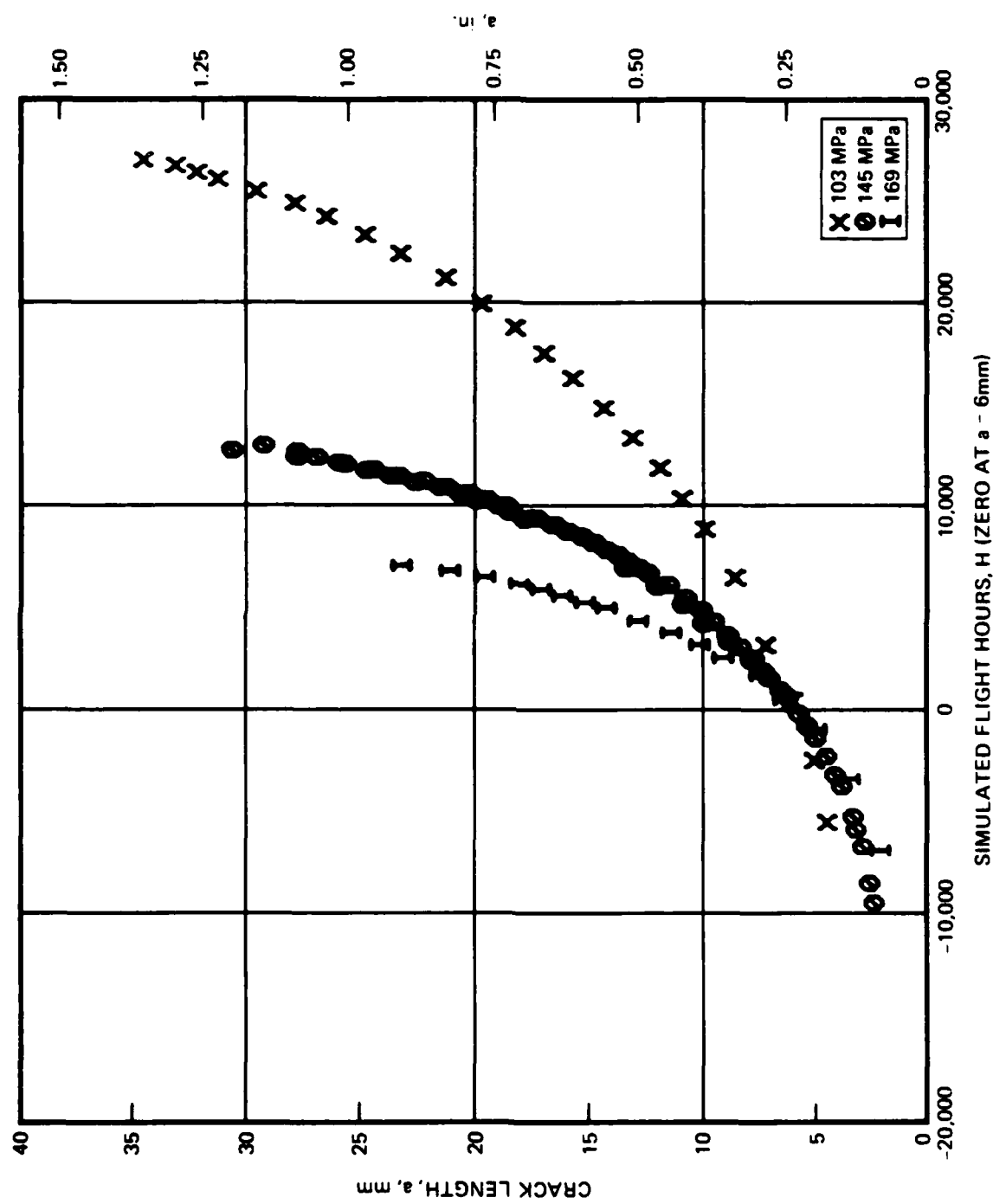


FIGURE B-3. 7150-T6E189, TD SPECTRUM

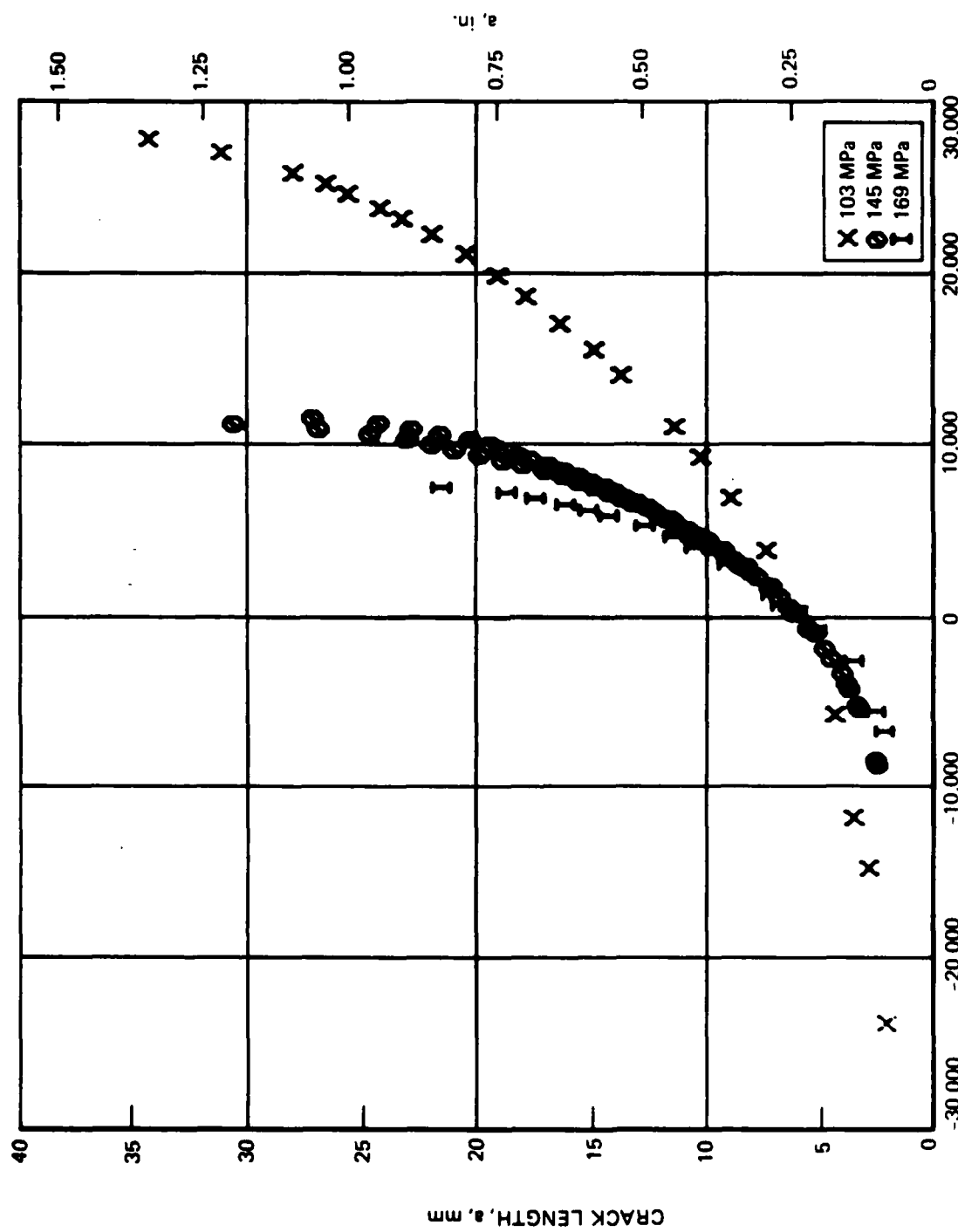


FIGURE B-4. 7150-T6E189, TC SPECTRUM  
SIMULATED FLIGHT HOURS,  $H$  (ZERO AT  $a = 6$  mm)

## APPENDIX C

### SPECTRUM CRACK GROWTH RATE VERSUS MAXIMUM PEAK STRESS INTENSITY $da/dH$ VERSUS $K_{hmax}$

1. The scales for both axes are identical on each graph.
2. Crack growth rates are calculated by the two-point secant method per ASTM E647 based on the data in Appendix B, and applying the ASTM E647 requirement that the minimum crack growth interval,  $a$ , be greater than or equal to 0.25 mm. This is performed using Northrop Support Services Laboratory computer program designated \$FITPTO from data on files designated .DDN, created from crack length measurement versus pass raw data. The data are plotted with a program designated \$SPCPT1.
3. Almost all tests had a crack growth rate which initially decreased for a few data points after precracking; therefore, all data up to the first local minimum crack growth rate were not plotted.

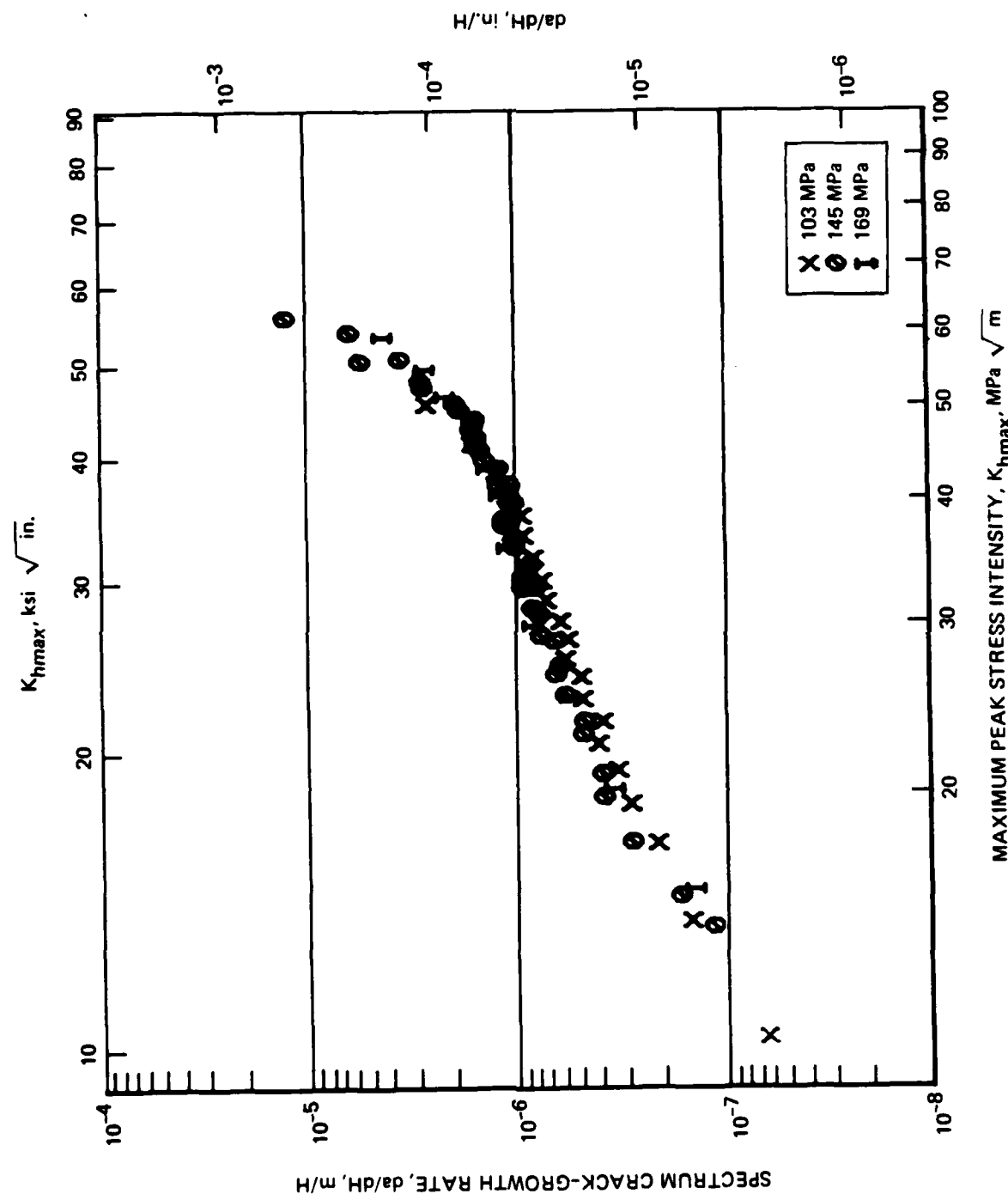


FIGURE C-1. 2124-T351, TD SPECTRUM

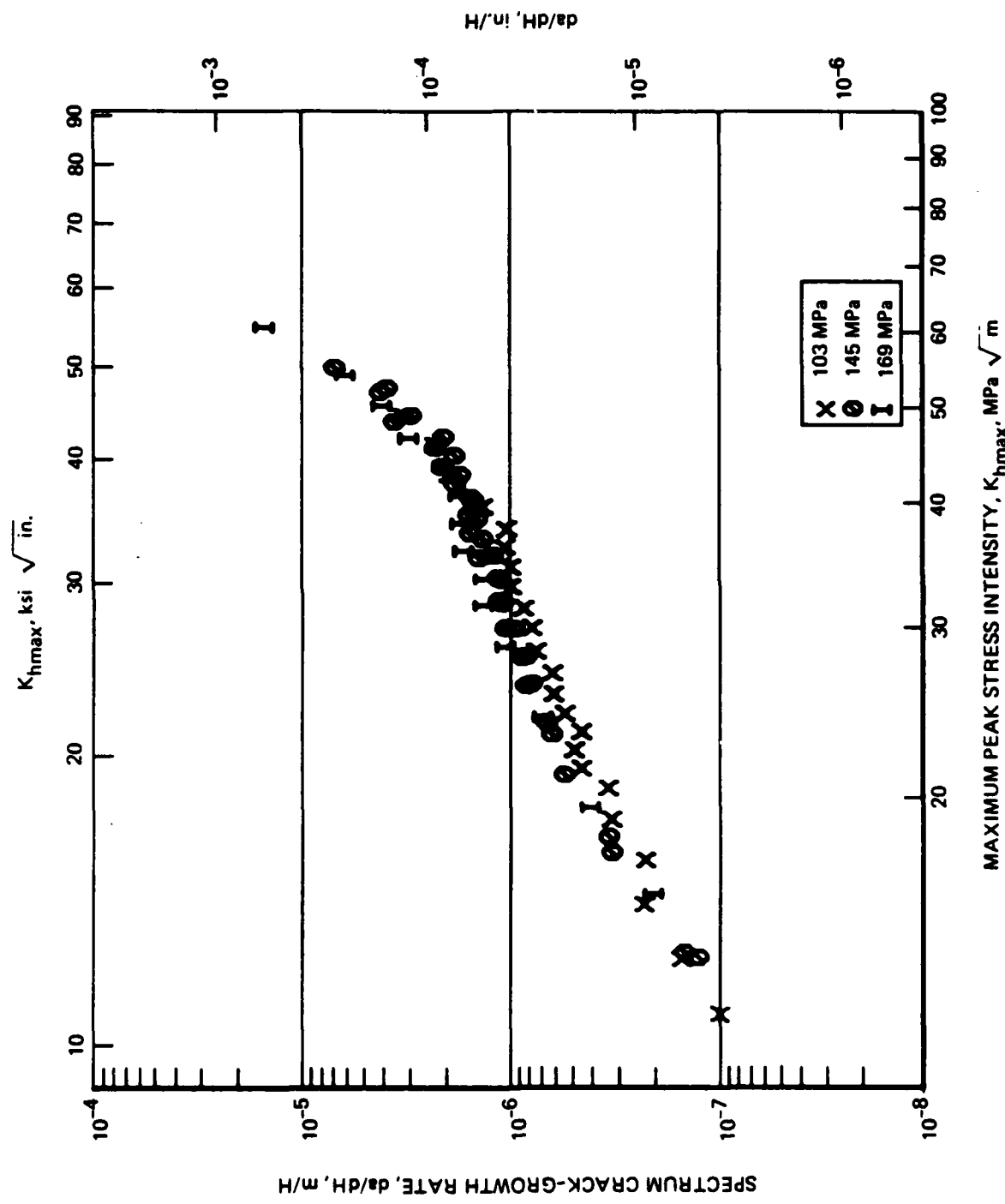


FIGURE C-2. 2124-T351, TC SPECTRUM

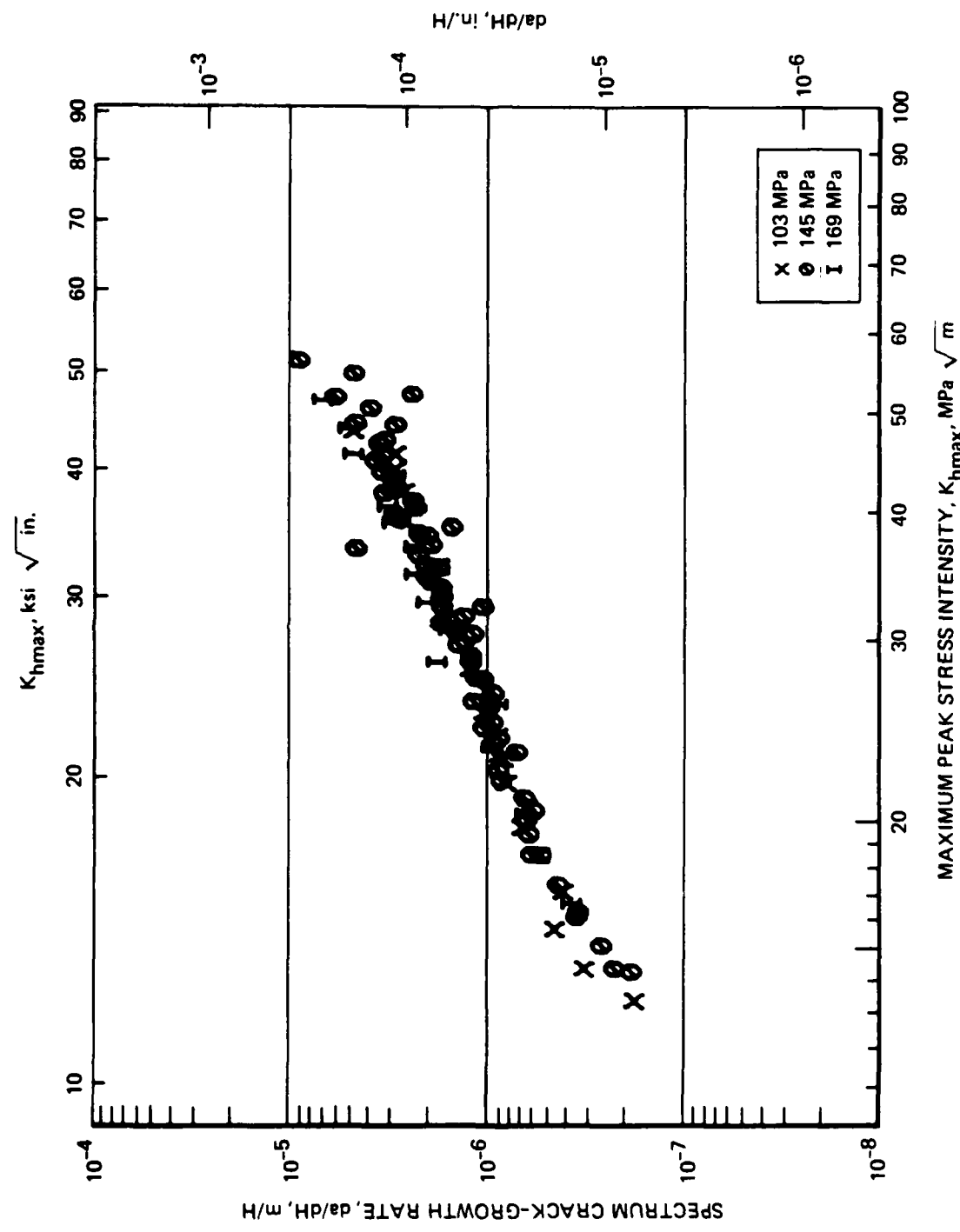


FIGURE C-3. 7150-T6E189, TD SPECTRUM

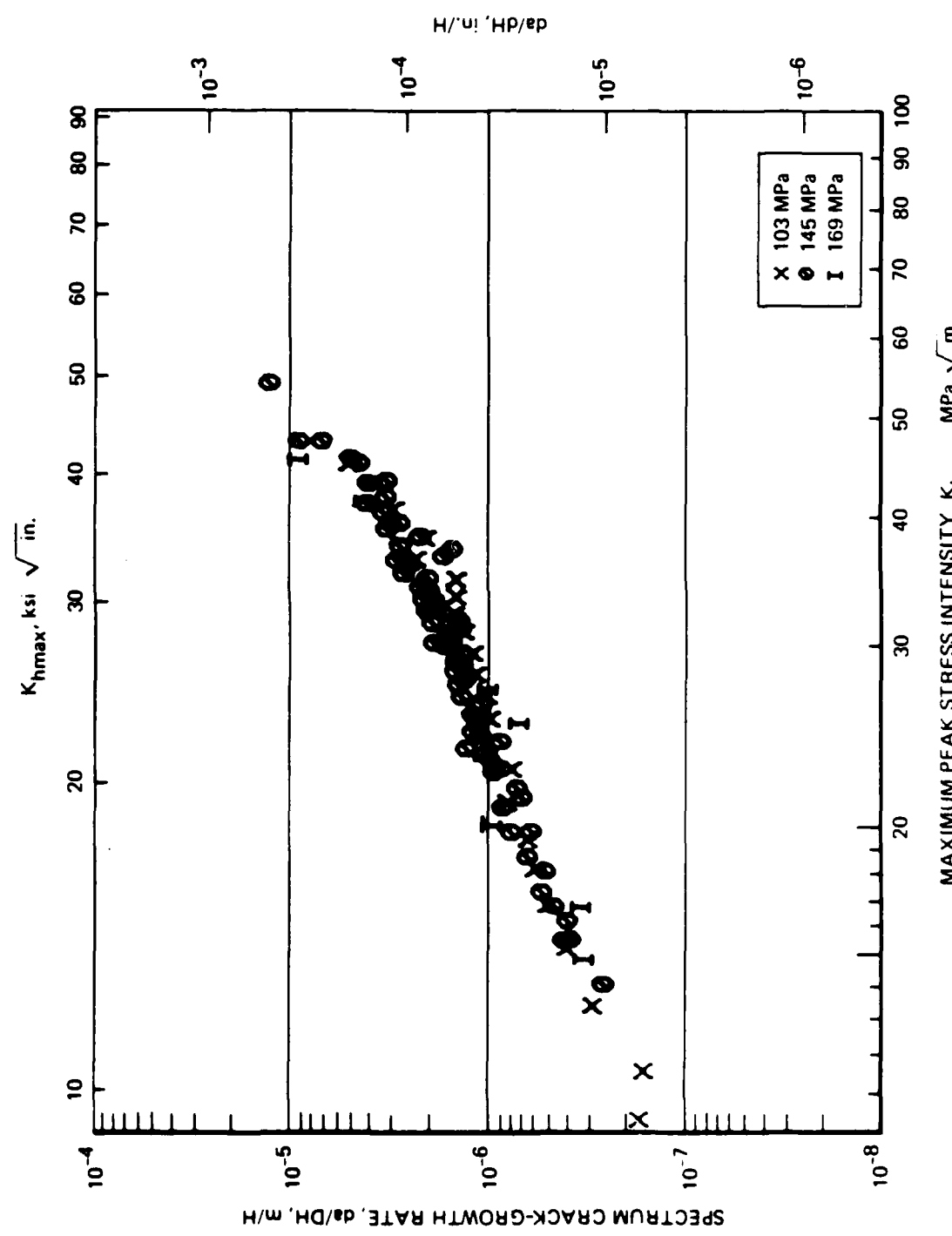


FIGURE C-4. 7150-T6E189, TC SPECTRUM

## APPENDIX D

### PREDICTION

Spectrum fatigue crack growth analyses were conducted on 10 alloys under two F-18 aircraft spectrums for a truncation of these two spectrums. These spectrums were a tension-dominated wing spectrum (TD), a tension-compression tail spectrum (TC), and the racetrack modification of these two spectrums (TDR and TCR).

The NORCRAK program was used to predict the spectrum crack growth lives. This program sums incremental crack growth on a cycle-by-cycle basis. It uses the Paris, Forman, or Walker equations, or tabulated  $da/dN$  versus  $\Delta K$  data to provide a crack growth rate basis. Retardation due to load interaction can also be accommodated using any of the Wheeler, Willenborg, or Northrop models. A number of commonly used stress intensity solutions are built into the program for use in the crack growth equations, and in addition it is possible to input  $K$  versus beta factors in tabular form for problems in which a  $K$  solution is not available. Tabulated data with a modified Willenborg retardation scheme was used for the present analyses. The  $K$  solution for the specimen was determined by combining (beta) factors for a center through crack and a crack emanating from a hole. The sensitivity to  $R$  ratio was based on data for 2024-T351 and 7075-T7351 and those sensitivities used for the 2000 and 7000 series alloys respectively.

The predictions for 7075-T7351 were normalized so that total life matched the test data for the two baseline (untruncated) spectrums. This was accomplished through the use of a "Shut-Off Load Ratio." This parameter was assumed to be only spectrum dependent and was utilized for all other predictions.

Total life predictions were made and the predicted spectrum lives were divided by the actual specimen lives and both are presented in Table D-1. A reasonable correlation was obtained for most materials. The most glaring exception was 7475-T651 which exhibited actual life far longer than predicted.

Life predictions were plotted in the form of crack length versus flight hours for 2024-T351, 7475-T651, and 7075-T7351 for the TD and TC spectrums. The general characteristic of all these predictions was that crack growth rate was underpredicted at short crack lengths and overpredicted at longer crack lengths. This can be seen in the  $K_{hmax}$  versus crack growth rate shown in Figure D-1. Note that the predicted and actual lives for 7075-T7351 were adjusted to be identical.

This rate error effect could be due to either geometrical parameter errors at short crack lengths or to stress intensity effects of some other nature. Other apparent errors are the effect of yield strength on retardation (no substantial effect was observed) and the neglect of compressive loads on retardation leading to different normalization for the TC versus TD spectrums.

TABLE D-1. SPECTRUM LIFE PREDICTIONS

AVERAGE ROUNDED TO NEAREST HUNDRED HOURS.  
MAXIMUM PEAK STRESS,  $\sigma_{hmax}$  = 145 MPa, "a" FROM 6mm TO FAILURE.

a. TENSION-DOMINATED SPECTRUMS

MATERIAL	TD SPECTRUM			TDR SPECTRUM		
	SIMULATED FLIGHT HOURS		PREDICTED ACTUAL	SIMULATED FLIGHT HOURS		PREDICTED ACTUAL
	ACTUAL	PREDICTED		ACTUAL	PREDICTED	
2020-T651	18,500	18,900	1.02	26,300	18,900	0.72
2024-T351	22,100	22,500	1.02	24,900	21,600	0.87
2024-T851	8,500	8,100	0.95	9,400	8,100	0.86
2124-T851	11,200	10,200	0.91	-	-	-
2324-T39	17,800	13,500	0.76	-	-	-
7050-T7451	14,900	10,800	0.72	16,800	11,100	0.66
7075-T651	10,800	6,300	0.58	12,600	6,900	0.55
7075-T7351	12,900	12,000	1.00	14,200	13,200	0.87
7475-T651	19,000	4,800	0.25	21,300	4,800	0.23
7475-T7351	15,000	11,100	0.74	13,800	11,100	0.80

b. TENSION-COMPRESSION SPECTRUMS

MATERIAL	TC SPECTRUM			TCR SPECTRUM		
	SIMULATED FLIGHT HOURS		PREDICTED ACTUAL	SIMULATED FLIGHT HOURS		PREDICTED ACTUAL
	ACTUAL	PREDICTED		ACTUAL	PREDICTED	
2020-T651	13,100	15,900	1.21	-	-	-
2024-T351	15,400	16,500	1.07	15,700	16,500	1.05
2024-T851	7,100	6,600	0.93	7,400	6,300	0.85
2124-T851	9,100	8,700	0.96	-	-	-
2324-T39	14,400	11,400	0.79	-	-	-
7050-T7451	13,200	9,600	0.73	13,500	9,500	0.71
7075-T651	8,900	6,000	0.67	9,500	6,000	0.63
7075-T7351	10,700	10,800	1.01	11,400	10,800	0.95
7475-T651	14,900	4,500	0.30	19,400	4,500	0.23
7475-T7351	12,400	4,300	0.69	13,000	4,300	0.72

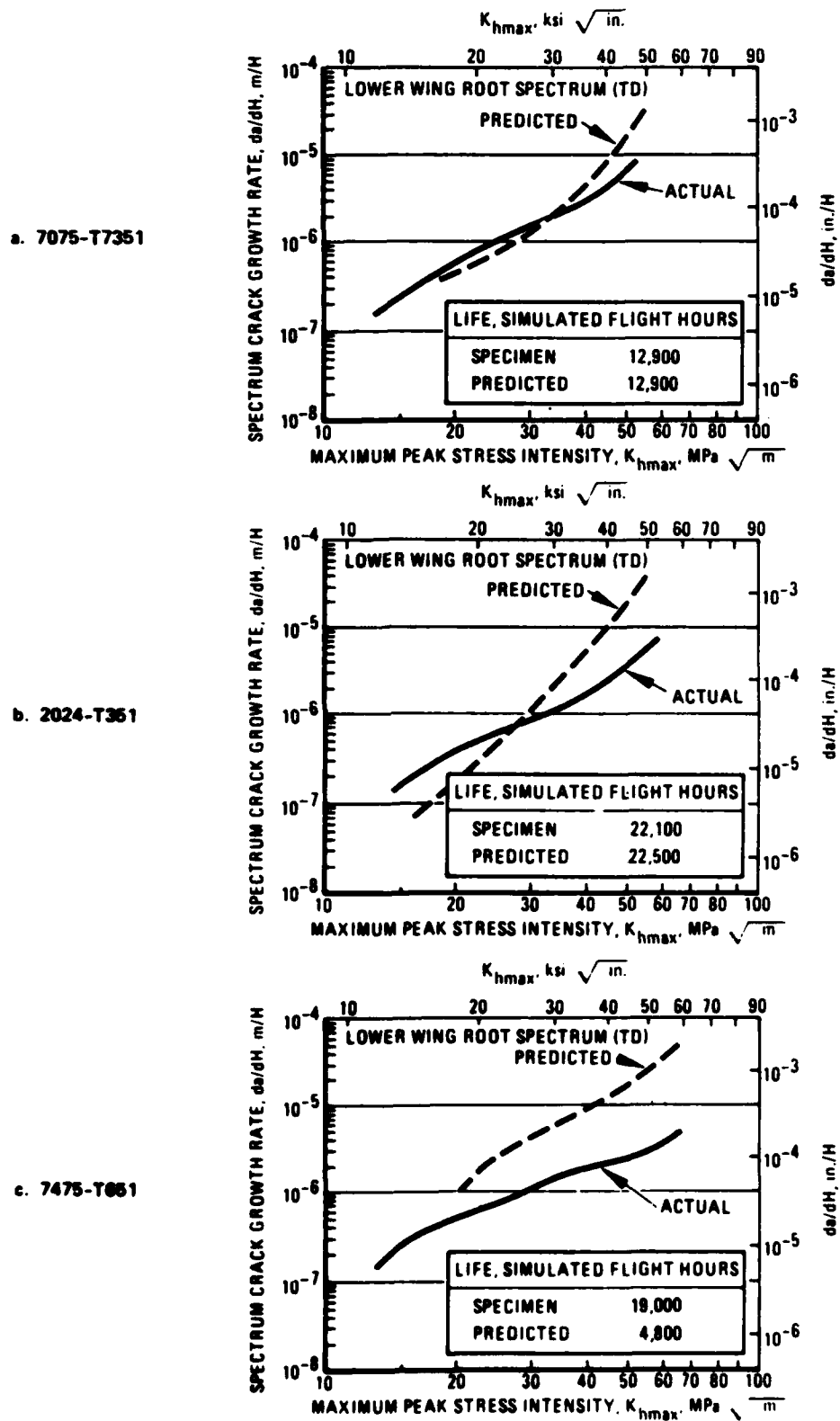


FIGURE D-1. PREDICTED AND ACTUAL SPECTRUM FCGR CURVES FOR TD SPECTRUM

## APPENDIX E

### EVALUATION OF SECOND HEAT OF 7475-T651

Alloy 7475-T651 had the best spectrum fatigue lives of all the 7000 series alloys which was not expected from the fracture toughness and constant-amplitude-fatigue behavior. To confirm this unexpected behavior Northrop and Alcoa at their own expense evaluated a second lot of 7475-T651.

In summary, this second lot did not have as good a spectrum fatigue behavior as the first lot, but still was the best of the six 7000 series alloys evaluated. The results are discussed in detail below.

The second lot was identified as 511348. The original first lot was identified as 511463.

#### E.1 TENSILE

The tensile properties at the T/2 location in the longitudinal direction were 598 MPa (86.7 ksi) ultimate strength, 550 MPa (79.8 ksi) yield strength, and 12 percent elongation and in the long transverse direction were 584 MPa (84.7 ksi) ultimate strength, 530 MPa (76.9 ksi) yield strength, and 14 percent elongation. In the longitudinal direction the strengths are about 11 MPa (2 ksi) higher than the first lot and the elongation is the same.

#### E.2 TOUGHNESS

Toughness was measured using a slow bend Charpy test at the T/2 location. The toughness in the L-T direction was 49.2 MPa  $\sqrt{\text{m}}$  (44.8 ksi  $\sqrt{\text{in.}}$ ) and in the T-L orientation was 41.4 MPa  $\sqrt{\text{m}}$  (37.7 ksi  $\sqrt{\text{in.}}$ ). These values cannot be directly compared to those obtained for the first lot using ASTM E399 procedures.

### **E.3 FATIGUE CRACK GROWTH RESULTS UNDER CONSTANT-AMPLITUDE LOADING**

Data are shown in Figure E-1. At  $K$  less than about  $7 \text{ MPa} \sqrt{\text{m}}$  the FCG rates for the second lot are faster.

### **E.4 SPECTRUM TEST RESULTS**

A single test was performed for each of the five spectrums, TD, TDR, TC, TCR, and TCZ.

Graphs of crack length versus number of flight hours are shown in Figure E-2 and the graphs of spectrum FCG rates versus maximum peak stress intensity are shown in Figure E-3. A comparison of the spectrum fatigue crack growth lives is given in Table D-1. The lives for the first lot are longer than the second lot, except for the TCZ spectrum.

### **E.5 SUMMARY**

The superiority of 7475-T651 over the other six materials was preserved, as a comparison of Table E-1 with Tables 7 and 9 will show.

**TABLE E-1. SPECTRUM FATIGUE LIVES FOR THE TWO LOTS OF 7475-T651**

$\sigma_{h\max} = 145 \text{ MPa}$  FROM  $a = 6\text{mm}$  TO FAILURE

SPECTRUM	LOT 1 (511463)	LOT 2 (511348)	DIFFERENCE*
TD	18,303 19,792	15,315	22
TDR	21,259	18,404	14
TC	14,744 15,141	14,188	5
TCR	19,387	15,991	19
TCZ	22,630 23,364	27,389	-17

$$* \text{ DIFFERENCE} = \frac{\text{LIFE (LOT 1)} - \text{LIFE (LOT 2)}}{(\text{LIFE (LOT 1)} + \text{LIFE (LOT 2)})/2} \times 100\%$$

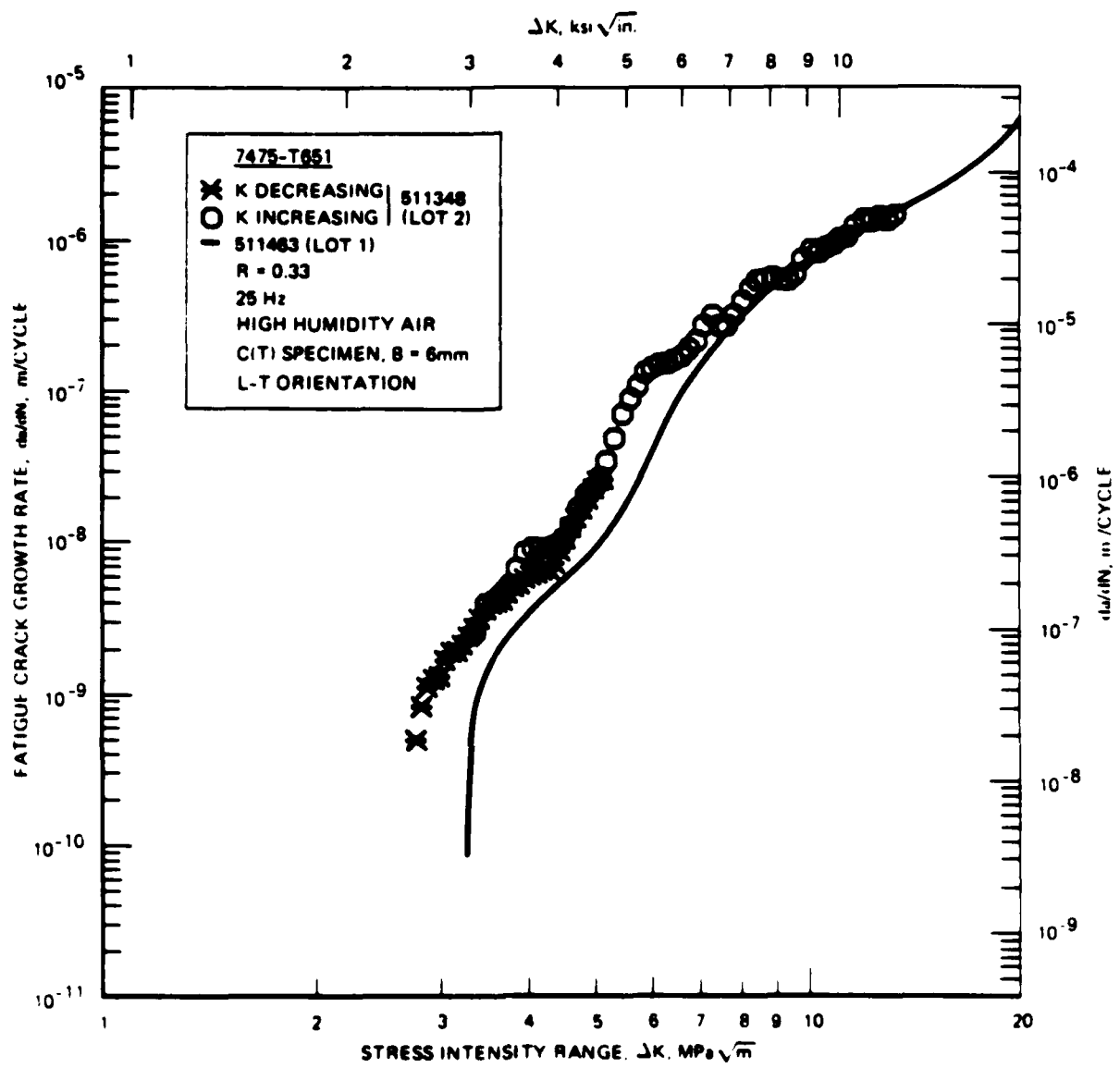
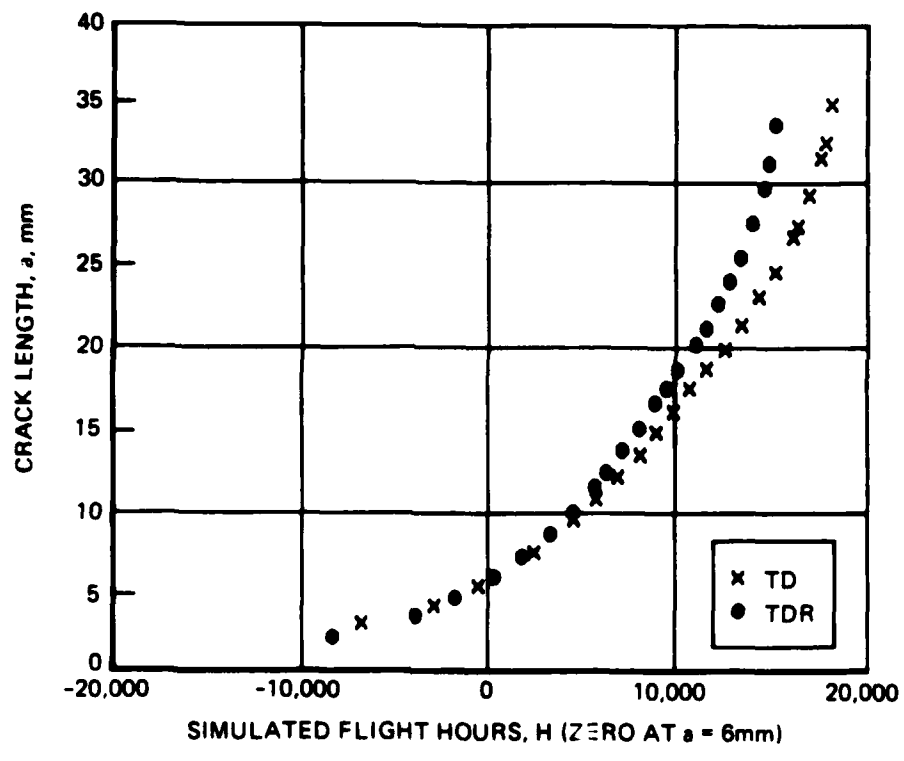


FIGURE E-1. CONSTANT-LOAD-AMPLITUDE FATIGUE CRACK GROWTH RATE DATA FOR 7475-T651



a. TD AND TDR SPECTRUMS

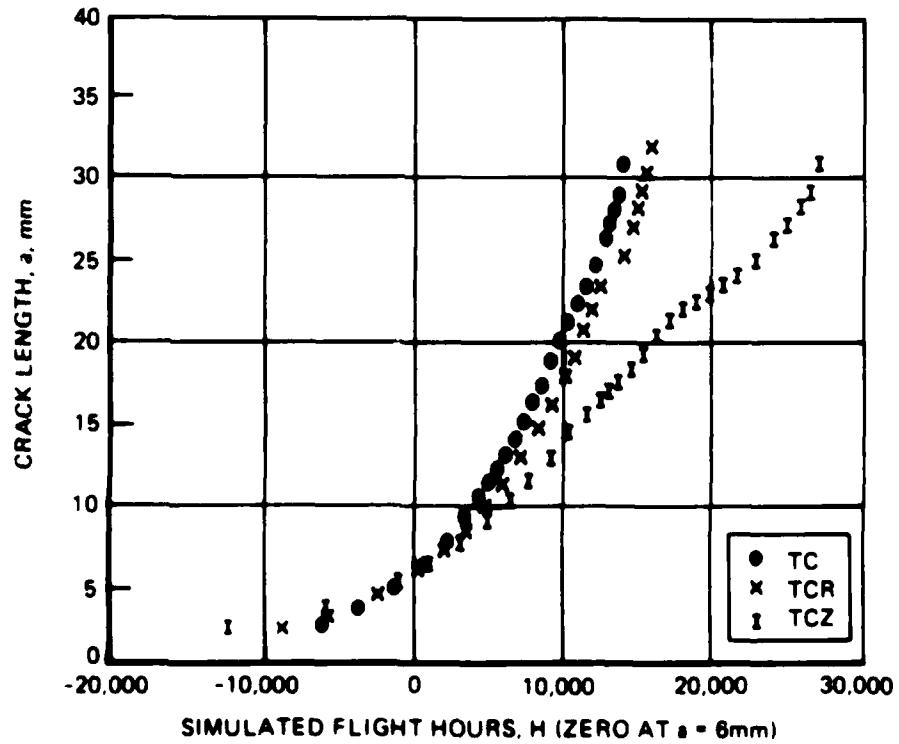
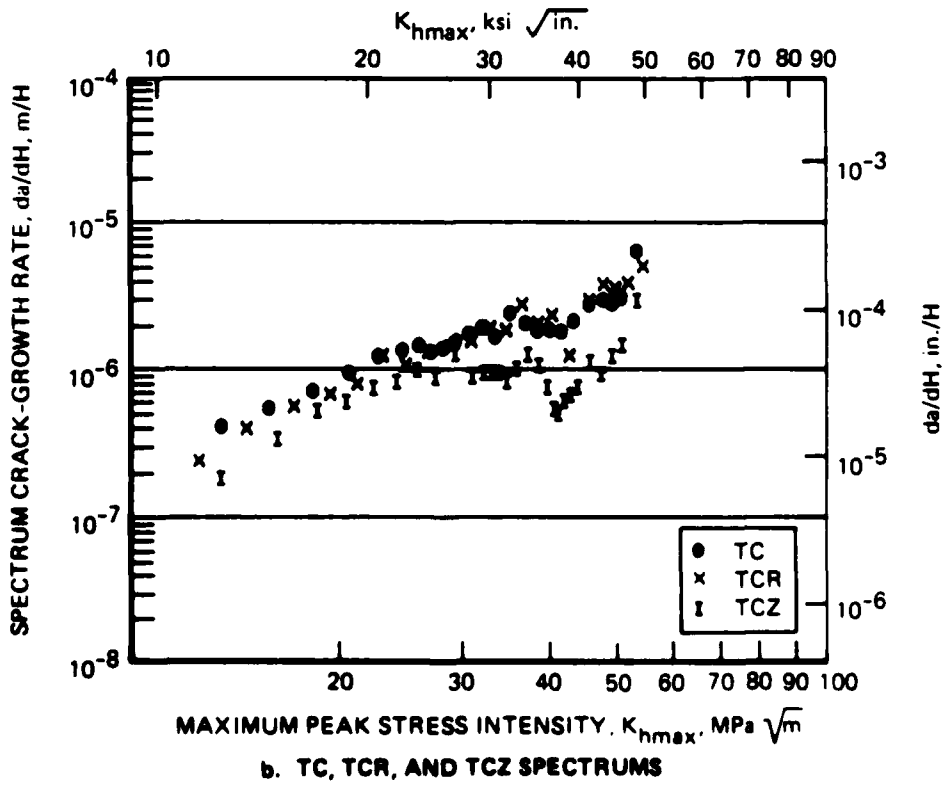
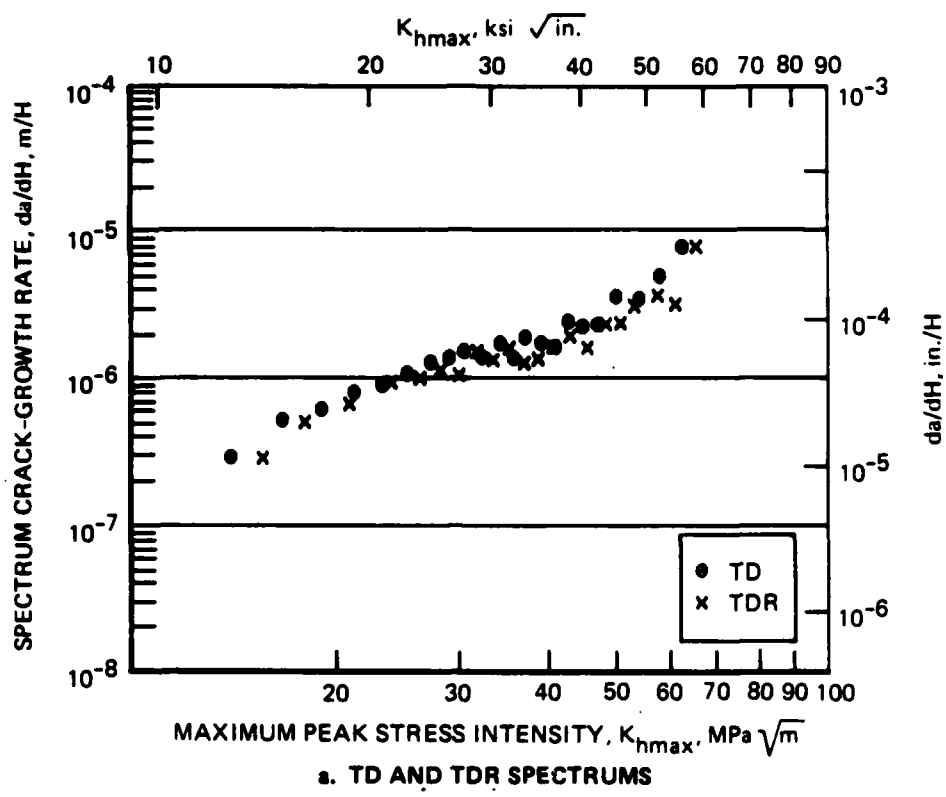


FIGURE E-2. CRACK LENGTH VERSUS SIMULATED FLIGHT HOURS  
FOR 7475-T851, LOT 2



**FIGURE E-3. SPECTRUM CRACK GROWTH RATE VERSUS MAXIMUM PEAK STRESS INTENSITY FOR 7475-T651, LOT 2**

**DISTRIBUTION LIST**  
(One copy only unless otherwise noted)

Commander  
Naval Air Systems Command  
Attn: Code AIR-5304B6 (2 copies)  
Washington, D.C. 20361

AIR-7226 (4 copies)  
AIR-5302 (1 copy)  
AIR-310A (1 copy)  
AIR-310B (1 copy)

Commander Naval Air Development  
Center  
Attn: M. Thomas, Code 6063  
(1 copy)  
E. Tankins, Code 6063  
(1 copy)  
R. Mahorter, Code 6063  
(1 copy)  
Warminster, PA 18974

Commander  
Naval Sea Systems Command  
Code 05R  
Department of the Navy  
Washington, D.C. 20361

Commander  
Naval Weapons Center  
Code 5516  
China Lake, CA 93555

Commander  
Naval Surface Weapons Center  
Metallurgy Div. -R32-D. Divecha  
White Oak,  
Silver Spring, MD 20910

Chief of Naval Research  
Code ONR 423  
ONR 431  
800 N. Quincy Street  
Arlington, VA 22217

Director  
Naval Research Laboratory  
Attn: Codes 6300 (1 copy)  
6370 (1 copy)  
6390 (1 copy)  
Washington, D.C. 20375

Air Force Wright Aeronautical  
Laboratory  
Attn: Code LLM (1 copy)  
LLN (1 copy)  
Metals Branch, Mfg.  
Tech Div (1 copy)  
Wright-Patterson AFB  
Dayton, OH 45433

Army Aviation Systems Command  
P.O. Box 209  
Attn: Mr. R. Vollmer-AMSAV-FRE  
St. Louis, MO 63166

Army Research & Tech. Lab  
Applied Technology Lab  
DAVDL-ATL-ATS  
Attn: T. Mazza  
Ft. Eustis, VA 232604

Army Research Office  
Box CM, Duke Station  
Attn: Metallurgy & Ceramics Div  
Durham, NC 27706

Army Mat'l's & Mech. Research Ctr  
Attn: Dr. George Thomas  
Watertown, MA 02171

Defense Advanced Research Project  
Agency  
Attn: Dr. B.A. Wilcox Code 641  
1400 Wilson Boulevard  
Arlington, VA 22209

NASA  
Ames Research Center  
Code 240-10  
Moffett Field, CA 94035

NASA Jet Propulsion Laboratory  
4800 Oak Grove Drive  
Pasadena, CA 91103

NASA  
Langley Research Ctr  
Attn: R.A. Pride  
Langley Station, MS 15d  
Hampton, VA 23365

Air Force Office of  
Scientific Research  
Dept. of the Air Force  
Bolling Air Force Base  
Washington, D.C. 20322

U.S. Department of Energy  
Division of Reactor Research  
& Technology  
Attn: A. Van Echo  
Mail Station B-107  
Washington, D.C. 20545

National Academy of Sciences  
National Materials Advisory Board  
2101 Constitution Ave.  
Attn: Dr. J.C. Lane  
Washington, D.C. 20418

National Science Foundation  
1800 G St., N.W.  
Washington, D.C. 20550

Battelle Memorial Institute  
Mfg. & Design Interaction  
Attn: Dr. Bryan R. Noton  
505 King Ave.  
Columbus, OH 43201

Bell Helicopter Co.  
Adv. Sys. Programs  
Attn: James Kenna  
P.O. Box 482  
Ft. Worth, TX 76101

The Boeing Company  
Aerospace Division  
P.O. Box 3707, M/S 73-43  
Attn: Mr. Rod Boyer  
Seattle, WA 98124

Boeing Company  
Vertol Division/MS P62-06  
Attn: R. Pinckney  
P.O. Box 95006  
Philadelphia, PA 19142

EXXON Materials Division  
Attn: Jerry Dixon  
P.O. Box 95006  
Raleigh, NC 27625

NASA  
Marshall Space Flight Ctr  
Attn: R. Schwinghamer  
Huntsville, AL 35812

General Dynamics  
Attn: C.F. Herndon  
P.O. Box 748, MS 2830  
Ft. Worth, TX 76101

General Dynamics Materials  
Research  
Attn: W.G. Scheck  
P.O. Box 80847, MZ 640-00  
San Diego, CA 92138

Grumman Aerospace Corp.  
MS AD-12, Materials & Proc. Dept.  
Attn: R.J. Herizman  
South Oyster Bay Road  
Bethpage, NY 11714

Grumman Aerospace Corp.  
Ad. Mtls & Process Div.  
Attn: Carl Micillo  
Dept. 447, Plan 12  
Bethpage, NY 11714

Hughes Aircraft Co.  
Components & Materials Lab  
Attn: L.B. Keller  
Bldg. 6, Main Station, D-134  
Culver City, CA 90230

Kaman Aerospace Corp.  
Matl's & Process Engineering  
Attn: A.S. Falcone  
Old Windsor Road  
Bloomfield, CT 06002

LTV Aerospace Corp.  
Vought Systems Division  
P.O. Box 5907  
Attn: Mr. A.E. Hohman, Jr.  
Dallas, TX 75222

Lockheed California Co.  
Department 76-31 Bldg. 63  
Attn: R. Kaseko/J. Pengra  
Burbank, CA 91520

Lockheed Missile & Space Co.,  
Inc.  
Dept. 86-73  
Attn. F.B. Yarborough  
P.O. Box 504, Bldg. 153  
Sunnyvale, CA 94088

Martin Marietta Corp.  
Denver Division  
Attn: Dr. A. Feldman  
P.O. Box 179, MZ 1630  
Denver, CO 80201

McDonnell Douglas Aircraft Co.  
Mrg. R&D Dept (MS1-22)  
Attn: Robert Zwart  
3855 Lakewood Blvd.  
Long Beach, CA 90846

McDonnell Douglas Corporation  
Engineering Division  
Attn. B.B. Leonard  
5301 BOLSA/MS A3-248/13-3  
Huntington Beach, CA 92847

McDonnell Douglas Research Labs  
P.O. Box 516  
Attn: Dr. D.F. Ames  
Dr. Charles Whitsett  
St. Louis, MO 63166

Northrop Corporation  
Attn: E. Jaffe  
One Northrop Ave  
Hawthorne, CA 90250-3277

Rockwell International Corp.  
Attn. M. Mahoney  
Science Center  
1049 Camino Dos Rios  
Thousand Oaks, CA 91830

Sikrosky Aircraft  
Mfg. Engineering Dept.  
Attn. J.D. Ray  
North Main Street  
Stratford, CT 06602

United Technologies Company  
Research Center  
400 Main Street  
East Hartford, CT 06108

Kaiser Aluminum Chemical  
Corporation  
Aluminum Division of Research  
Center for Technology  
P.O. Box 870  
Pleasanton, CA 94566  
Attn: T.R. Prichett

Reynolds Metals Company  
Metallurgical Research Division  
4th and Canal Streets  
Richmond, CA 23219  
Attn: Dr. Grant Spangler

Professor R. Ritchie  
Department of Materials Science  
and Mineral Engineering and  
Lawrence Berkeley Laboratory  
University of California  
Berkeley, CA 94720

Professor S. Suresh  
Brown University  
Division of Engineering  
Providence, RI 02912

Dr. E.A. Starke, Jr.  
School of Engineering and Applied  
Science  
University of Virginia  
Charlottesville, VA 22903

Prof. A.J. McEvily  
Department of Metallurgy  
U-136  
University of Connecticut  
Storrs, CT 06268

Southwest Research Institute  
8500 Culebra Road  
P.O. Box 28510  
San Antonio, TX 78284  
Attn: Mr. J. Fitzgerald  
Dr. D. Davidson

Aluminum Company of America  
1200 Ring Bldg.  
Washington, D.C. 20036  
Attn: Mr. G. Barthold

Aluminum Company of America  
Alcoa Center, PA 15069  
Attn: Mr. Paul L. Mehr

D. Brook  
123 Meadow Drive  
Patafkala, OH 43062

Roy L. Hewitt, P. Engr., PhD.  
Research Officer  
Structures and Materials  
Laboratory  
National Aeronautical  
Establishment  
Montreal Road  
Ottawa, Canada  
K1A 0R6

Prof. J. Schijve  
Delft University of Technology  
Dept of Aerospace Engineering  
P.O. Box 5058  
2600 GD Delft  
The Netherlands

Anders F. Blom, PhD.  
The Aeronautical Research  
Institute of Sweden  
P.O. Box 11021  
S-161 11 Bromma, Sweden

Douglas Aircraft Company  
3855 Lakewood Blvd.  
Long Beach, CA 90808  
Attn: P.R. Abelkis  
Mail Code 36-90  
Dept. C1-E84

Douglas Aircraft Company  
3855 Lakewood Blvd.  
Long Beach, CA 90846  
Attn: Dr. David Cho  
Mail Code W5-20

Dr. Richard Hertzberg  
Lehigh University  
Bethlehem, PA 18015

Metals & Ceramics Info. Center  
Battelle, Columbus Laboratories  
505 King Avenue  
Columbus, OH 43201

END

6-81

DTIC